EÖTVÖS LORÁND UNIVERSITY

FACULTY OF INFORMATICS

DEPARTMENT OF CARTOGRAPHY AND GEOINFORMATICS

Spatiotemporal Analysis of the Sea of Galilee Area Using Remote Sensing and GIS-Based Model: Markov – Cellular Automata

Ahmed Adwan

Student of Cartography MSc

Prof. Dr. László ZENTAI

Head of Department

ELTE Department of Cartography and Geoinformatics

Budapest, 2018

Abstract

The Sea of Galilee is considered as the only natural surface freshwater reservoir between all the main water resources in Palestine. Concerning the fact, that water is fundamental to the survival of every single living thing. This study aimed to conduct an assessment and mapping of the changes – Spatiotemporal analysis – occurred in the Sea of Galilee area based on satellite imagery. In this research, fifteen satellite imageries are gathered from 1972 to 2017 besides to 2011-ASTGTM-DEM. All the satellite imageries corrected atmospherically and radiometrically.

The period from 1972 to 2000, the decreasing and increasing of the water body of the Sea of Galilee behave as a wave. Consequently, the water level and the volume were changing. However, the Sea of Galilee in this era reaches the largest area and volume over the research time, which is 167.67 km^2 and 209.41 meters under the mean sea level. From 2000 to 2017 the real significant decreasing of the yearly average area of the Sea of Galilee started. The shrinkage in the Sea of Galilee happened in every direction mainly from the north, the north-eastern, the north-western and the south-eastern, the decreasing continue till 2010 when the Sea of Galilee area reaches the deck then started increasing again. The water body area in 2017 and nowadays follow the general trend of the 2000s period, which is decreasing. The essential explanation behind the shrinkage of the Sea of Galilee because of the intensive human water consumption by Israel in the first place knowing there are other factors affect the area of the Sea of Galilee like the evaporation, the amount of inflow released from Jordan River, and precipitation.

The research made a logical prediction of the Sea of Galilee [shape and area]. This prediction based on suitability maps and applying Markov chain analysis and Multicriteria Evaluation [MCE] analysis. Spatial validation indices are used after that for validation. Base on the validation statistics the standard Kappa index was 0.9423 that means a complete agreement and strong relationship between the model and reality. After that, the predictions process continued knowing that the predicted water body [shape and area] of the Sea of Galilee in 2036, 2055 and 2074 following the same circumstances from 1998 to 2017. The final results were as follows: The predicted areas of 2036, 2055 and 2074 are 158.50, 155.65 and 155.66 km^2, which can be considered as a logical extension of the trend of the 2000s period, which is decreasing. The research recommended to implement a water rationing system and adopt regular programs for monitoring the Sea of Galilee by the local authorities. It is also recommended to use the results of this research to develop the prediction model by including the amount of inflow released from the watershed of the Sea of Galilee to get a very accurate prediction.

DEDICATION

This thesis is especially dedicated to…

… My parents who never stop giving, who weave my happiness with strings from their merciful heart, who taught me that with faith and determination you could overcome any obstacle.

…my homeland, and my beloved people in Palestine.

Table of Contents

Table of Figures

List of Tables

1. Introduction

1.1 Background

Water is fundamental to the survival of every single living thing. Part of this resource is stored in lakes, which most are a freshwater resource used to satisfy environmental and human needs. Unfortunately, the water of these resources is becoming degraded, and some of them has recently been perceived to be wholly desiccated and almost extinct due to human activities and the fact that extreme climatic condition (for example, droughts).

Understanding changes in water surface, wetlands, land-uses, seashores and vegetation areas over time is essential to many aspects of cartography, geographic and planning researches. Imagery acquired by airborne or satellite sensors provide a necessary source of information for mapping and monitoring the natural and human-made features on the land surface. Interpretation and analysis of remotely sensed imagery require an understanding of the processes that determine the relationships between the property sensor measures and the surface properties we are interested in identifying and studying (Smith, 2012). However, dealing with imageries, which describe these temporal changes, is still a little bit restricted because these imageries depict only a past data.

1.2 Research Problem

The area of the Sea of Galilee (Lake Kinneret) surface was and still threatened by decreasing, In this research many satellite imageries will be collected and both of the geographic information system and remote sensing techniques will be used for spatiotemporal analysis, in order to detect the changes in the Sea of Galilee area, shape, water, level, and volume. Later Markov Cellular Automata model and spatial validation statistics will be part of this research to make a rational prediction of the Sea of Galilee shape.

1.3 Aim and Objectives

The primary objective of the current study is to conduct an assessment and mapping of the changes – Spatiotemporal analysis – occurred to in the Sea of Galilee area based on satellite imagery using GIS/remote sensing techniques. To achieve this objective, the accompanying points are to be considered:

- Detecting the magnitude and direction of change occurred at the Sea of Galilee, water level, and shape.
- Predict the total area and shape of the Sea of Galilee in the future.

1.4 Significance

The importance of the current study comes from the fact that it will represent a baseline and a geodatabase for the Sea of Galilee, which is the only natural surface freshwater reservoir among the significant water resources of Palestine that can benefit both planners and decision-makers for any future developmental projects to save the lake.

The GIS/remote sensing techniques are excellent and sufficient tools having the ability to cover large-scale areas to monitor temporal and spatial changes of the lake zone compared to the traditional tools that lack the required updating.

The use of satellite imagery is cost-effective in the sense that it is relatively cheap and sometimes free of charge such as Landsat images.

1.5 Research Justifications

Sea of Galilee has recently been perceived in the way to be decreased. This whole area needs more attention and research, the continuous changes occurring to the Sea of Galilee regarding the area and the water level due to the natural dynamic changes and the anthropogenic activities make the Spatiotemporal technique essential to analysis the decreasing. The reasons standing behind the conduction of this study are as follows:

- Lack of up-to-date geodatabase regarding the lake including the information of the bathymetry from the water authority.
- Change detection of the magnitude and direction of change occurred at the Sea of Galilee requires a more powerful system like GIS/remote sensing techniques which can provide a better way to effective mapping and monitoring. GIS/remote sensing systems provide analytical tools and modelling processes that can be used in environmental monitoring actions, mapping, and extraction of new information.
- This research will help for better planning of the lake and future development projects. It is considered as a baseline for any development projects.

1.6 Methodology

The methodology procedure in this research involves five phases figure (1-1). Step one and two consists of search concept and data acquisition. Step three includes the practical part of data analysis, image classifications, and change detection. Step four consists of the GIS-Modelling

for this study and predicting the future shape of Sea of Galilee. The findings of the current research and their analysis are completed in step five.

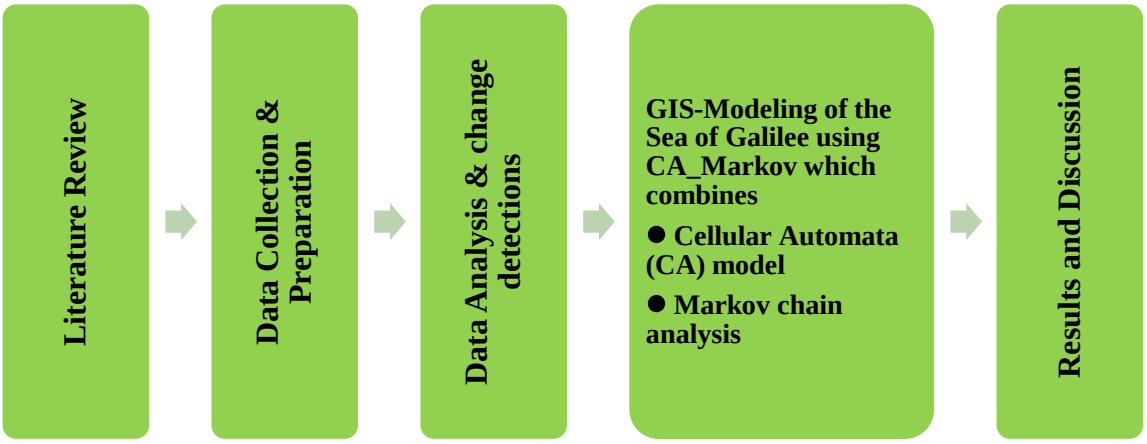

Figure (1-1). Methodology flowchart.

1.7 Research Structure

This thesis is comprised of six chapters as follows:

Chapter one includes a general background followed by the research problem, then, aim and objectives, significance and research justifications. Finally, a general description of the methodology to achieve the objectives and the research outline.

In chapter two, GIS, RS, image classification [supervised and unsupervised classification] change detection and spatiotemporal analysis are defined. Then, previous studies about the spatiotemporal analysis presented. Then, Markov chain analysis and cellular automata explained besides an overview of the statistical validation methods and equations. In the end, case studies about the Sea of Galilee are discussed.

Chapter three gives an overview of the study area, which is the Sea of Galilee concerning its geographic location, hydrology, and geology background.

Chapter four highlights the materials and methods and describe the methodology in details; image gathering, image pre-processing, supervised classification, spatiotemporal analysis, and prediction analysis are explained.

Chapter five presents and discusses the results gained throughout the methodology in chapter four. The changes of Sea of Galilee, the validation results of the CA_Markov model discussed. Finally, the result of predicted shape and area are illustrated and explained. In the end, chapter six draws the main conclusions and recommendations of the study.

2. Literature Review

2.1 Overview

Remotely sensed images are ordinarily used in analysing the spatial and temporal patterns of environmental variables over past decades due to the dynamic changes happening to the water bodies worldwide (Jianya, et al., 2008).

In this chapter, GIS, Remote Sensing and Image Classification Techniques in Remote Sensing are summarized from previous literature. Then, change detection and spatiotemporal analysis [time series analysis for spatial scenes] are outlined. At that point, change detection development over time is overviewed. Then, methods, algorithms and case studies about wetlands change detection are summarized again from previous literature. After that, Markov chain, Cellular Automata and statistical validation are defined. In the end, previous studies about CA_Markov and the Sea of Galilee Area are summarized from previous literature.

2.2 Introduction

There is no doubt that change information of the earth's surface is becoming more and more critical in monitoring the local, regional and global resources and environment. The magnificent collection of past and present remote sensing imagery makes it plausible to analyse a spatiotemporal pattern of environmental elements and impact of human actions in past decades (Jianya, et al., 2008).

2.3 Geographic Information Systems

The geographic information system (GIS) can be defined as a computer system capable of assembling, storing, manipulating, and displaying geographically referenced information. Based to (Dueker, 1979), the GIS is a particular case of information systems where the database consists of observations on spatially distributed features, activities or events, which are definable in space as points, lines, or areas. The concept of the geographic information system emerged during the 1960's and 1970's as a new trend to produce maps to be used for resource assessment, land evaluation, planning and environmental monitoring. Geographic information systems consist of three main elements: computer hardware, sets of application of software modules, and a proper organization context (Burrough, 1986). GIS is useful and valuable for organizations of all sizes and in almost every industry as there are an escalating interest and awareness of the economic and strategic values of GIS.

2.4 Remote Sensing

The remote sensing is the science of gathering information about objects or areas from a distance, typically from aircraft or satellites depending on the energy reflected from Earth. In current utilization, the term alludes to the use of aerial sensor technologies to detect and classify objects on Earth both on the surface, in the atmosphere and oceans using propagated signals, for example, electromagnetic radiation released from aircraft or satellites (Aggarwal, 2003). Remote sensing imagery has many applications in mapping land use and land cover (LULC), agriculture, soil mapping, city planning, forestry, archaeological investigations, surveying, bathymetric, shoreline changes, deforestation, vegetation dynamics, water quality dynamics, urban growth, … etc. (Abd Rabou, 2017).

2.5 Image Classification Techniques in Remote Sensing

Remotely sensed images are classified to specify corresponding levels, which called "class" or "themes" concerning groups with a similar characteristic, with the aim of discriminating multiple objects from each other within an image (Lillesand & Kiefer, 1994). Here, digital image classification uses the spectral information represented by the digital numbers in one or more bands that are a spectral figure (2-1). Analysis by humans uses the elements of visual interpretation to identify homogeneous groups of pixels that represent various features or land cover classes of interest (Abd Rabou, 2017) (Lillesand & Kiefer, 1994).

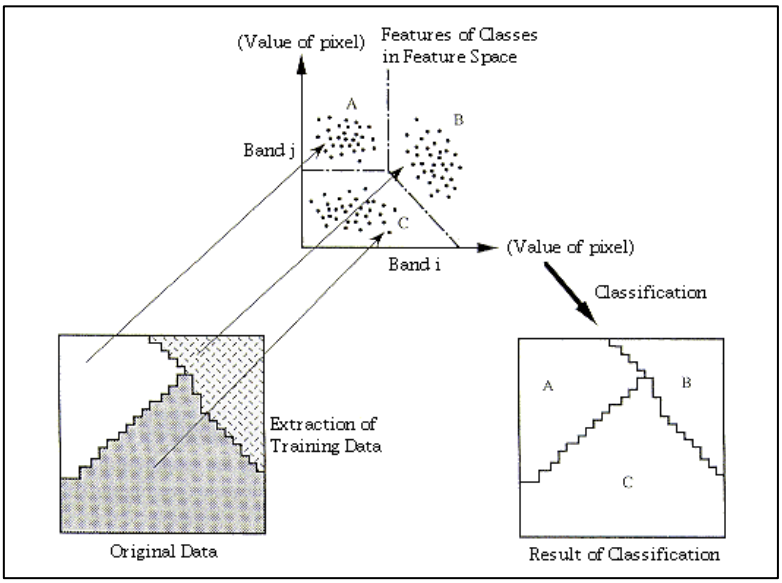

Figure (2-1). Concept of classification.

(Hashimoto, Takagi, & Kajiware, 1999)

They are two type of image classification techniques in remote sensing are generally known: unsupervised and supervised image classification.

2.5.1 Unsupervised Classification

In unsupervised classification method, spectral classes are gathered first, in view of the numerical information in the data, and are then matched by the analyst to information classes (if possible). Programs, called clustering algorithms, are used to determine the natural (statistical) groupings or structures in the data. Pixels are grouped based on the reflectance properties of pixels, which are called "clusters." In this regard, the image classification software generates clusters (Abd Rabou, 2017). There are different image clustering algorithms for example K-means and ISODATA. The user merges clusters into a land cover type as shown in figure (2-2). The unsupervised classification method is regularly used when no sample sites exist. In fact, Unsupervised classification is not working completely without human intervention. Even though may, it does not begin with a pre-determined set of classes as in a supervised classification (J. R. Eastman, Jin, Keym, & Toledano, 1995).

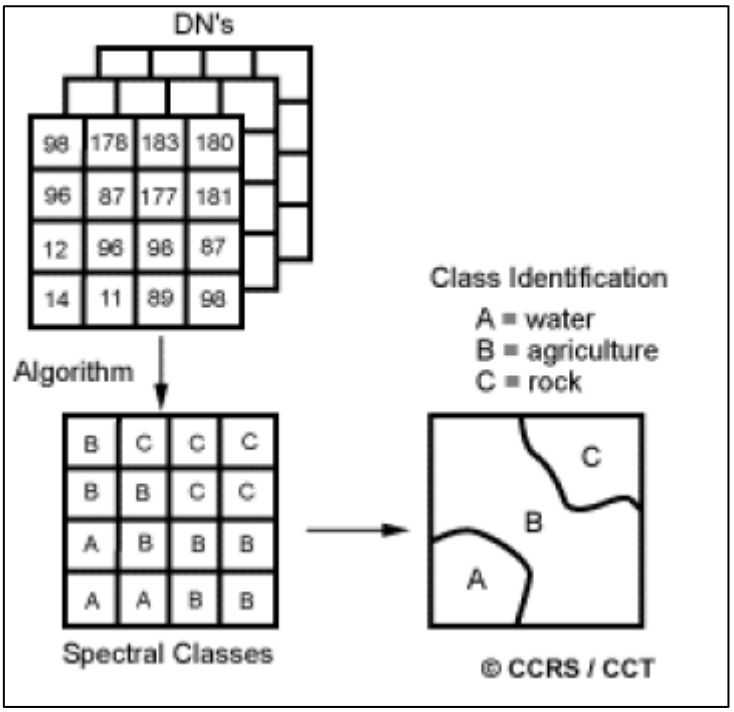

Figure (2-2). Schematic of the unsupervised classification procedure.

(CCRS/CCT, 1998)

2.5.2 Supervised Classification

"In supervised classification technique, the analyst identifies in the imagery homogeneous representative samples of the different surface cover types information classes (e.g., land cover type) of interest. The analyst selects representative samples for each land cover class in the digital image. These sample land cover classes are called "training sites" as shown in figure (2-3). The selection of appropriate training areas remains on the analyst's familiarity with the geographical area and their knowledge and insight into the real surface cover types present in the image. The image classification software uses the training sites to identify the land cover classes in the entire image. Thus, in a supervised classification technique are first defining the information classes which are then used to determine the spectral classes which represent them" (Blaschke, 2010; J. R. Eastman et al., 1995; Weih Jr, Riggan Jr, 2010 & Abd Rabou, 2017).

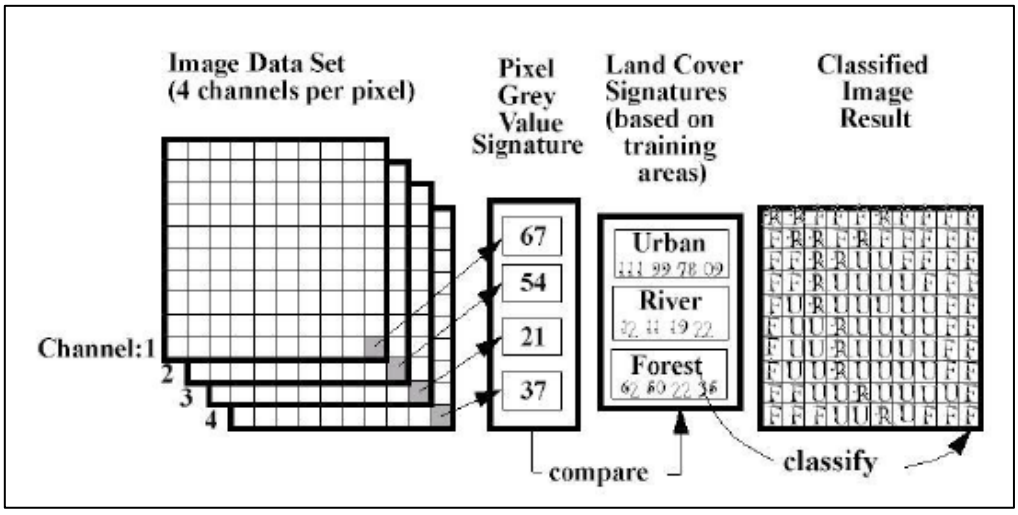

Figure (2-3). Scheme of supervised classification.

(T. Lillesand et al., 1994)

2.6 Change Detection Concept

"Change detection is the process of identifying differences in the state of an object or phenomenon by observing it at a different time" (Singh, 1989). Change detection, in other words, is a technology ascertaining the changes of specific features within a specified time interval. It gives the spatial distribution of features and quantitative and qualitative information of features changes (Kandare, 2000).

2.7 Change Detection History

Many sources say the history of the change detection begins with the history of remote sensing. It is important to know the development of change detection is intimately connected with military technology during the first and the second world wars and the strategic advantage provided by temporal information obtained by remote sensing. On the other side, the civilian applications development of digital change detection era started with the establishment of Landsat 1 in July 1972, but the improvement was constrained by data processing technology and computer technologies (Théau, 2012).

2.8 Change Detection Techniques

According to (AUG signals, 2008) change detection algorithms analyse multiple images of the same scene captured at different times to identify regions of change. (Singh, 1989) lists change detection methods into two types, namely, classification comparison and direct comparison. (Deer, 1999) suggests a classification of three categories, including pixel-based, feature-based and object-based change detection. LU, et al., 2004 concludes the change detection methods into seven types, namely: arithmetic operation, transformation, classification comparison, advanced models, GIS integration, visual analysis and some other techniques. (Richard, et al., 2005) reviews change detection methods in general terms and propose a classification of direct difference, statistical hypothesis testing, predictive models, shading model, and background modelling and so on. Jianya, et al., 2008 classifies change detection from its approaches, namely, bi-temporal change detection and temporal trajectory analysis. The former measures changes based on a ‘two-epoch’ timescale, i.e., the comparison between two dates. The last analysis the changes based on a ‘continuous’ timescale, i.e., the focus of the analysis is not only on what has changed between dates but on the progress of the change over the period as well. AUG signals, 2008 classifies change detection algorithms as algorithms based on pixel amplitude, both the magnitude and phase or on transformed pixel values. Théau, 2012 classifies change detection methods based on history since the algebra techniques , for example, image differencing or image rationing were the first techniques used to characterize changes in digital imagery then more complex techniques were developed since then with the improvement of processing capacities but also with the development of new theoretical approaches.

2.9 Time Series (Spatiotemporal) Definition

The data gathered sequentially over time called a time series. For instance, Environmental modeling, hydrology, meteorology, Digital Elevation Model (DEM) graphics and engineering are such examples in which spatiotemporal (time series of spatial scenes) arise.

The purest form of data used in time series is a longish series of continuous measurements at equally spaced time points. That is, observations are made at distinct points in time, these time points being evenly spaced and, the observations may take values from a continuous distribution. Assume that the series Xt runs throughout the time that is (Xt) t=1±2±3… but is only observed at times t = 1, . . . , nn (Reinert, 2010).

Time series analysis is a technology finding the changes of specific features within a predetermined time interval. It gives the spatial distribution of features and qualitative and quantitative information of features changes (Kandare, 2000).

In fact, there are various reasons to record and to analyze the data of a time series. Among this, there is a desire to gain a better understanding of the data generating mechanism, the prediction of future values or the optimal control of a system. The characteristic property of a time series is the fact that the data are not generated independently, their dispersion varies in time, they are frequently governed by a trend, and they have cyclic components. Statistical procedures that suppose independent and identically distributed data are, consequently, excluded from the analysis of time series. This requires proper methods that are summarized under time series analysis (Falk, et al., 2011).

The quantitative analysis for recognizing the characteristics and processes of surface changes are identified through from the different times of remote sensing data. It incorporates the number of changes and turns, the distribution that is the ground surface types, boundary changes, patterns and trends before and after the changes (Shaoqing, 2008).

Time series analysis technique is principally used for temporal trajectory analysis. In contrast to bi-temporal change detection, the temporal trajectory analysis is mostly based on low spatial resolution images such as Advanced Very High-Resolution Radiometer (AVHRR) and Moderate Resolution Imaging Spectroradiometer (MODIS), which have a high temporal resolution. The trade-off of using these images, however, is the loss of spatial details that makes auto-classification very hard, so that the temporal trajectory analysis is usually restricted in, for instance, vegetation dynamics in large areas, or change trajectories of individual land cover classes. Quantitative parameters such as Normalized Difference Vegetation Index (NDVI) or

area of given land cover class are often used as the dependent variables for the establishment of change trajectories (Jianya, et al., 2008).

2.10 Previous Studies about the Spatiotemporal Analysis

Many studies followed by using multiple methodologies and algorithms to map and assess the spatiotemporal changes of wetlands or water surfaces using various sets of remotely sensed data. Some works relevance are presented below.

Habboub, 2013 used the spatiotemporal analysis to study the water body of the Dead Sea. In this study, fourteen satellite imageries collected from 1972 to 2010 in addition to 2011-ASTGTM-DEM. Geographic information system and remote sensing techniques besides the satellite imageries were used for spatiotemporal analysis to detect the changes in the Dead Sea area. The result showed that the Dead Sea shrinks by 2.5 km^2/year while the water level decreases by 0.7 m/year. Consequently, the volume changes by -0.33 km^3/year. The direction of this shrinkage is from the north, northwest and from the south direction of the northern part due to slopes of bathymetry. A prediction of the Dead Sea shape was prepared using Markov Cellular Automata model and spatial statistics. The validation process shows a standard Kappa index of 0.9545, which means a strong relationship between the model and reality. The study shows that *"predicted shapes of 2020, 2030 and 2040 following the same conditions from 1984 to 2010. The predicted areas of 2020, 2030 and 2040 are 610, 591 and 574 km^2, which are considered a logical extension of the trend from1984 until 2010".*

Moayeri, et al., 2012 studied Hurol Azim wetland which bordering Iran and Iraq in the Middle East, Landsat satellite images captured by the users in the former years show the fact that Hurol Azim wetland area has been smaller in recent decades. The goal of this study is the wetland changes of Thematic Mapper (TM) and Enhanced Thematic Mapper Plus (ETM+) sensor of Landsat imagery in 1990 and 2005. The principal components analysis (PCA) method was used to determine the aim. The result showed that the wetland area of Hurol Azim has been smaller of 515.4 km^2 in 1990 to 230.59 km^2 in 2000. The principal reasons for wetland reduced water levels are the dam of Karkheh and drought.

Ndzeidze, 2009 used RS and GIS to define the extent of change of the wetland area and other land use and land cover classes in the Upper Noun drainage basin from 1973 to 2007. In this study, a supervised maximum likelihood algorithm classification method is used on available Landsat Multispectral Scanner (MSS), (TM) and (ETM+) imagery from 1978 to 2002. A significant drop in the area of permanent and seasonally flooded prairies was observed. This

study, therefore, provides base data for monitoring human impacts on the Upper Noun drainage basin and its natural habitats, especially within and around the wetland.

Ruan et al., 2008 proposed to study the potential of a time series of remotely sensed data for the change detection of wetland in Hongze Lake in the Northern Jiangsu Province. The raw data comprised three digital images acquired between 1979 and 2002. The task proceeded in three parts. First, following pre-processing and registration to the topography at the scale of 1:100,000, the ETM+ image of 2002 was classified by using hybrid classification techniques. A thematic feature space image of near-infrared versus red was created based on the above classification results. Second, the historical remotely sensed data were clustered using standard unsupervised classification technique; Iterative Self-Organizing Data Analysis Technique (ISODATA). Then the clusters were labelled into information classes utilizing the selection of core clusters, the relationship of clusters between clusters in feature space and geographical space. Third*, "the class "Emergent" was extracted from the three dates of thematic maps and recorded respectively as three files. The three files were then overlaid for the analysis of wetland change. The distribution of the class "Emergent" and its change as time and in space were utilized as indicators for the difference in wetland condition"*. The results showed that a significant loss of wetland has occurred in the study area in the past more than 20 years.

Baker et al., 2007 this study used Landsat-based satellite imagery in time series from 1988 and 2001 to map the changes in wetland ecosystems in the Gallatin Valley of southwest Montana. Stochastic Gradient Boosting (SGB) algorithm was applied to classify the 2001 image and Change Vector Analysis (CVA) was used to recognize *"locations where wetland areas might have changed between 1988 and 2001. These potentially changed locations again were classified for the 1988 Landsat image using SGB. Areas of change constituted 3.4% of the study area. Thus only this small percentage of the image was reclassified for the 1988 image. Overall change detection accuracy was 76%, although changes along the periphery of wetland boundaries and in areas of smaller upland inclusions were not distinguished as well as other changes. Overall accuracies of the SGB wetland classification maps were 81% for 1988 and 86% for 2001. CVA significantly reduced the number of pixels involved in the historical image classification compared to conducting independent classifications, thus reducing the potential for compounding classification errors in unchanged areas"*.

2.11 Markov Chain Analysis Definition

Markov process is *"the state of a system at time 2 can be predicted by the state of the system at time 1 by given a matrix of transition probabilities from each cover class to every other cover class"* (Eastman, 2012).

Markov analysis is primarily utilized to study land use change and land use impact assessment. Latterly, Markov analysis of land use change has been combined with GIS to make such a tool for visualizing and projecting the probabilities of land use change among categories of land use. The inputs and outputs of Markov chain illustrated in figure (2-4).

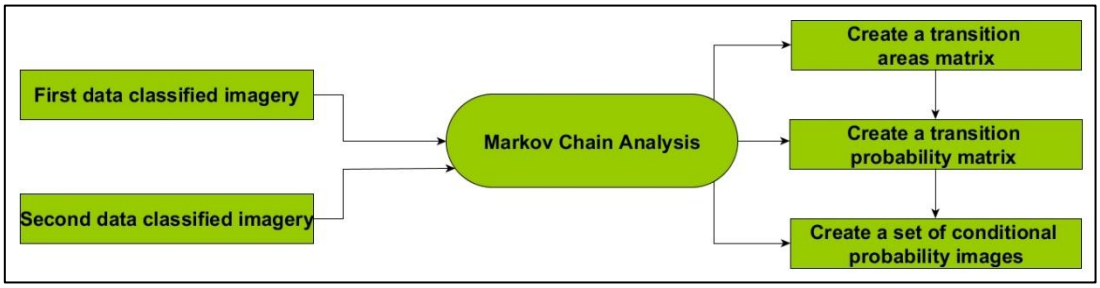

Figure (2-4). Markov Chain Analysis flowchart.

(Habboub, 2013)

"All landscape spatial transition models can be expressed in a simple matrix equation as follows (Tang, et al., 2007):

$$\boldsymbol{LU_{t+1} = LU_t * P} \qquad \textit{Equation (2-1)}$$

LU_t and LU_{t+1} are vectors composed of the fractions of each landscape type at time t and time t+1, respectively (Briassoulis, 2012).

(Tang et al., 2007) *defined P as a square matrix, whose cell P_{ij} is the transition probability from landscape i to j during times t and t + 1, while* (Memarian et al., 2012) *portrayed the transition probability, Pij, as the probability of moving from one state i then onto the next state which could be appeared in the form of a transition matrix, P. Equation 2-2 demonstrates the P matrix.*

A transition areas matrix shows the total area (in cells) expected to be changed in the next time period. A set of conditional probability images expresses the probability that each pixel will belong to the designated class in the next time period.

They are called conditional probability maps since this probability is conditional on their current state (Eastman, 2012).

$$“ p = \begin{bmatrix} P_{11} & P_{12} & P_{1n} \\ P_{21} & P_{22} & P_{2n} \\ P_{n1} & P_{n2} & P_{nm} \end{bmatrix}$$ *Equation (2-2)*

The transition probabilities P in K steps are derived from the landscape transitions happening during some time interval as shown in equations 2-3 and 2-4 (Tang, et al., 2007):

$$\boldsymbol{P_m(i,j) = \frac{N(i,j)}{\sum_{k=1}^{k} n_{ij}}}$$ *Equation (2-3)*

$$\boldsymbol{P(i,j) = \sum_{k=1}^{k} \frac{P_m(i,j)}{K n_m}}$$ *Equation (2-4)*

Where N(i, j) is the observed data amid the transition from state i to j, nij is the years number between time step i and step j, the total quantity of years is m; P(i,j) is the yearly transition probability subsequent to normalizing the transition probability in multiyear, and K is the number of steps. (Tang, et al., 2007).

(Briassoulis, 2012), (Bell et al., 1977) and (Tang et al, 2007) *mentioned that there are several assumptions for Markov chain;*

- *The change is stochastic, not deterministic.*
- *Markov chain gives a set of discrete classes, which has to be identified clearly, since the process can be in one and only one of these classes at a given time.*
- *It moves successively from one state to the other with some probability that depends only on the current state and without considering the other historical values, LU_1, LU_2, LU_3….*
- *The cells in the transition matrix are probabilities; it follows equation 2-5.*

$$\boldsymbol{\sum_{j=1}^{m} P(i,j) = 1}$$ *Equation (2-5)*

One of the downsides of Markov chain is that it has an insufficient spatial knowledge. To enhance the spatial sense of these conditional probability images, using Cellular Automata model will be a good decision.” (Habboub, 2013).

2.12 Cellular Automata (CA) Description

CA is a grid of cells with every cell refreshing its value in light of its neighboring cell values (Yao, 2010) while (Eastman, 2012) describes CA as a cellular entity that independently varies its state based on its former state and that of its immediate neighbors depending on a specific rule. Despite the fact that this definition is so near to Markov chain, the main contrast is that the application of the transition rule which relies on not only upon the previous state but the state of the local neighborhood as well. So, the state of a cell is specified by the earlier states of the surrounding neighborhood of cells. Each cell in a regular spatial lattice can have any one of a finite number of classes. CA consists of different elements. They are; cell space which is one cell that can be in any geometric shape, cell state that represents any spatial variable, a sequence of discrete time steps, transition rules which is a rule specifies the state of the cell before and after updating based on its neighbours. A limited neighbourhood (Von Neumann) including 4 or 12 adjacent cells for 3x3 filter and 5x5 filter respectively as shown in Figures 2-5-A and 2-5-C or an extended neighbourhood (Moore) including the 8 or 24 adjacent cells for 3x3 filter and 5x5 filter respectively as shown in Figures 2-5-B and 2-5-D. See (equation 2-7) below which illustrated the effect of the neighbourhood type (Collet, et al., 2012) (Fonstad, 2006) (Habboub, 2013).

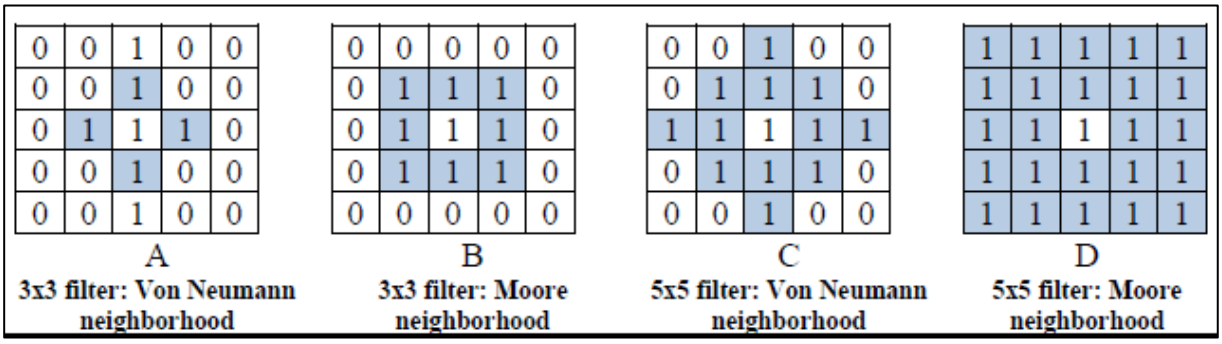

Figure (2-5). Neighborhood type.

(Fonstad, 2006) (Habboub, 2013)

2.13 CA_Markov

According to (Memarian, et al., 2012) CA_Markov can simulate land use changes among numerous classifications and combines the CA and Markov chain procedures. Furthermore, Markov analysis does not explain the causes of land use change, and it is insensitive to space as well.

"IDRISI software illustrates a technique of CA_Markov since a Markov chain analysis is performed to estimate the transition matrix between the two past dates and to estimate probabilities of change for the third date to be predicted. Then, a Cellular Automata (CA) estimates the spatial distribution of land cover at a later date.

Equations 2-6 and 2-7 down show the evaluation of cells from the time (t) to (t+1) is determined by a function of its state, its neighborhood space and a set of transition rule (Samat, et al., 2011).

$$LU_{i,j(t+1)} = f\left(LU_{i,j(t)} \cdot S_{i,j(t)} \cdot P_{x,y,i,j(t)} \cdot N_{i,j(t)}\right)$$

Equation (2-6)

$$N_{i,j(t)} = \frac{\sum^{t} N_{i,j(t)}}{\#\ \text{ofadjacent cells}}$$

Equation (2-7)

- *Where:*
- $LU_{i,j\,(t+1)}$*: The potential of cell i,j to change at time t+1,*
- $LU_{i,j\,(t)}$*: States of cell i,j at time t,*
- $S_{i,j\,(t)}$*: Suitability indexes of cell i,j at time t [see equation 4-4] ,*
- $P_{x,y,i,j\,(t)}$*: Probability of cell i,j to change from state x to state y at time t (as shown in equation 2-3above, and;*
- $N_{i,\,(t)}$*: Neighbourhood index of cell i,j"* (Habboub, 2013).

2.14 The Validation of CA-Markov Analysis

For the validation IDRISI is one of the software which can offer a very comprehensive statistical analysis that answers how competently a pair of maps agrees concerning the quantity and location of cells in every category, different Kappa Indices of Agreement (KIA) and related statistics derived to show how much the comparison map agrees with the reference map. Gil Pontius (Pontius, et al., 2011) have designed these strategies of validation not long ago at Clark University (Habboub, 2013).

Habboub, 2013 defined the validation as a procedure determine the disagreement and the contrast between predicted map and real classified imagery. So two types of disagreement will

be calculated; first, quantity disagreement: this happens when the quantity of the cells of a category in the comparison map is unlike from the amount of the cells from the same category in the reference map. Second, allocation disagreement happens where the location of a class in the comparison map is unlike from location of that class in reference map (Memarian, et al., 2012) (Pontius, et al., 2011).

The equations which are used for validation shown in (Pontius, et al., 2011) and display these two parameters where (J) indicates a number of strata – classes – and the number of categories in typical stratified sampling design. Every category in the comparison map is indexed by i, which ranges from 1 to J. The number of pixels in every stratum is denoted by Ni. Every observation is recorded based on its category in the comparison map (i) and the reference map (j) as well. The number of these observations is summarized as the entry n_{ij} in row i and column j of the contingency matrix (Memarian, et al., 2012) (Habboub, 2013).

"The ratio of the study area (P_{ij}) that is category i in the comparison map and category j in the reference map is calculated roughly by equation 2-8.

$$P_{ij} = \left(\frac{n_{ij}}{\sum_{j=1}^{J} n_{ij}}\right)\left(\frac{N_i}{\sum_{i=1}^{J} N_i}\right)$$

Equation (2-8)

Quantity disagreement (q_g) has been calculated for an arbitrary category g using equation 2-9

$$q_g = \left|\left(\sum_{i=1}^{J} p_{ig}\right) - \left(\sum_{j=1}^{J} p_{ig}\right)\right|$$

Equation (2-9)

Equation 2-10 calculates the total quantity disagreement (Q) which incorporates all J categories.

$$Q = \frac{\sum_{g=1}^{J} q_g}{2}$$

Equation (2-10)

Allocation disagreement (ag) for an arbitrary category g is calculated through Equation 2-11. The first argument within a minimum function is the omission of category g, on the other hand, the second argument is the commission of category g. Where: a pixel is called omission for a class when the pixel in the reference map is like that class, and it is a different class in the

comparison map. A pixel is called commission for a class when the pixel in the comparison map is the same of that class, and it is a different class in the reference map.

$$a_g = 2min\left[\left(\sum_{i=1}^{J} p_{ig}\right) - p_{gg'}, \left(\sum_{j=1}^{J} p_{gj}\right) - p_{gg}\right]$$

Equation (2-11)

Equation 2-12 estimates the overall allocation disagreement (A).

$$A = \frac{\sum_{g=1}^{J} a_g}{2}$$

Equation (2-12)

The proportion of agreement (C) is estimated by Equation 2-13.

$$C = \sum_{j=1}^{J} p_{jj}$$

Equation (2-13)

The total disagreement (D) is the sum of the overall quantity of disagreement and overall allocation of disagreement as illustrated in equation 2-14" (Habboub, 2013).

$$D = 1 - C = Q + A$$

Equation (2-14)

To summarize all the previous equations and according to Pontius, et al., 2011 IDRISI offers three more different kappa indices of agreement besides to the standard KIA, which are:

1. Kappa for no information (K_{no}).
2. Kappa for the grid cell level location, which represents how well the grid cells are located on the ground ($K_{location}$).
3. Kappa for stratum level location, which shows how competently the grid cells are located within the strata ($K_{location\ Strata}$).

Every Kappa is an index that shows how well the comparison map agrees with the reference map on a scale [0 to 1]. (1) means that the agreement between both of the maps is complete, on the other hand (0) means the agreement is much more closer to the statistically expected random agreement (Memarian, et al., 2012) (Habboub, 2013).

2.15 Previous Studies about the Sea of Galilee

(Markel, 2014) studied the watershed of the Sea of Galilee. The study found out that the watershed of the Sea of Galilee is populated and contains urban, agricultural and minor industrial activities, which produce a variety of nutrient and pollution loads that endanger water quality in the lake. The study aimed to outline the organizational structure, the monitoring program, and the management frameworks of the Sea of Galilee and its watershed. It is concluded that ongoing and expanded lake and watershed management is promising means for maintaining a healthy ecological system and improved water quality in the Sea of Galilee.

Markel et al., 2006 in their study presented an application of AVGWLF (a GIS-based watershed load model) to the Sea of Galilee watershed. The model lets one simulate daily stream flows, and monthly sediment, nitrogen, and phosphorus loads discharged to the lake from the surrounding watershed. Results gained from simulations yield satisfactory correspondence between simulated and measured daily water volume. Partition by the source of total phosphorus delivered to the lake from 2000 to 2004 confirms the reduction in point source nutrient contribution due to the improvement of wastewater treatment facilities in the area. The study concluded that future management should focus on reduction of nutrients originating from septic systems (point sources) and pasture and cropland areas (diffuse sources). Results from simulations will enable watershed managers to prioritize effective management alternatives for protecting the water quality in the lake.

Schwabe et al., 2004 in their study reconstructed the limnological history (level and composition) of the Sea of Galilee *"during the past ~40,000 years and compared it with the history of the contemporaneous Lake Lisan from the aspect of the regional and global climate history. The Sea of Galilee level reconstruction was achieved through a chronological and sedimentological investigation of exposed sedimentary sections in the Kinnarot basin trenches and cores drilled at the Ohalo II archaeological site. Shoreline chronology was established by radiocarbon dating of organic remains and Melanopsis shells. The results of this study show the major changes in the Sea of Galilee level were synchronous with those of the southern Lake Lisan. Both lakes dropped significantly ~42,000, ~30,000, 23,800, and 13,000 years ago and rose ~39,000, 26,000, 5000, and 1600 years ago. Between 26,000 and 24,000 years ago, the lakes merged into a unified water body, and lake level achieved its maximum stand of ~170 m below mean sea level (m bsl). However, the fresh and saline water properties of Lake Kinneret and Lake Lisan, respectively, have been preserved throughout the 40,000 years studied. Calcium carbonate was always deposited as calcite in Lake Kinneret and as aragonite in Lake*

Lisan– the Dead Sea, indicating that the Dead Sea brine (which supports aragonite production) never reached or affected Lake Kinneret, even during the period of lake high stand and convergence".

2.16 Evaluating the Literature Review

- The past literature review considers the main base of this study through it the structure of this research built, the model of the change detection made to suit with the study area, the understanding of Markov chain analysis became easy, and finally, the problem of this research solved.
- The majority of the previous studies that mentioned before used the spatiotemporal analysis in a time period not more than 40 years, but this study used it in a time period time 45 years.
- The overviewing of the previous studies focused on many topics. However, none of them reviewed the change on the Sea of Galilee over the time in details like what this study made.
- Some of the previous studies used old satellite images to detect the changes meanwhile this study used the most recent imageries and up-to-date methods of change detection

3. The Study Area Description

3.1 Overview

This chapter consists of four sections. The names of the Sea of Galilee discussed first, then the geographic location of the Sea of Galilee presented, after that, the hydrology of the Sea of Galilee reviewed in details including the watershed. Finally, the geological background of the Sea of Galilee discussed.

3.2 Names

Although, the Sea of Galilee has many names most of the modern maps recognize "the Sea of Galilee" as its common name, the name Galilee points to the region of Galilee which is situated on it. In Arabic, it calls "Lake Tiberias". It is also called in different names; these names came through the history and religions for instance "Lake Kinneret," "the Sea of Kinnereth," "the Lake of Gennesaret" and sometimes simply "the lake" (Washah, 2002).

3.3 The Geographic Location

The Sea of Galilee located on 32° 49' 59.99" N, 35° 34' 59.99" E, WGS84 coordinate system, set in the hills of northern Palestine among the hills of the Galilee. Bordering Jordan to the east, historical Palestine and the West Bank to the west as illustrated in Figure (3-1).

The Sea of Galilee is not a sea by any reasonable definition; it is called a sea just because of tradition. It is a lake, approximately 53 kilometres (33 miles) in circumference, about 21 km (13 miles) long, and 13 km (8 miles) wide; it has an aggregate area of 166 square km and the greatest depth of roughly 48 meters. At 213 meters below sea level, it is the lowest freshwater lakes on earth and the second-lowest point on the planet after the Dead Sea. The Sea of Galilee is fed by underground springs, but its primary source is the Jordan River that, after exiting the lake, continues farther south to its final destination, which is the no-outlet Dead Sea. (Kessler, 1999).

The Sea of Galilee is situated down in the Jordan Great Rift Valley, the valley caused by the detachment of the African and Arabian Plates. In the past, the area was liable to quakes and, before, volcanic action. (Markel, 2004) That proved by the superabundant basalt and different igneous rock that characterize the topography of the Sea of Galilee region. Because of its low-lying position in the rift valley, encompassed by hills, the Sea of Galilee is prone to sudden violent storms.

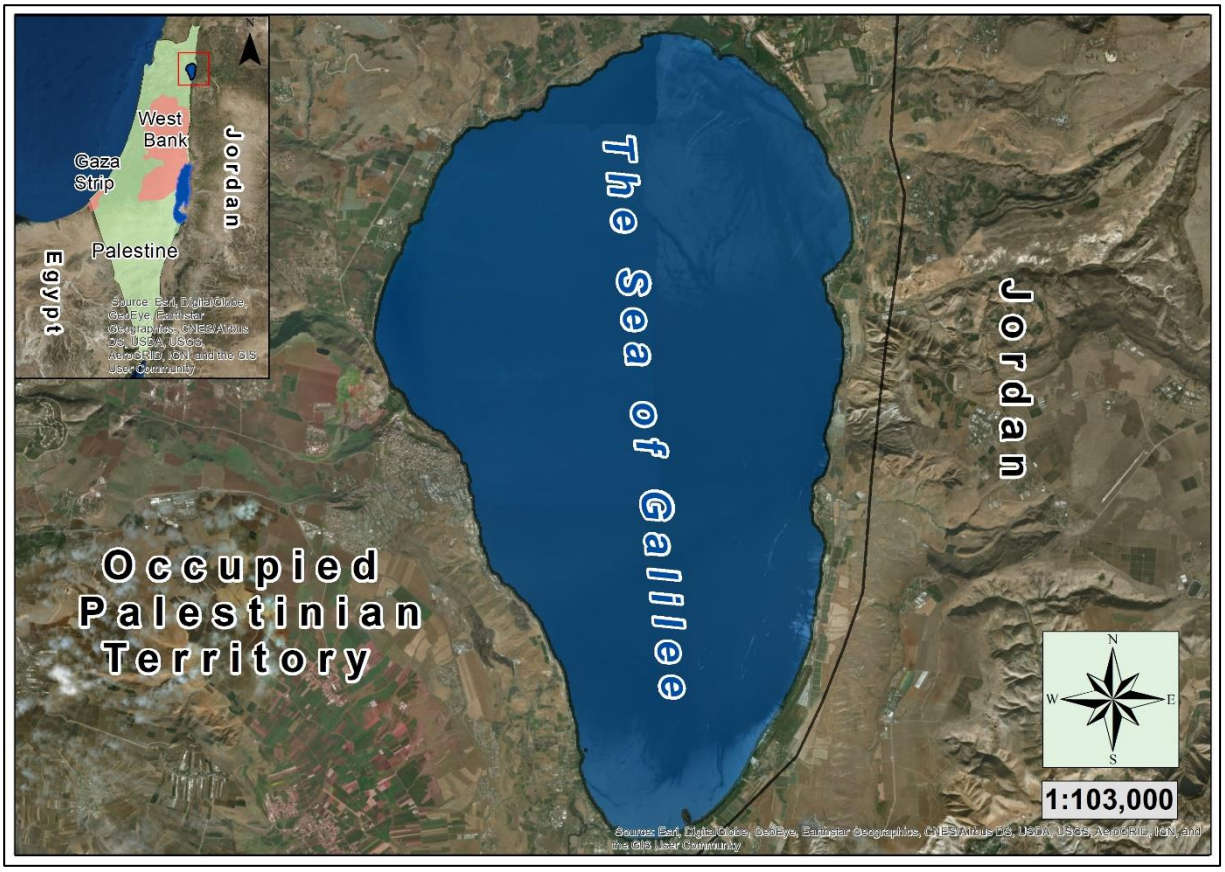

Figure (3-1). The Sea of Galilee location[1]

3.4 Hydrology Background

3.4.1 Temperature

The Sea of Galilee average water temperature varies from 10°C in winter to 32°C in summer reaches the maximum in August while in January, it reaches the minimum value see figure (3-2) shows the average monthly water temperature in Sea of Galilee minimum and maximum. The temperatures are calculated based on the data over the past ten years. The sea affects temperature nearby because of the moderating effect a large body of water has on climate. During the winter, sea temperature tends to be higher than land temperature, and the other way around/round during the summer months this is the consequence of the water's mass and specific heat capacity. On average, there are 192 days above 30°C. (U.S. Geological Survey, 1998).

[1] All the maps of The Sea of Galilee beginning from here made by the researcher based on the research geodatabase and the coordinate system used WGS_1984

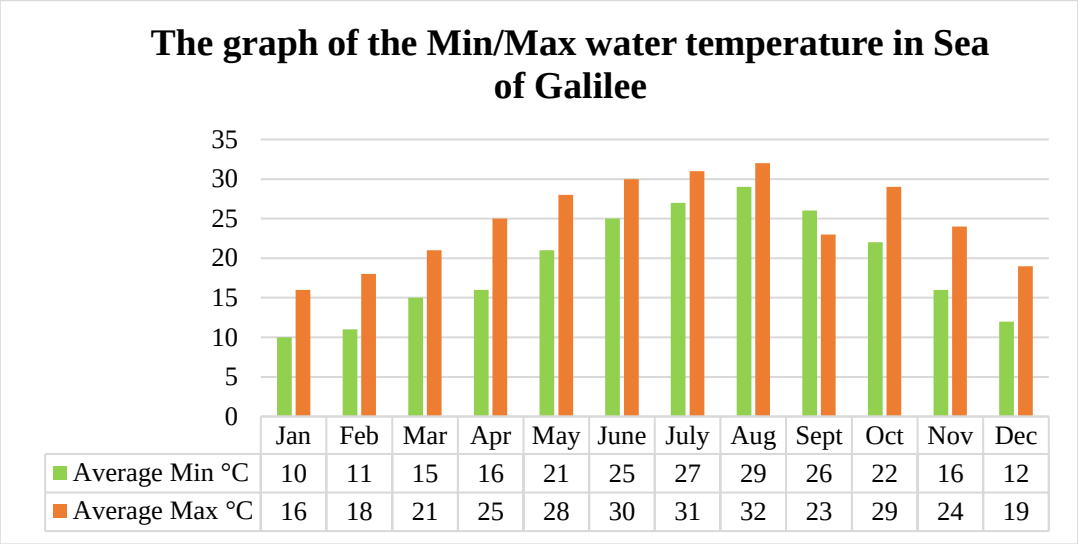

Figure (3-2). The average monthly water temperature in Sea of Galilee (min-max).

(WORLD SEA WATER TEMPERATURES, 2018)

3.4.2 Precipitation

The average annual precipitation on the Sea of Galilee area is 400 mm/year; most of the water flowing to the Sea of Galilee comes from the relatively high rainfall areas of the Jordan River watershed to the north, and the rift valley escarpments to the east and west of the Sea. Figure (3-3) illustrates the average rainfall on the Sea of Galilee area.

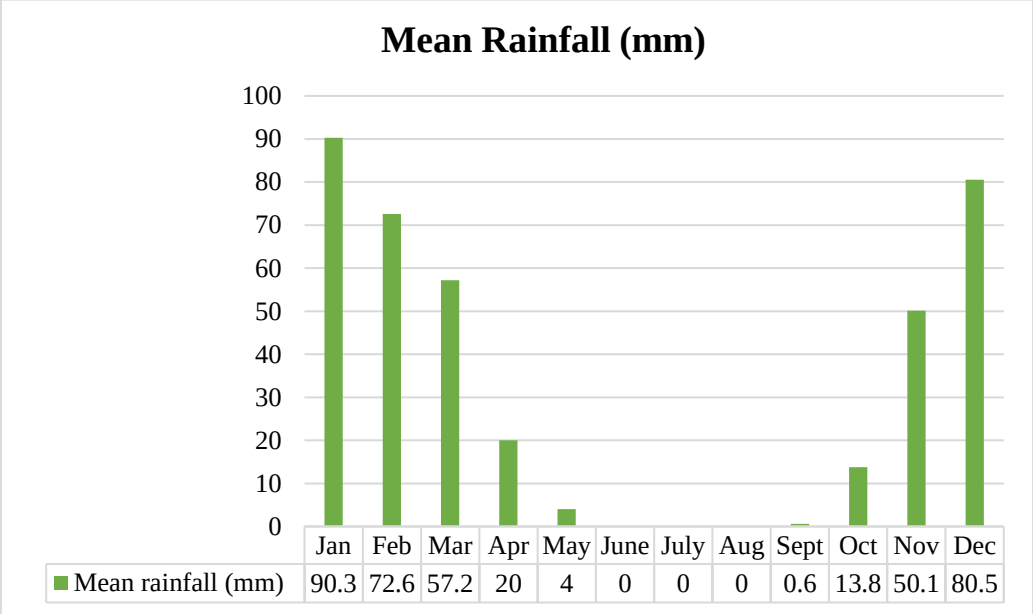

Figure (3-3). The average precipitation on the Sea of Galilee.

(Israel Meteorological Service Massada Station, 2016) modified

3.4.3 Watershed (Catchment Area)

Sea of Galilee drains a catchment area of 2730 km^2, of which 2,070 square kilometres are in historical Palestine, and 660 square kilometres are in Lebanon and Syria. From an altitude of 2800 m (Mount Hermon) down to the Lake itself, located 209 m below sea level figure (3-4) and figure (3-5), in the central part of the Jordan Rift Valley "Northern Palestine" (Kessler, 1999). It is the most critical surface water resource in Palestine. The major water source for the lake is the 1,700 km^2. Upper Catchments of the Jordan River (UCJR) including 920 km^2 in Palestine and the remainder located in Syria and Lebanon. In the north of the UCJR, the high elevation of the Mt. Hermon range (between 1,200 – 2,800 m) is the wettest area in the Sea of Galilee watershed, where the average annual precipitation ranges between 1200 – 1500 mm. The Mt. Hermon basins feed the three major tributaries of the Jordan River: the Dan with 250 million m^3 (Mm^3) annually, the Hermon (110 Mm^3, also known as Banias), and the Snir (115 Mm^3, also known as the Hazbani River). The other part of the Sea of Galilee basin is the direct watershed, located near the lake. The area of the direct watershed is 965 km^2, 577 km^2 of which are in the southern part of the Golan Height to the east of the lake, and the other 388 km^2 are in the Eastern Galilee Mountains to the west of the lake (Israel Water Authority, 2012).

Figure (3-4). Orientation map of the Sea of Galilee watershed.

(Israel Water Authority, 2012)

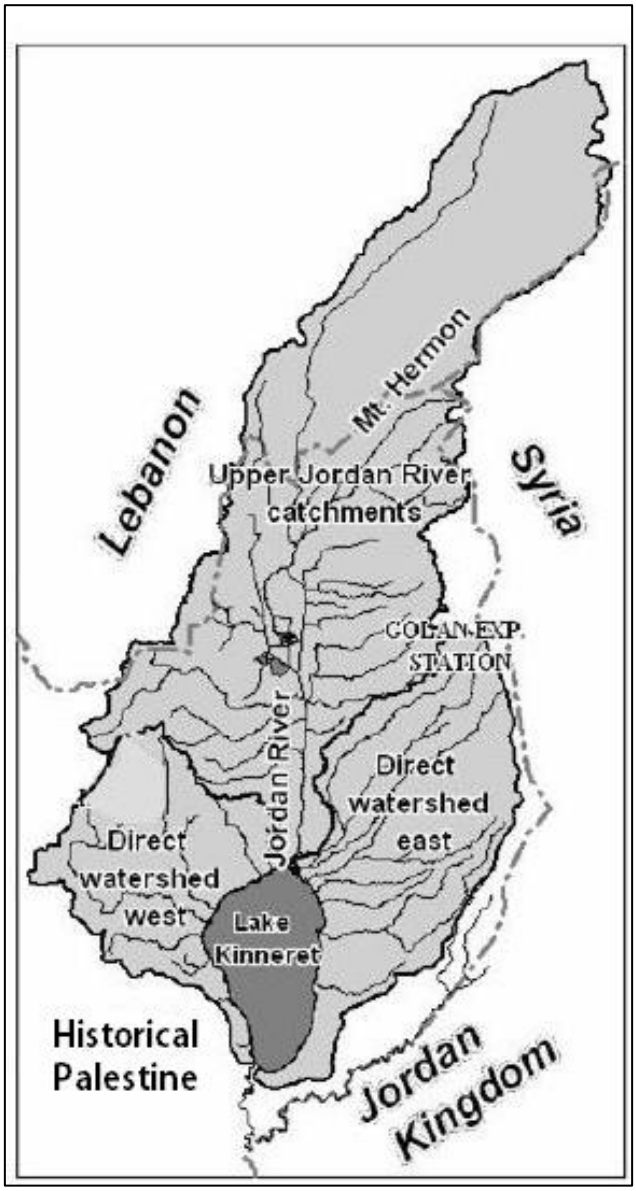

Figure (3-5). The Sea of Galilee watershed including the international borders, the Upper catchments of the Jordan River and, the direct watersheds (east and west).

(Israel Water Authority, 2012)

3.4.4 The Change of the Sea of Galilee Hydrological Parameters over Time

3.4.4.1 The History of the Water Level

The total inflow from the watershed plus the direct rain exceeds ca. 600 10^6 m^3/year, while the Jordan River contributes about 70% of the total (Rimmer and Givati 2014). The annual available water (inflows minus evaporation) in Sea of Galilee has decreased significantly during the last 40 years figure (3-5). The decline in the net replenishment to the lake was ca. 150 10^6 m^3 yr^{-1} over 36 years. Sixty percent of this reduction is attributed to decreased precipitation and a

change in the rain pattern (Givati and Rosenfeld 2007). The remaining 40% is attributed to increased water consumption in the watershed, including in Lebanon. It is also clear from the figure (3-5) that the inflows to the lake vary from year to year (annual evaporation is approximately constant). As shown in figure (3-5), there have been extended periods of low inflow years, while the extractions were driven by demands. As a result, water levels have declined during these dry years, as seen in figure (3-6). In 1986, the level dropped for the first time below -212 m, reaching -213 m (the "Lower Red Line") by 1990. During the high rainfall winter of 1991/1992, the water level rose back to the Upper Red Line, but over the next ten years, the total amount pumped exceeded the available water year after year. The years 1992-2002 and 2004-2009 experienced cumulative declines of lake level by 6 m and 5.5 m, respectively, dropped below the "Lower Red Line." The wet years of 1991-2 and 2002-4 produced periodic recoveries but were soon succeeded by normal and low inflow years that resulted in lowering the lake levels (Markel, 2014).

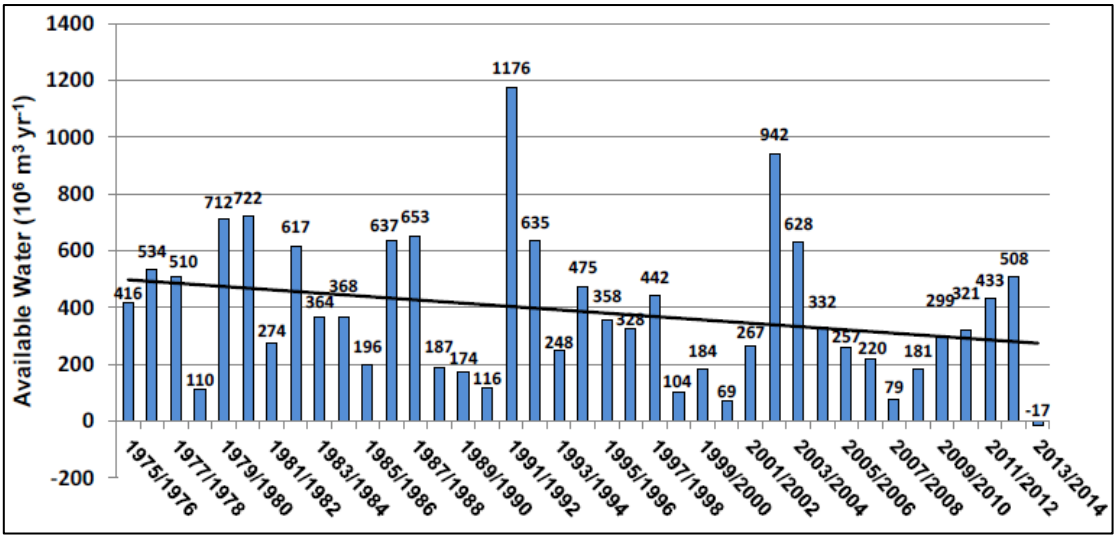

Figure (3-6). Annual available water in the Sea of Galilee
(10^6 m^3) The black line represents a linear regression from 1975/1976 to 2013/2014.
(Israel Hydrological Service, 2012)

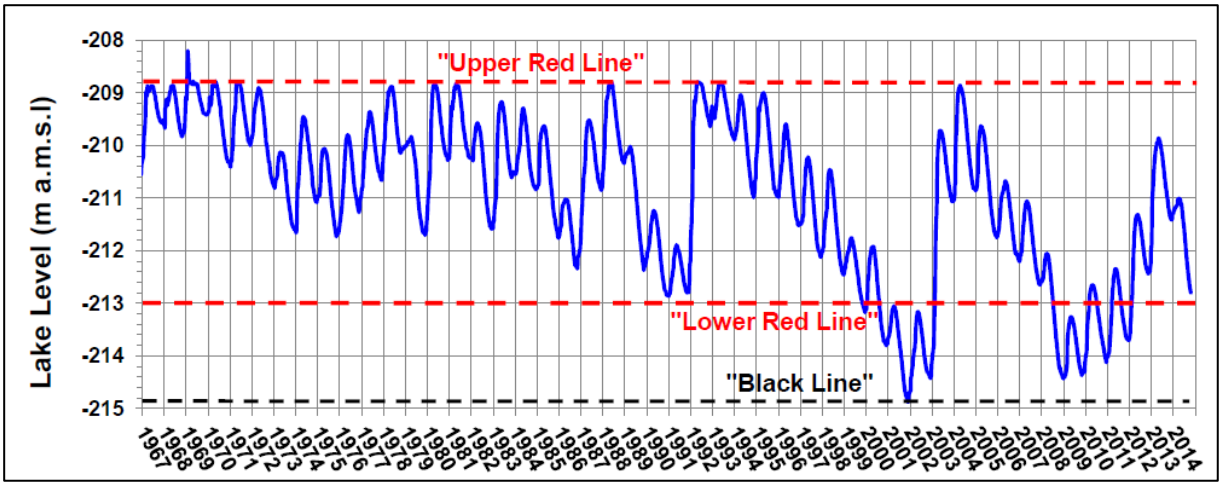

Figure (3-7). The Sea of Galilee Daily Water Levels 1967-2014.

(Israel Hydrological Service, 2012) modified

[Upper Red Line]. This sign shows that the Sea of Galilee is full (maximum capacity). When this level is reached, the Degania Dam[2] is being opened. [Lower red line]. The line height is 213.0 meters below sea level. *"According to ecology experts with the decline of the water level under this line starts damage to ecological balance and water quality begins to decline. After the arrival of water to this level, it is forbidden to pump or use water from the Sea of Galilee"* (Water Level of Lake Kinneret, 2018).

3.4.4.2 The Recent Water level

Based on the last update in 28th February 2018 form Water Level of Lake Kinneret website, the current water level of the Sea of Galilee is 213.6 meters below the sea level.

3.4.4.3 The Evaporation of the Sea of Galilee

The Evaporation of the Sea of Galilee is presented annually in figure (3-7) for the years of 1997-2008. The average evaporation is about 240 million cubic metre [MCM] based on Mekorot "the national water company of Israel" and the country's top agency for water management. (Israel Water Authority, 2012).

[2] The Degania Dam is a small barrage across the Jordan River just below the Sea of Galilee near Degania Alef and Yardenit in the north. The purpose of the dam is to regulate water levels in the Sea of Galilee and flows into the lower Jordan River. It has two floodgates capable of releasing 800 m^3/s (28,000 cu ft/s). The dam was completed in the early 1930's as part of the Naharayim Rutenberg hydroelectric power plant project. Although the floodgates have been opened partially in the past they were first opened fully in May 2013 after heavy spring flooding and a need to replenish the river (Wikipedia, 2018).

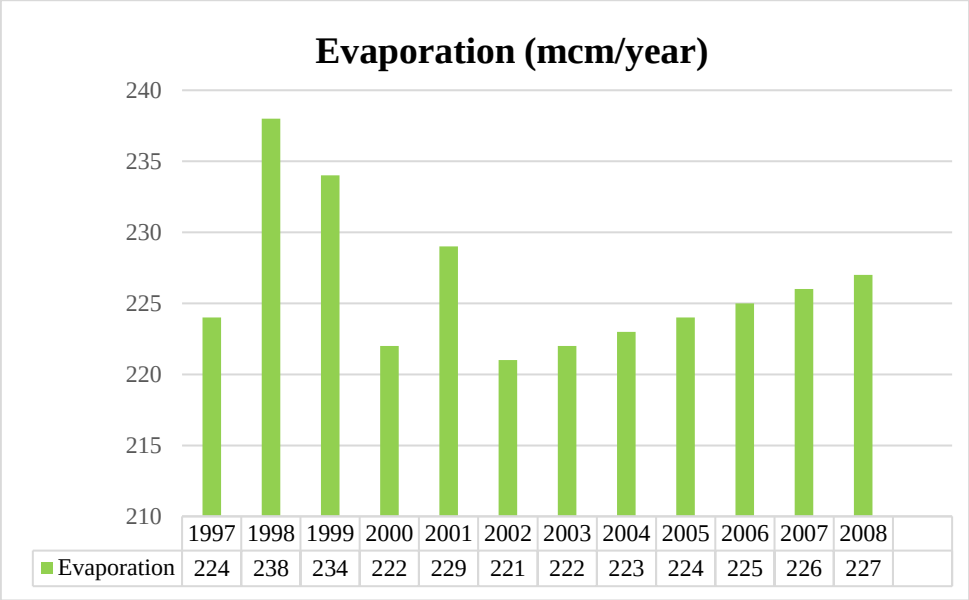

Figure (3-8). The Evaporation of the Sea of Galilee (1997-2008).

(Israel Water Authority, 2012) modified

3.4.4.4 The Water Balance in the Sea of Galilee Basin

The average annual water flowed into Sea of Galilee over the past decades is 610 Mm^3 (for the period (1985-2009) including the Jordan River (415 Mm^3), direct rainfall (65 Mm^3), direct watershed runoff and artificial diversion (70 Mm^3), and springs flowing directly into the lake (55 Mm^3). An average of 240 Mm^3 evaporates every year so that the average annual volume of available water is 370 Mm^3. Most of this volume is pumped out from the lake every year for consumption, while some water occasionally overflows to the Lower Jordan River towards the Dead Sea.

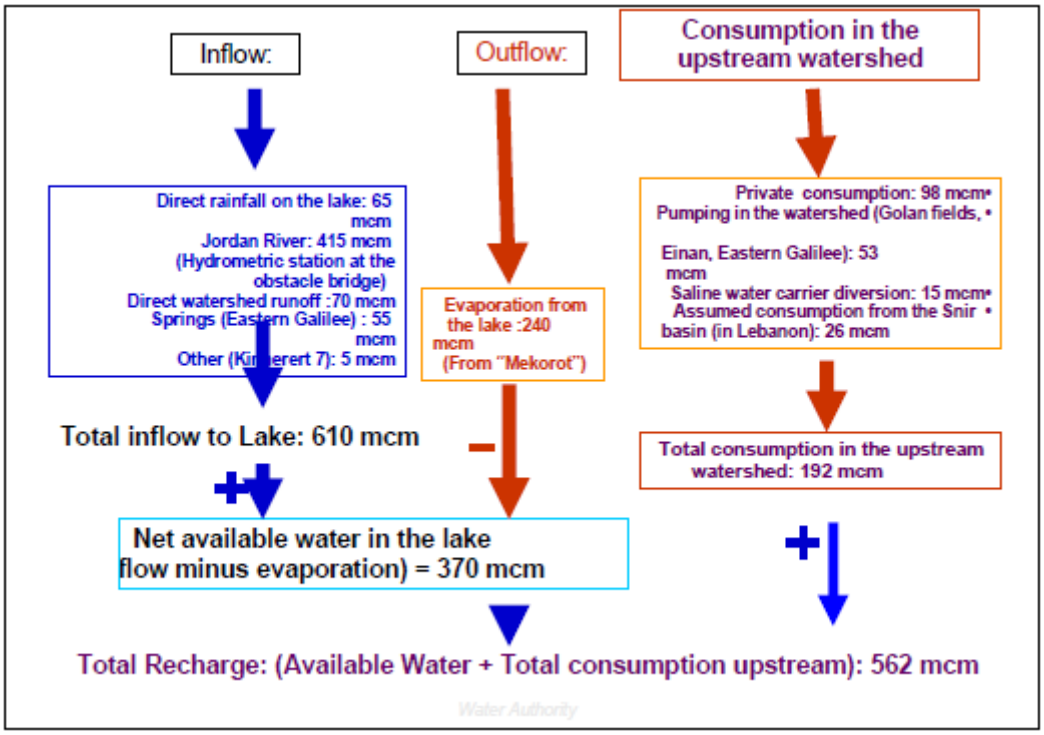

Figure (3-9). Water Balance in the Sea of Galilee Basin

average values for the Period 1985-2009.

(Israel Water Authority, 2012)

3.5 Geological Background of the Sea of Galilee

As with many things in history, geological or otherwise, the Sea of Galilee didn't happen overnight. It took several million years before it formed into its current state. The present Sea of Galilee is a remnant lake that evolved from the ancient water bodies filling the Kinnarot basin northern part of the Jordan Valley amid the Pleistocene–Holocene periods. The Sea of Galilee considers as one of a few lakes that occupied the tectonic depression along the Dead Sea transform, for example, the Pleistocene Lake Amora (Samra), (Neev and Emery, 1967; Stein, 2001).

The salt broke down in the lakes began from the old Sedom brine, and freshwater mixed with the brine reflects the hydrological–climatic conditions in the region that changed from wet to arid during the Quaternary" (Stein, 2001). The various lakes along the Dead Sea–Jordan rift were characterized by distinct salinities. Lake Kinneret, a flow-through water body, was fresher than the southern terminal lakes occupying the Dead Sea basin. This difference is manifested by the abundance of fauna in mid-late Holocene Lake Kinneret; e.g., diatoms, ostracods, and mollusks (cf. Ehrlich, 1985; Pollinger et al., 1986).

4. Materials and Methods

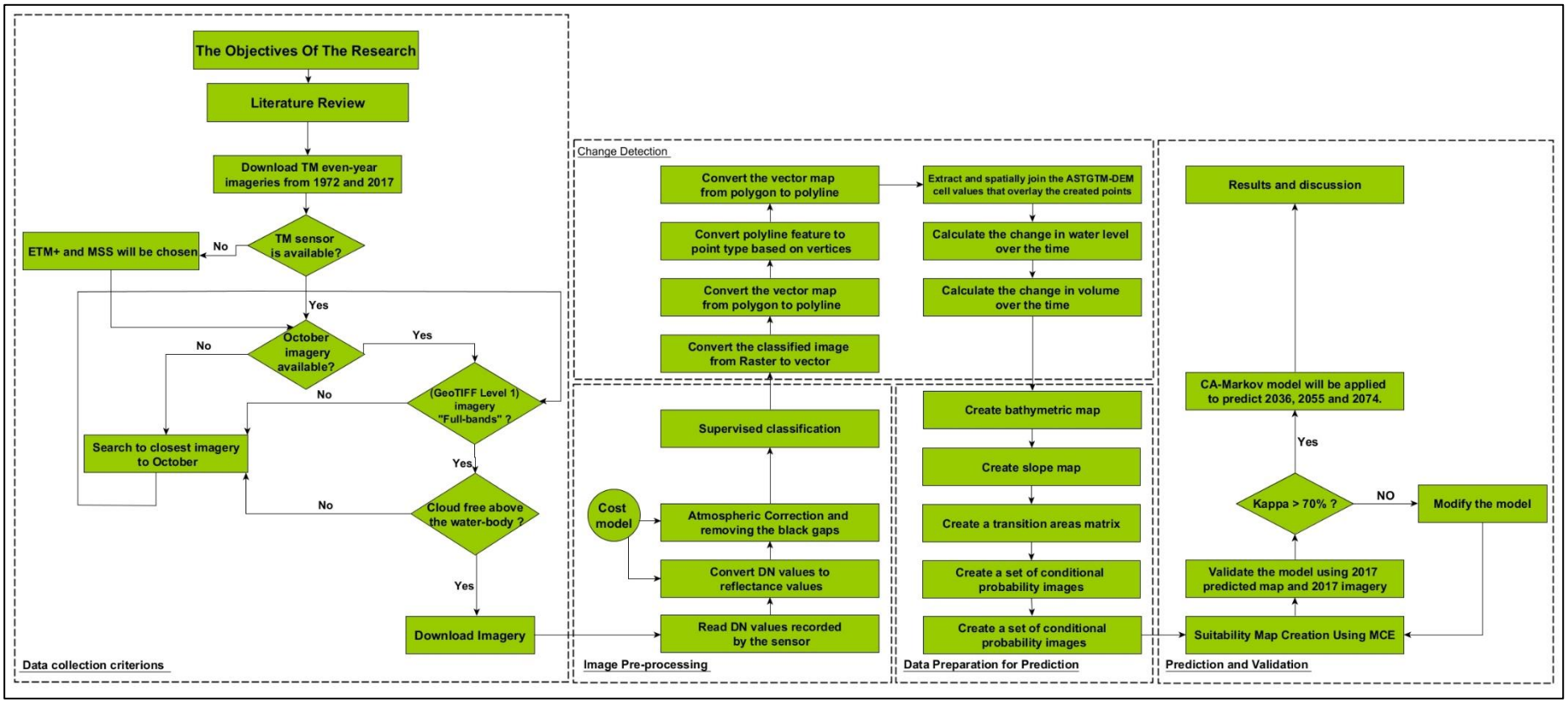

Figure (4-1). The methodology of the research.

(Habboub, 2013) modified

4.1 Overview

In this chapter, the research methodology structure is outlined in sub-elements. At that point, data-gathering criteria are clarified and advocated. From that point forward, image pre-processing and normalization of satellites imageries are represented. Next, the supervised classification process is talked about. Then, change detection analysis portrayed. At long last, prediction and expectation process is clarified in subtle elements.

4.2 Methodology Framework[3]

Figure (4.1) illustrates the methodology followed in this research, which consists of many stages to achieve the aims and objectives of the research as it deals with three principal axes:

1. Mapping the Sea of Galilea area from 1972 to 2017 based on the satellite images.
2. Change detection analysis for the area of sea Galilea from 1972 to 2017.
3. Prediction of the area and the shape of sea Galilea using Remote Sensing and GIS-Based Model: Markov - Cellular Automata.

4.3 Tools used

In order to achieve this methodology, the following software and supporting tools are uses:

- ERDAS Imagine 2015.
- ESRI ArcGIS 10.2.
- IDRISI Selva.
- Excel 2016.

[3] The methodology followed in this research is a combination between many methodologies in previous studies had the same purpose of this research, which detects the changing of a water body through a time [spatiotemporal analysis]. One of these studies was in Palestine to detect the changes of the Dead Sea area, the methodology used in the research give very accurate measurements comparing with the measurements from fieldwork. Very important to say that writer of this research [Adwan Ahmed] contacted with the writer of the Dead Sea research [Habboub Mohammed] and agreed that the study area "Sea of Galilee" is very close to the Dead Sea and both are located under the same circumstances. Based on this research will follow the same methodology framework to solve the research problem and achieve its goals.

4.4 Data Collection and Acquisition

In this study the satellite images data was acquired at irregular periods between 1972 and 2017, covering a period time of 45 years where the seven-satellite imagery of good-quality was obtained and covered the study area.

As it discussed before, this research following the same criterions of data collection, which is used to detect the changes in the Sea of Galilee area in Palestine. Figure (4-2).

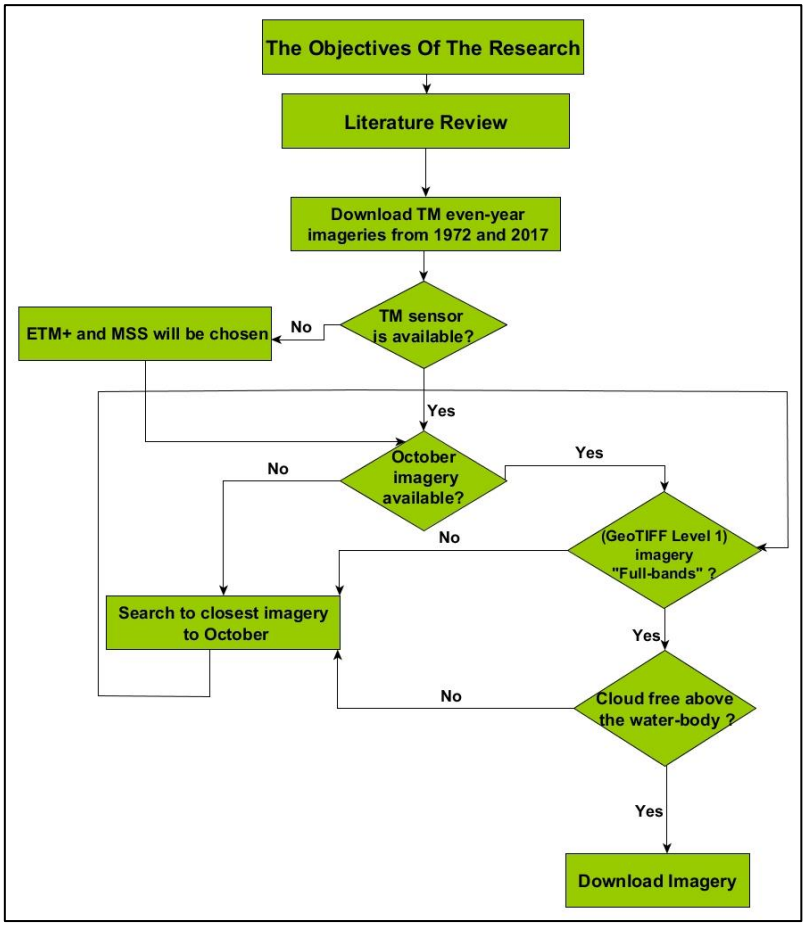

Figure (4-2). The criterions of data collection in this research.

(Habboub, 2013)

"The first criterion in data collection is to download even-year imageries including the oldest and newest Landsat archived imageries, 1972 and 2017. The second criterion is to give TM imagery a priority over ETM+ and/or MSS since TM sensor lifespan is more extended than ETM+ (approx. 20 years) so consistent data will be collected. In contrast, Landsat ETM+ imageries have the problem of the Scan Line Corrector Failure (SLCoff) which presented in black gaps. Moreover, Landsat ETM+ has the only advantage of the panchromatic band existence. However, the resolution in the multispectral bands in ETM+ is the same of TM, 30

m. The third criterion is reducing the pre-processing by downloading all imageries in the same date, the month of October is chosen to avoid clouds in the scene. In case of October imagery does not match the listed criteria, the closest imagery to October matching the listed criteria will be downloaded. The fourth criterion is downloading full-bands imagery in a Geostationary Earth Orbit Tagged Image File Format (GeoTIFF). In case of GeoTIFF does not available, the closest imagery to October matching the listed criteria will be downloaded. The fifth criterion is downloading free clouds scenes, at least above the water-body. In case of cloud existence above the water-body, the closest imagery to October matching the listed criteria will be downloaded, all the data downloaded from U.S. Geological Survey (USGS) website" (Habboub, 2013). At the end the final satellite images used in this research listed in Table (4-1).

The Advanced Spaceborne Thermal Emission and Reflection Radiometer Global Digital Elevation Model (ASTGTM-DEM) for 2011 is downloaded from (USGS) too for creating a slope map which is an essential element for the prediction.

Table (4-1). Satellite images characteristics in this research.

Acquisition Date	Satellite	SENSOR	Acquisition Date	Satellite	SENSOR
1972-09-15	LANDSAT 1	MSS	2002-10-18	LANDSAT 5	TM
1975-06-29	LANDSAT 2	MSS	2004-08-28	LANDSAT 5	TM
1984-09-06	LANDSAT 5	TM	2006-10-05	LANDSAT 5	TM
1986-09-28	LANDSAT 5	TM	2008-07-22	LANDSAT 5	TM
1988-12-30	LANDSAT 4	TM	2010-12-03	LANDSAT 5	TM
1990-08-30	LANDSAT 4	TM	2014-09-17	LANDSAT 7	ETM
1992-08-11	LANDSAT 5	TM	2017-10-27	LANDSAT 7	ETM
2000-10-04	LANDSAT 5	TM			

Source:(Habboub, 2013) modified

4.5 Image Pre-processing

The aim of the image pre-processing that all images should appear as if they were acquired from the same sensor. It is also essential procedure to make the image more clearly and suitability to obtain the best results for image classification that requires many initial processing steps to improve the image, for example, radiance calibration, atmospheric correction, geometric correction and image enhancement. Akhter, 2006. Figure (4-3) shows the Image Pre-processing flowchart that used in the research.

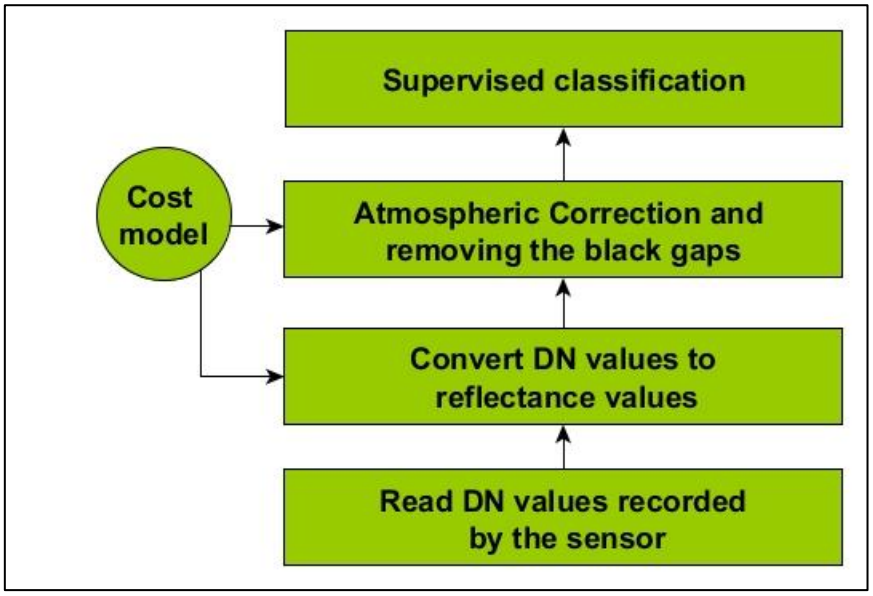

Figure (4-3). The Image Pre-processing flowchart.

4.5.1 Atmospheric Correction

This step is reducing the effects of atmospheric conditions on the image values. The value recorded at a given pixel includes not only the reflected radiation from the surface but the radiation scattered and emitted by the atmosphere as well (path radiance) as is shown below.

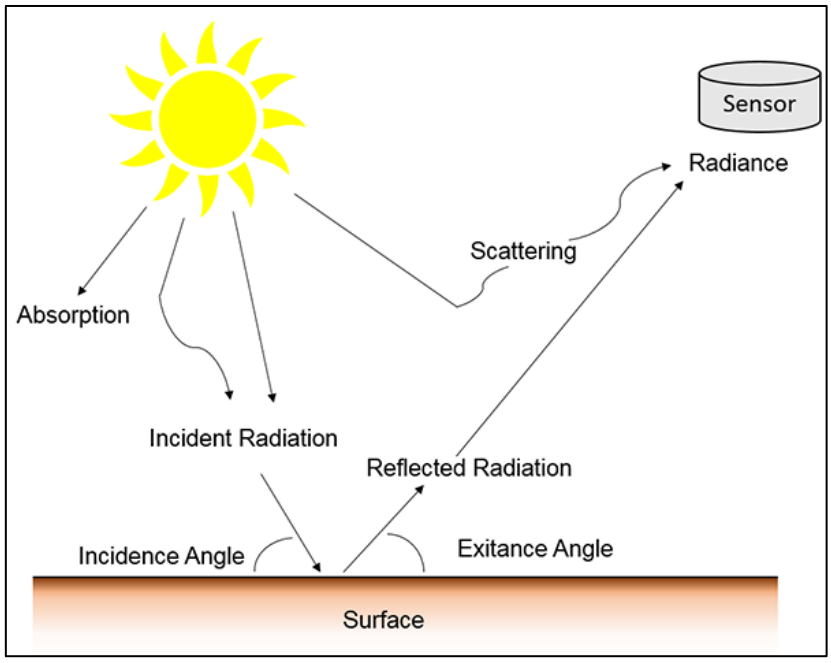

Figure (4-4) Atmospheric effects on the satellite sensor.

(GPS 216, 2018)

At that point, removing atmospheric effects are finished using Dark Object Subtraction (DOS) technique, which expels the impacts of scattering from the image data.

Dark objects have little to no reflectance observed by the scanner, so the DN values represent path radiance or the influence of atmospheric effects, by subtracting the value of the DN in each band the artefact can be removed.

In this research and by using the Cosine of the Solar Zenith Angle (COST) method, the atmospheric correction using DOS is done, this technique included in the Chavez (1996) COST method and many types of research before like (Wen, 2008) (Ramsey, 2010) Figure (4-5-C).

4.5.2 Radiance calibration

The digital sensors of the satellites record the intensity of electromagnetic radiation (ER) from each point viewed on the Earth's surface and store it as a digital number (DN) for each spectral band.The exact range of DN that sensor mange depends on its radiometric resolution. For example, a sensor such as Landsat MSS measures radiation on a 0-63 DN scale while Landsat TM measures it on a 0-255 scale (Green, et al., 2000).

In this research, radiance calibration is required since it is useful in general for comparing across sensors or comparisons across time (Green, et al., 2000). This procedure used in this research to convert DN to absolute radiance values that are imperative for comparative analysis of images taken by different sensors [MSS, TM and ETM+ imagery].

In this step converting the atmospherically corrected reflectance (at the sensor) to reflectance of pixels at the Earth's surface is done[4] figure (4-5-B) using COST model again which is based on this following equation (Ramsey, 2010) (Habboub, 2013).

[4] The satellite images of the Sea of Galilee before and after image pre-processing are included in the annex [The attached CD]

$$\rho_{Band\ N} = \frac{\pi((L_{band\ N} \times Gain_{band\ N} + Bias_{band\ N}) - (H_{band\ N} \times Gain_{band\ N} + Bais_{band\ N})) \times D^2}{E_{band\ N} \times (COS((90 - \theta) \times \frac{\pi}{180}))}$$

Where:

$\rho_{Band\ N}$ = Reflectance for Band N.

$Gain_{bandN} = \frac{L_{max\ \lambda}}{254} - \frac{L_{min\ \lambda}}{255}$.

$Bais_{bandN} = L_{min\ \lambda}$.

$L_{max\ \lambda}$: The spectral radiance that is scaled to (QCALMAX=255), watts × (m^2 * ster * μm) $^{-1}$.

$L_{min\ \lambda}$: The spectral radiance that is scaled to (QCALMIN=254), watts × (m^2 * ster * μm) $^{-1}$.

$L_{band\ N}$ = Digital Number for Band N.

$H_{band\ N}$ = Digital Number representing Dark Object for Band N.

$E_{band\ N}$ = Solar Irradiance for Band N, watts/ (m^2 * μ).

θ = Sun Azimuth.

D' =Normalized Earth-Sun distance, see equation 4-2.

$$D'^2 = (1 - 0.01674\ COS\ (0.9856\ (JD - 4)))^2$$

(Ramsey, 2010)

*"*JD is the Julian Day (day number of the year) of the image acquisition"* (Habboub, 2013).

Table (4-2). The characteristics of Landsat imagery 2008 in COST model.

Band	DNmin	S. Elev.	1%	H Lmin	L1%	Lhaze	(Lmax-Lmin)/255	L. Min	L. Max	S-E Dist.	S. Exo.	S. Elev.
1	71	63.07	0.01	4.1267	0.4798	3.6469	0.0602	-0.15	15.21	1.0159	195.7	63.07
2	28	63.07	0.01	3.0097	0.4484	2.5613	0.1175	-0.28	29.68	1.0159	182.9	63.07
3	19	63.07	0.01	1.4112	0.3817	1.0295	0.0806	-0.12	20.43	1.0159	155.7	63.07
4	11	63.07	0.01	0.7460	0.2567	0.4893	0.0815	-0.15	20.62	1.0159	104.7	63.07
5	5	63.07	0.01	0.0170	0.0538	-0.0367	0.0108	-0.037	2.719	1.0159	21.93	63.07
7	3	63.07	0.01	0.0021	0.0183	-0.0162	0.0057	-0.015	1.438	1.0159	7.452	63.07

The columns Lhaze, S-E Dist., and S. Elev. used as primary inputs in COST model file in ERDAS.

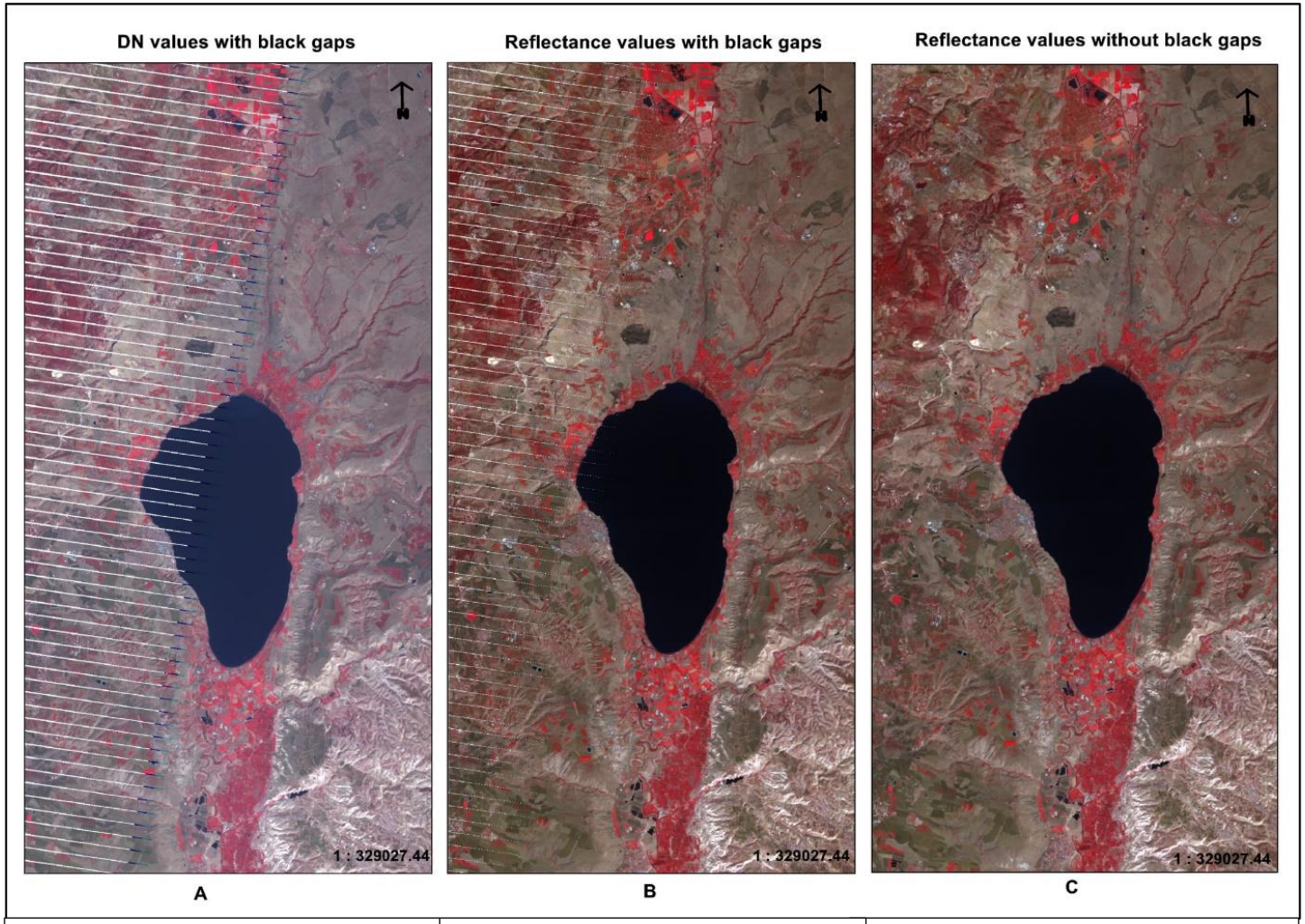

The Sea of Galilee before Image Pre-processing with DN values and black gaps	Atmospheric corrected reflectance values with black gaps, converted from spectral radiance	Reflectance values without black gaps, using cost model

Figure (4-5). Image Preprocessing. The satellite image of the Sea of Galilee in 2014.

4.6 Image Classification

One of the most significant applications of satellite remote sensing is to detect changes in land cover to discern those areas on digital images that change features of interest between two or more dates (Dewidar & Frihy, 2007).

In this research, supervised classification is used in the mapping of sea body and the land around through using training sites based on Areas of Interest (AOI), so the spectral signatures of classes are developed, and then the software assigns each pixel in the image to the type to which its signature is most similar. Figure (4-6) summarizes the steps performed for supervised classification.

In order to classify the images based on these signature files. Each pixel in the study area has a value in each of the Blue, Green, Red, Near Infrared, Middle Infrared, Thermal Infrared, and another Middle Infrared bands. The pixel is then assigned to the type that has the most similar signature.

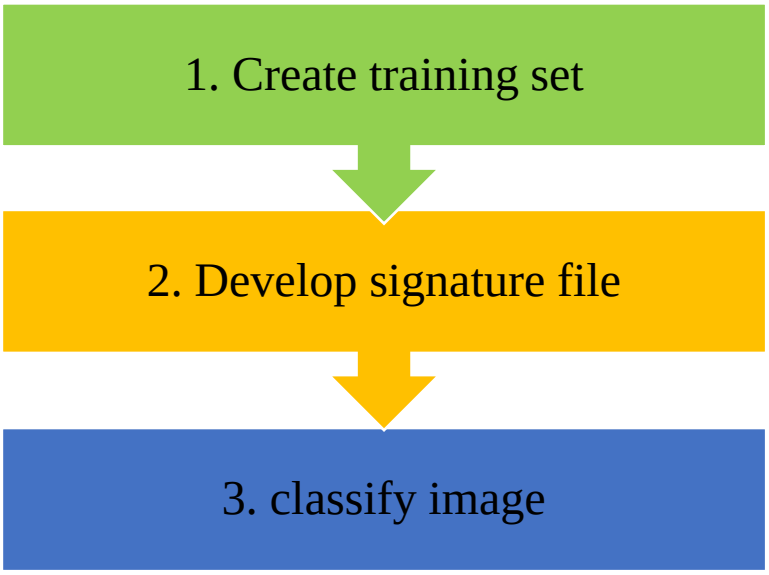

Figure (4-6). Steps for supervised classification.

4.6.1 Supervised Classification

The primary point of the image classification procedure is to categorize all pixels consequently in an image into classes. To classify the images agreeing on these signature files. Every pixel in the study area has a digital value/number in every one of the Blue, Green, Red and other bands then the pixel is assigned to the class compose that has the most comparable signature figure (4-7).

4.6.2 Evaluate the signatures files

It is critical to evaluate how similar are the signatures files to each other before the classification; several different statistical techniques can be used for the evaluating, for example, minimum distance, maximum likelihood classifier, and parallelepiped classifier.

In this research, the Maximum Likelihood Classifier (MLC) method is used for image classification using training sites as it recommended by (Jesús D. Chinea, 2006).

In The Maximum Likelihood Classifier, the distribution of reflectance values in a training site described by a probability density function developed based on Bayesian statistics. This classifier assesses the likelihood that a given pixel will belong to a category and classifies the pixel to the category with the most noteworthy likelihood of enrolment (Jesús D. Chinea, 2006).

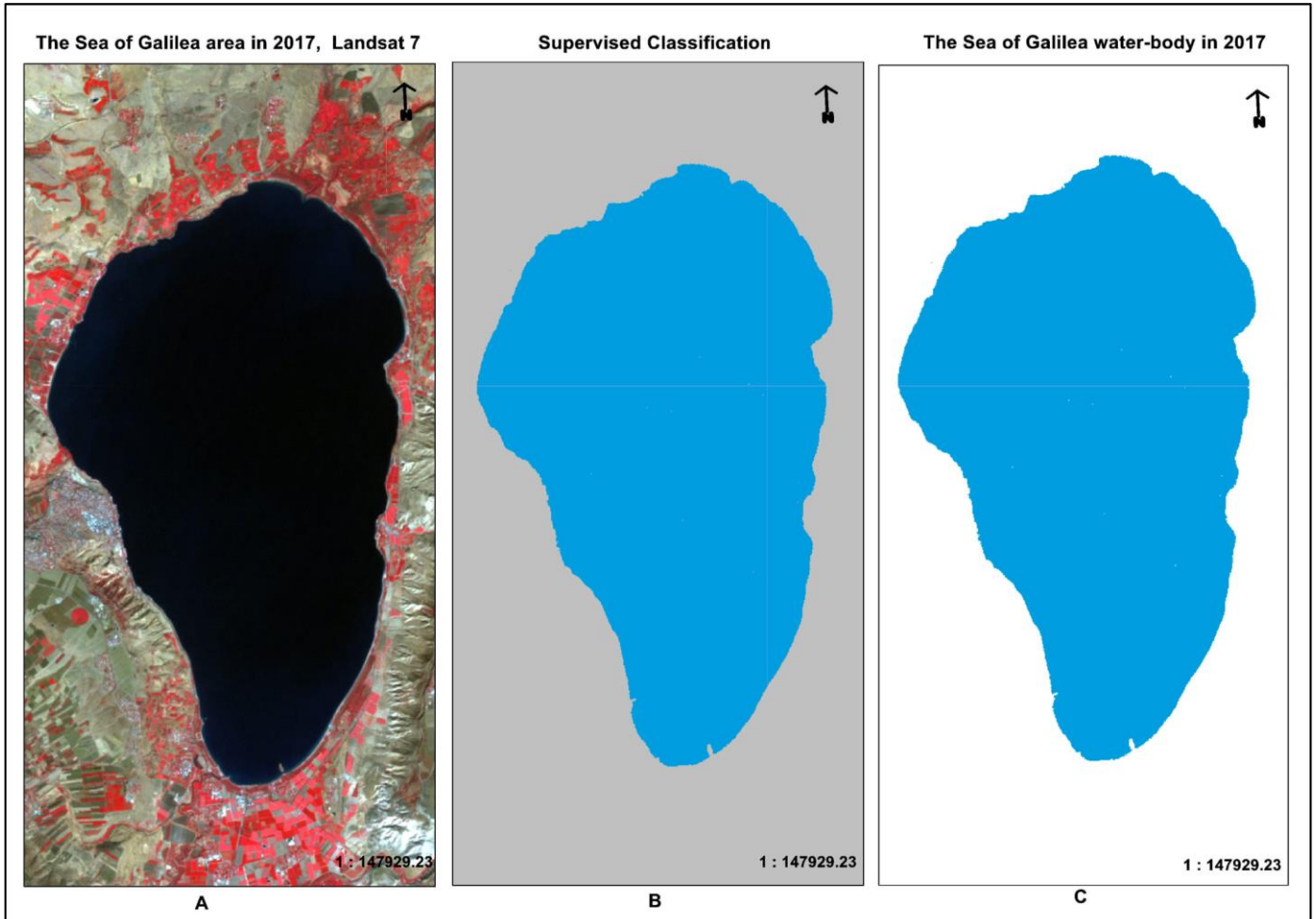

Imagery of the Sea of Galilee in 2017	**Supervised Classification of the imagery in 2017, the water class (blue) and the land class (gray)**	**The water-body of the Sea of Galilee in 2017 as a vector data type**

Figure (4-7). Supervised classification and vectorization.

4.7 Change Detection Analysis

In this step, detecting and calculating the changes in area, shape, water level and volume of Sea of Galilee over the time study are completed by used the ERDAS and ArcGIS toolbox.

Assessment the volume of a watershed can be possible by thinking about watershed as a bowl so its volume can be found by delineating two things Akin et al. (2013) and Cooley (2013):

1) A plane across its rim and its curved inner surface.
2) A capping surface can be built by connecting a set of points situated along the divide, while the inward surface is the modern topography represented by the ASTGTM-DEM. The volume is merely the difference between the cap elevation and topography

With a specific end goal to follow this technique to calculate the volume of Sea of Galilee water body, it needs a few changes since the ASTGTM-DEM does not give information about the bathymetry shape of Sea of Galilee because of the water existence. In this way, the change in volume is measured as opposed to measuring volume itself by using remote sensing images and ASTGTM-DEM. Figure 4-9 lists the methodology followed to analyse the spatial changes over time. As a matter of first importance, classified imageries will be converted from a raster to a vector format. Then, vectorized maps are converted from polygon type to polyline type in order to get the Sea of Galilee water shoreline contour as shown in figure 4-10-B, Next, the shoreline is converted to point type as shown in figure 4-10-C. From that point forward, the converted points are joined spatially with ASTGTM-DEM to assign the elevation of the ASTGTM-DEM cell to that point which overlaid it. At long last, the elevation of the Sea of Galilee surface is calculated by averaging the assigned elevation values in a converted point layer. Figure (4-8) shows the change detection flowchart. Figure 4-9 shows the results of the first three steps from the flowchart.

Figure 4-10 illustrates the change detection model, which is built in the model builder in ArcGIS. The model consists of two inputs, blue ellipses, six operations, umber rectangles and six outputs one of them is the result, green ellipses. The inputs are the Sea of Galilee polygon in a vector format and ASTGTM-DEM while the operations are the tools used in converting polygon to points, spatially joining, calculating area of the water body and averaging the assigned elevation values in a converted point layer (Habboub, 2013).

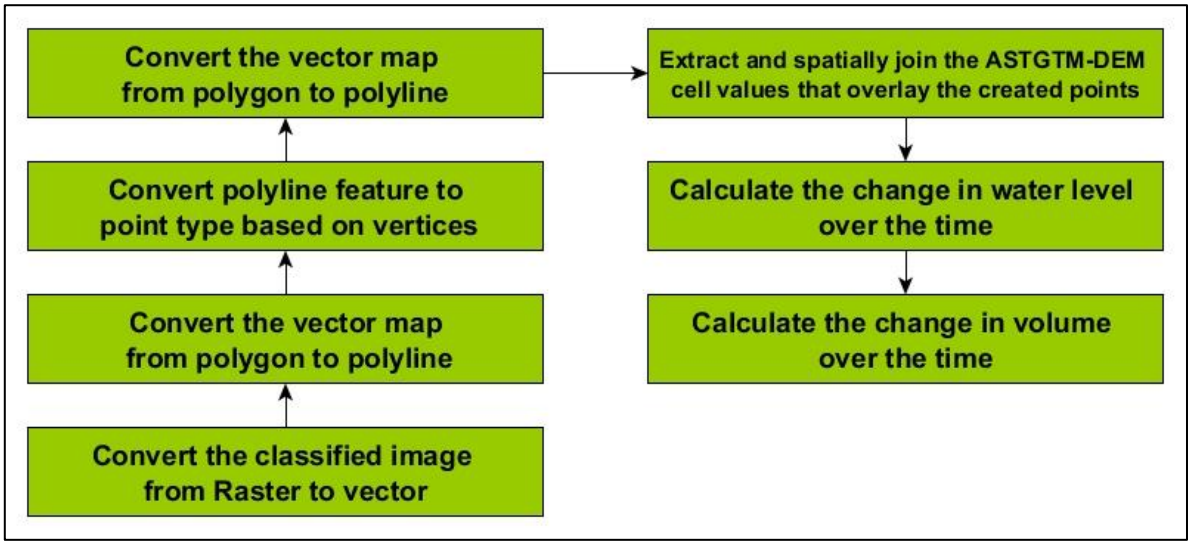

Figure (4-8). Change detection flowchart.

(Habboub, 2013)

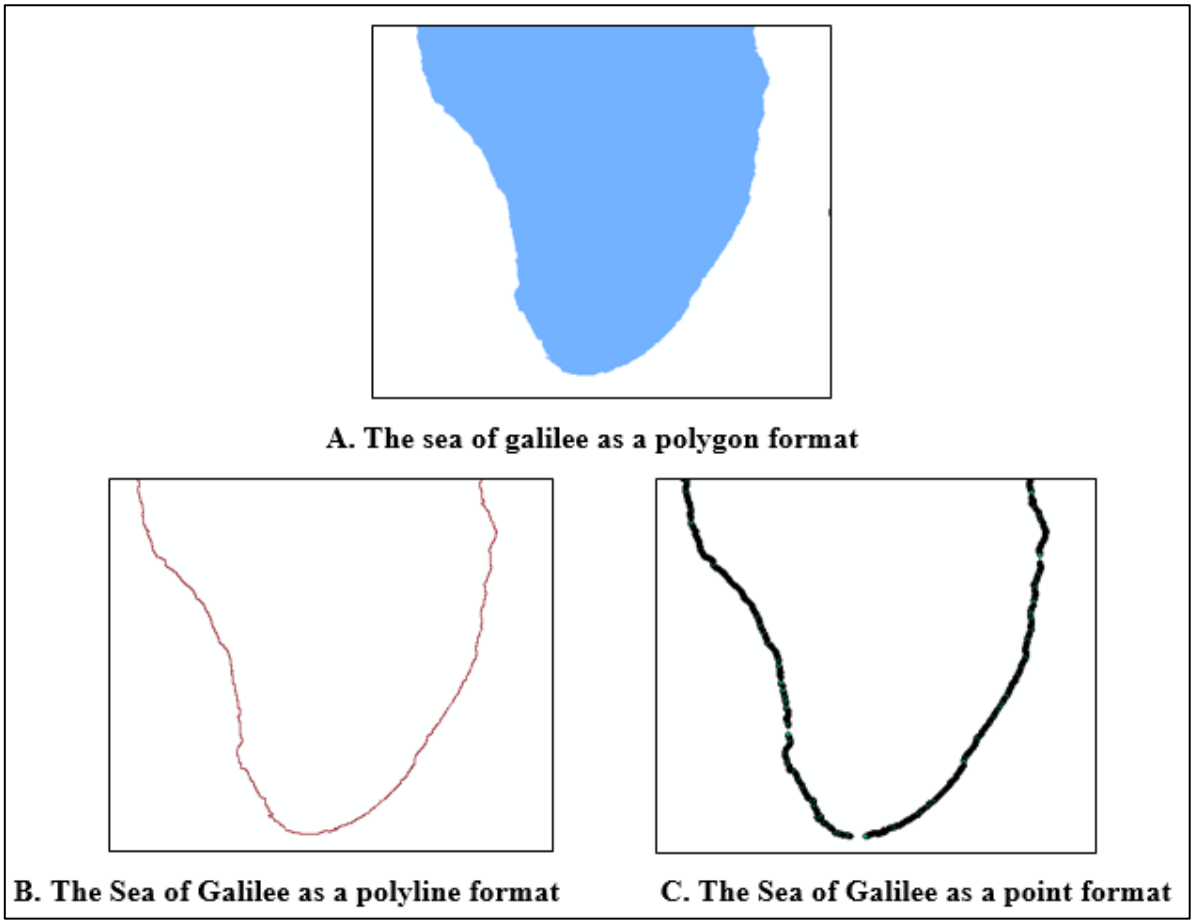

Figure (4-9). The sea of Galilee as a polygon, polyline and point format.

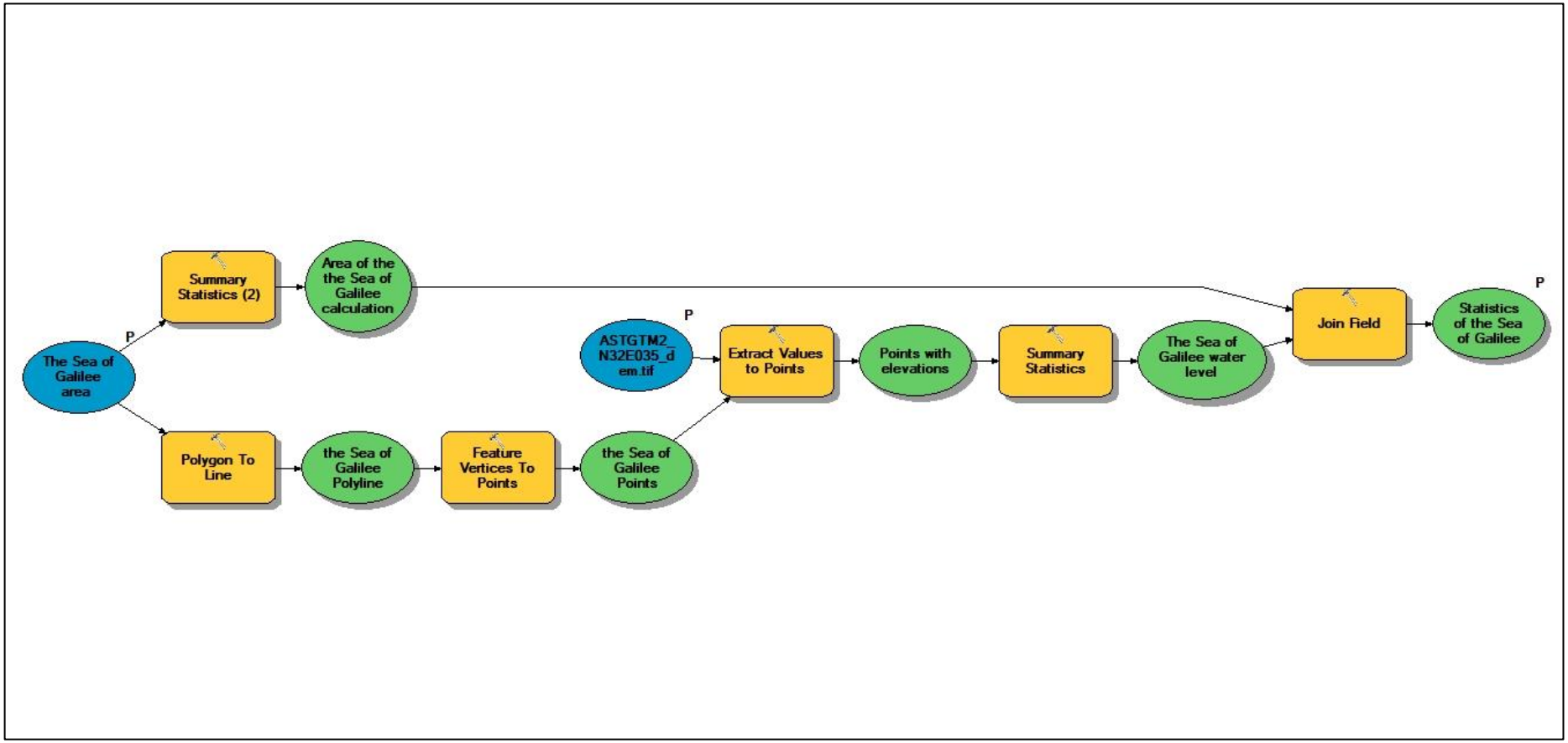

Figure (4-10). Change detection model in ArcGIS.

(Habboub, 2013)

4.8 Data preparation for prediction

This part of the research can be described as it shown in the figure below.

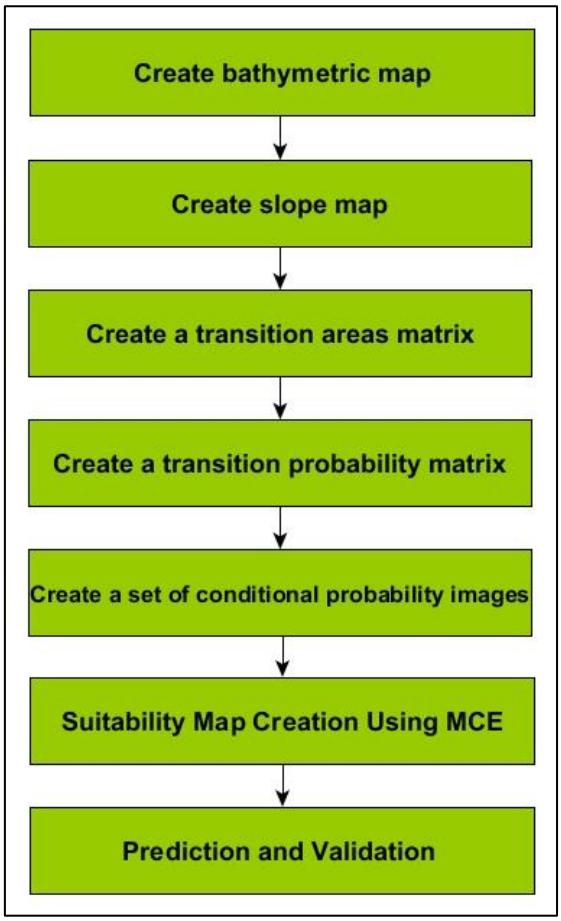

Figure (4-11). Data preparation for prediction flowchart.

(Habboub, 2013) modified

4.8.1 Bathymetric map

The bathymetric map is one of the fundamental criteria for prediction and expectation. Active remote sensing technologies, for example, Light Detection and Ranging (LiDAR), SONAR (Sound Navigation and Ranging) and ALB (Airborne Laser Bathymetry), have been fiercely used to study the water-secured region. Despite the fact that these advancements can give covering, high precision and have a better capacity for bathymetric mapping, however, these procedures are extremely costly (Jagalingam et al., 2015). All the above strategies are costly. In this manner, with the benefit of bigger scope and much lower cost, water profundity estimation with satellite picture is still of significant worth.

The essential rule of this retrieval of bathymetric data from satellite imagery is that when the light goes through water, it winds up attenuated by interaction with the water column. Deep

areas seem dim on the image since the water absorbs much of the reflected light (Australian Journal of Basic and Applied Sciences, 2014). Shallow zones seem lighter on the picture since less light reflected from the seabed is absorbed in the passage through the water column

The estimation of bathymetry can be required to be the best with Landsat TM information since that sensor identifies visible light from a wider portion of the visible spectrum, in more bands, than other satellite sensors. Landsat bands 1, 2 and 3 are overall valuable in estimating bathymetry, so too is band 4 in exceptionally shallow (<1 m), clear water over bright sediment (where bands 1-3 have a tendency to be saturated). Bands 5 and 7 are wholly consumed by even a couple of centimetres of water and ought to along these lines be expelled from the picture before bathymetric calculations are performed. Figure (4-12) demonstrates the schematic representation of Depth of Penetration (DOP); the DOP of band 1 is the biggest (from 20- 25m) in clear water, at that point DOP of band 2, 3 and 4 which are around 15, 5 and 1m (Green, et al., 2000) (Habboub, 2013).

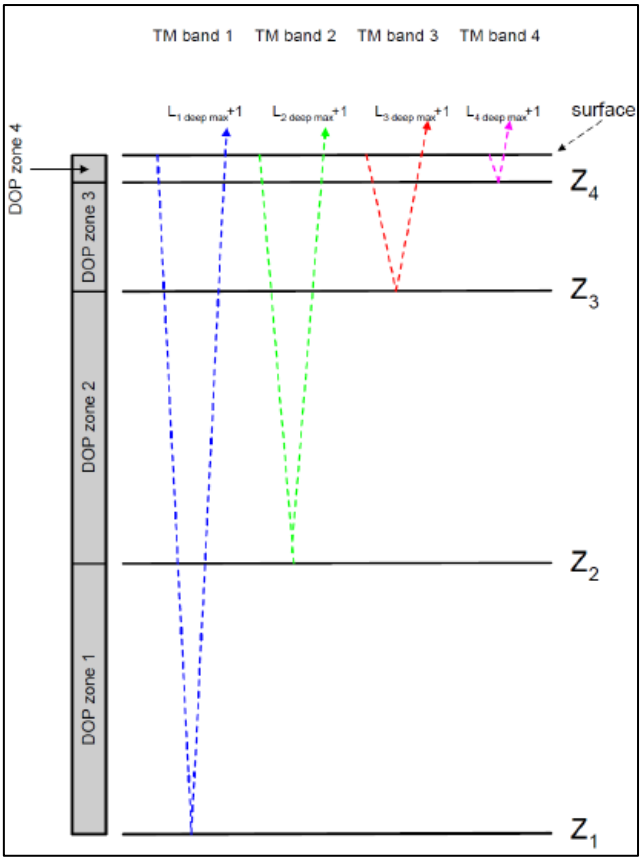

Figure (4-12). DOP zones of TM bands 1,2,3 and 4.

(Green, et al., 2000)

To make bathymetric zones map represents an exceptionally bathymetric map, the next advances must be refined one by one: First, discovering the average DN values of profound

water pixels in the blue, green, red and infrared bands of the 2010 Landsat TM image the results was in Table (4-3). That shows the maximum, minimum and average values for the first four bands.

Table (4-3). Maximum, Mean and Minimum DN-Value in TM Band 1, 2, 3 and 4 over a deep-water area.

	Band 1	Band 2	Band 3	Band 4
Max DN of deep water	58	29	22	16
Min DN of deep water	52	20	17	11
Mean DN of deep water	56	27	19	14

(Landsat 5, TM, 2010-12-03)

Second, creating the decision tree used to delineate the 5 exclusive DOP-zones (Green et al., 2000) clarifies that knowing the maximum DN values over deep water gives us a baseline. This baseline is utilized to decide the depth at pixels higher than background reflectance from the seabed. For every waveband, if DN values are higher than the maximum deep water values then it is assumed that the sensor is detecting light reflected from the seabed but in this study, the average values are used instead of maximum values which represent more convenient results and better visualization since when using maximum values the results often show that water-body is very deep which is not correct. The results of this step are the decision tree, which listed, and shown in Table (4-4) then modeled and layout in ERDAS. Figure (4-13) and figure (4-14).

Table (4-4). Decision tree used to delineate the 4 exclusive DOP-zones.

Landsat 5 TM	Band	1	2	3	4	DOP-zones
If DN value of Pixel		<=56	<=27	<=19	<=14	very deep
If DN value of Pixel		>56	<=27	<=19	<=14	deep
If DN value of Pixel		>56	>27	<=19	<=14	medium
If DN value of Pixel		>56	>27	>19	<=14	shallow
If DN value of Pixel		>56	>27	>19	>14	very shallow

(Habboub, 2013) modified

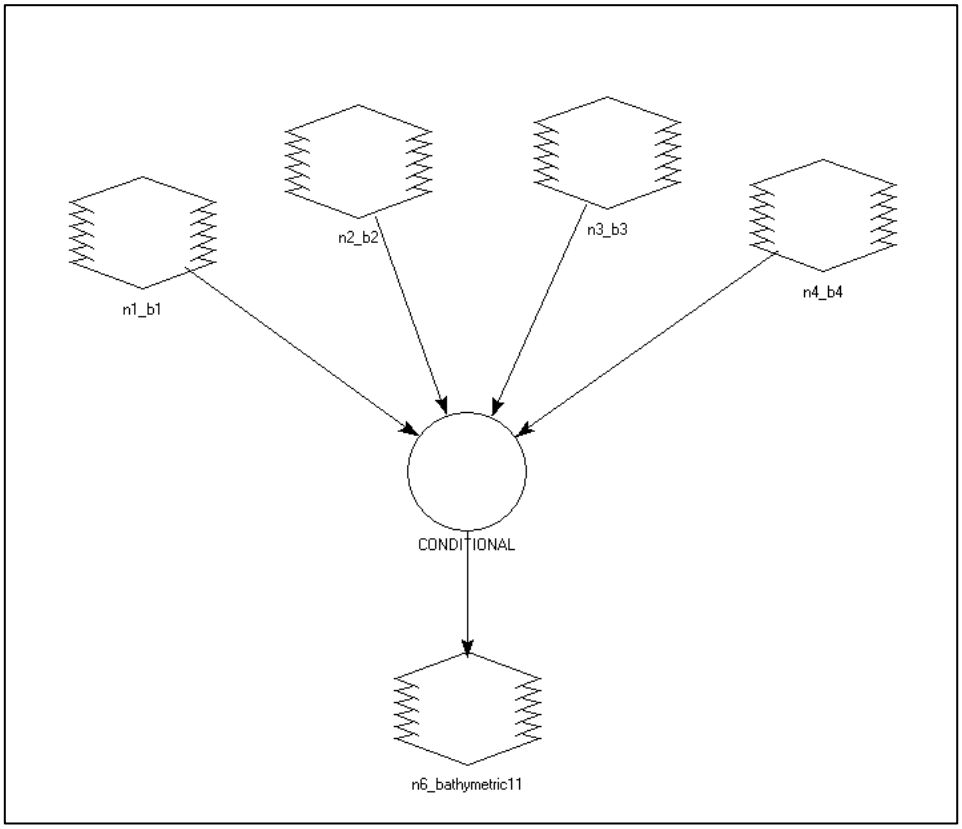

Figure (4-13). Bathymetric map model in ERDAS.

(Habboub, 2013) modified

The equation code used in the bathymetric map model in ERDAS is listed down.

CONDITIONAL {

($n1_b1 <= 56 AND $n2_b2 <= 27 AND $n3_b3 <= 19 AND $n3_b3 <= 14) 0,

($n1_b1 > 56 AND $n2_b2 <= 27 AND $n3_b3 <= 19 AND $n3_b3 <= 14) 63,

($n1_b1 > 56 AND $n2_b2 > 27 AND $n3_b3 <= 19 AND $n3_b3 <= 14) 127,

($n1_b1 > 56 AND $n2_b2 > 27 AND $n3_b3 > 19 AND $n3_b3 <= 14) 191,

($n1_b1 > 56 AND $n2_b2 > 27 AND $n3_b3 > 19 AND $n3_b3 > 14) 255},

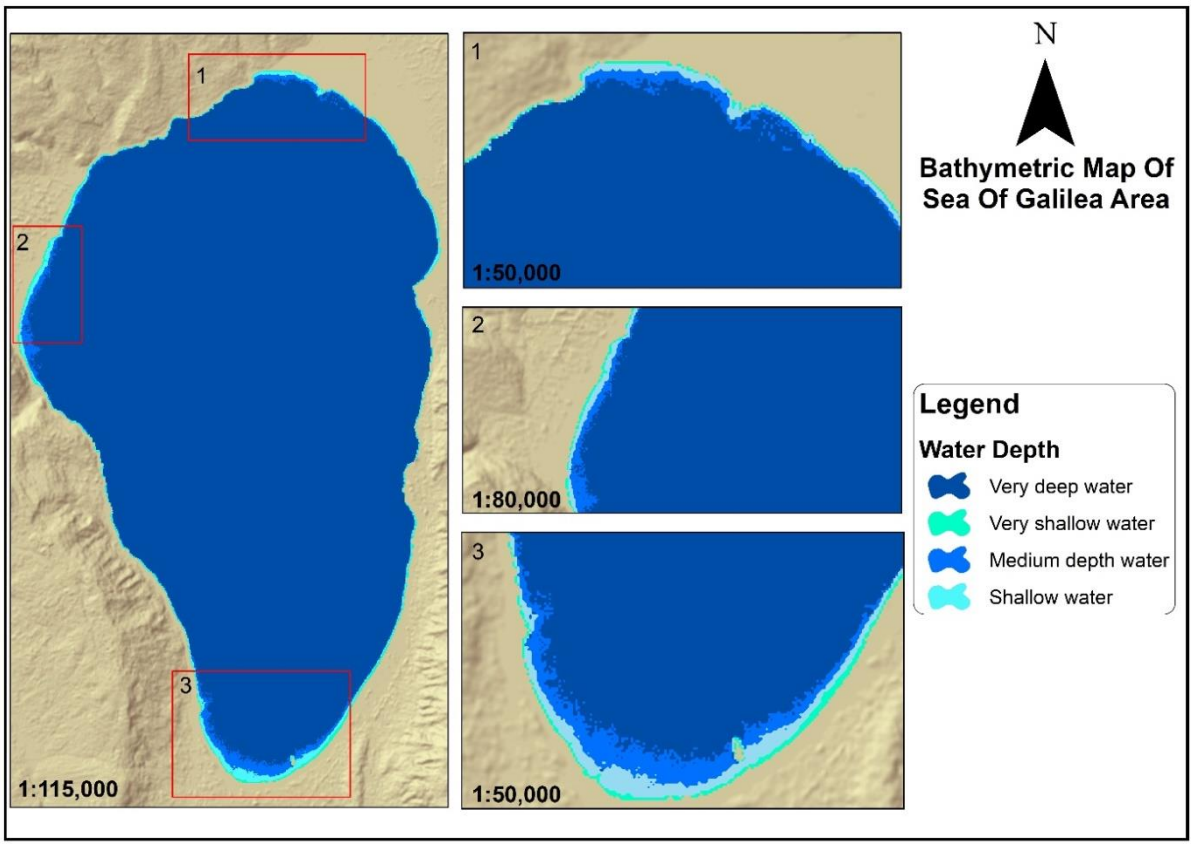

Figure (4-14). Bathymetric map of the study area based on equation code.

4.8.2 Slope map

Slope map one of the basic criteria map for prediction. The formation of the slop map a forward procedure using ArcGIS software spatial analyst extension. However, the idea of making slope map by computing the distinction between DN which saved in a ASTGTM-digital elevation model cell and the minimum value on the eight adjacent cells in that ASTGTM-DEM (Habboub, 2013). At that point, the computed contrast is isolated by the cell size of ASTGTM-DEM. This procedure is rehashed for each cell in ASTGTM-DEM to make the slope map (Habboub, 2013). Figure (4-15) represents ASTGTM-DEM and slope maps.

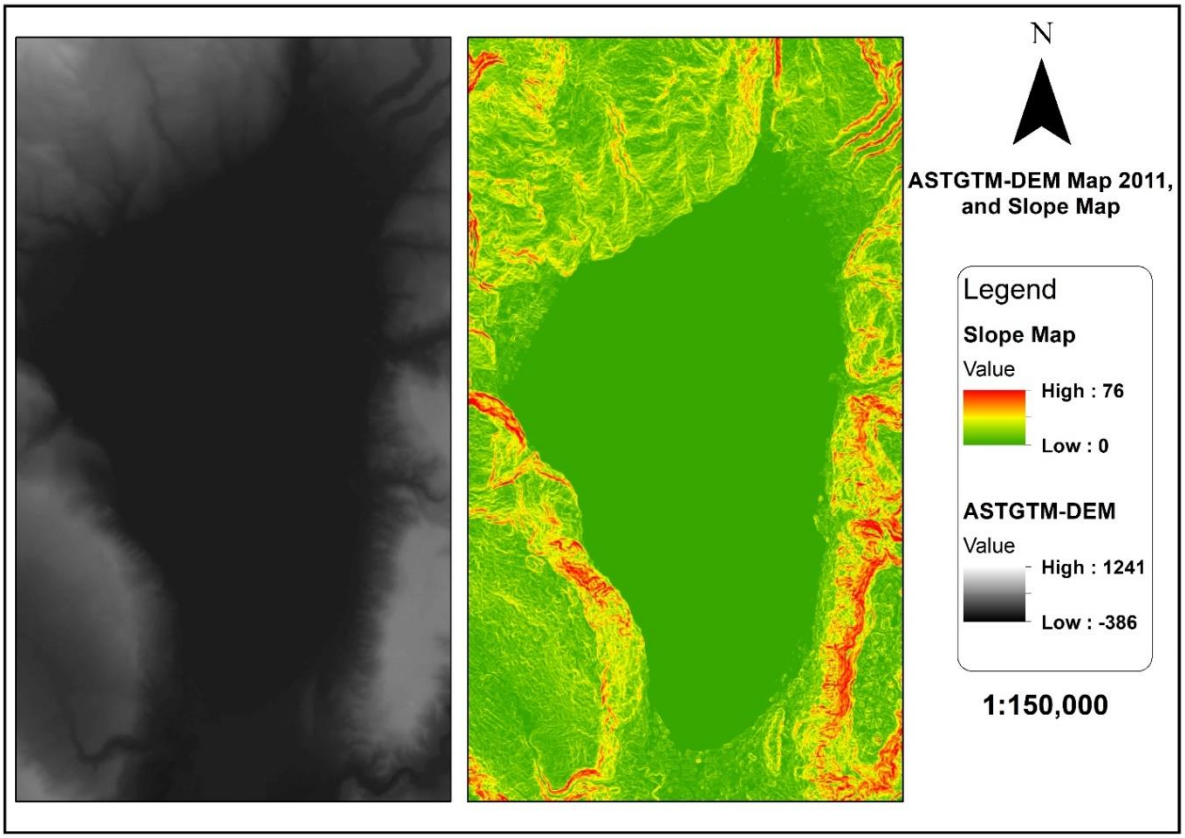

Figure (4-15). ASTGTM-DEM and Slope Map.

4.8.3 Suitability Map Creation Using MCE

"So as to utilize Cellular Automata, a suitability map for each class is considered as a pre-requirement. Suitability maps are acquired using Multi-Criteria Evaluation by combining the information from several criteria to form a single index of evaluation (Eastman, 2012*). A weight linear combination equation –Equation 4-4- is used to obtain suitability map for Sea of Galilee area*

$$S = \sum_{i=1}^{n} W_i C_i \prod_{i=1}^{n} r_i$$

where

S*: Is the suitability map*

W_i*: Weight for a criteria i*

C_i*: Criteria for suitability*

r_i*: Restriction*

By applying weights to each rated factor, the suitability map of Sea of Galilee Area was developed using three maps; the bathymetric map, the probability of classes map derived from Markov process and the slope map derived from ASTGTM-DEM. Table (4-5) illustrates the final weights for each rated map criteria for each suitability map.

Table (4-5). The final weights for the suitability map.

Suitability map for water class			
	i = 1	*i = 2*	*i=3*
C_i: Criteria for suitability	*Bathymetric zones map rated from 0.1 to 1 as very shallow to very deep water respectively.*	*The water class probability map of Sea of Galilee Area derived from Markov process.*	*Slope map derived from ASTGTMDEM map rated from 0.1 to 1 as the highest slope to the lowest slope respectively.*
W_i: weight for a criterion i	*34%*	*33%*	*33%*
r_i: Restriction	*Area boundaries*		
Suitability map for the land class			
	i = 1	*i = 2*	*i=3*
C_i: Criteria for suitability	*Bathymetric zones map rated from 0.1 to 1 as deep to very shallow water respectively*	*The land class probability map of Sea of Galilee Area derived from Markov process.*	*Slope map derived from ASTGTMDEM map rated from 0.1 to 1 as the lowest slope to the highest slope respectively.*
W_i: weight for a criterion i	*34%*	*33%*	*33%*
r_i: Restriction	*Very deep water*	*Area boundaries*	

Adopting the ArcGIS to predict the area of Sea of Galilee a model has been constructed, see Figure 4 -18 to create the suitability map for water/land class using MCE. The model comprises of three inputs, blue ellipses, four tools, umber rectangles, and four outputs one of them is the derived suitability map. The inputs are the conditional probability map, the bathymetric map and slope map, reclassification tools and weighted overlay tool. Figure (4-16) shows the model in ARC GIS" (Habboub, 2013).

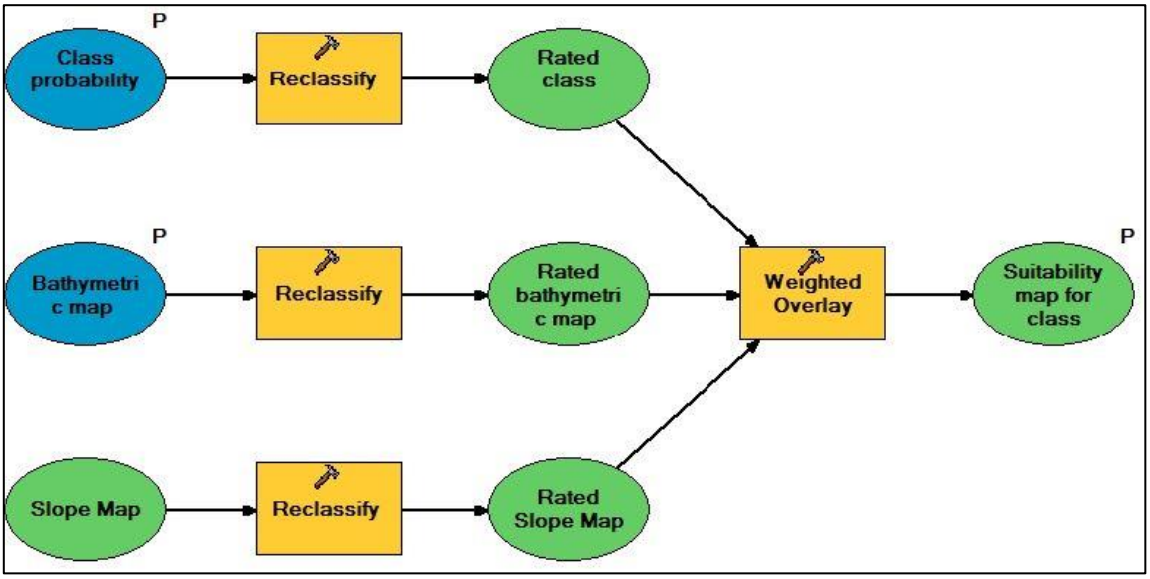

Figure (4-16). Suitability map model.

(Habboub, 2013) modified

4.8.4 Prediction and Validation

Utilizing the gained information carried out by the Markov chain analysis, the predicting model will be applied again to predict the shape and the area of the Sea of Galilee from imagery captured in the time of 1998 and 2017 to a future but first of all the Sea of Galilee map in 2017 will be predicted and compared with the real classified map 2017 using the validation, which provides a method to measure agreement between two categorical (integer or byte) images, a "comparison" map and a "reference" map. The standard Kappa Index will be used and other spatial-statistical parameters. (The model can be valid if Kappa Index > 70 %) (Wen, 2008). If the model has the Kappa Index under than 70 % at that point, Markov Chain Analysis should be repeated by choosing different years than it was before. Otherwise, both MCE model and CA-Markov analysis model will be applied again to create the spatial model for 2036, 2055 and 2074 years.

5. *Results and Discussion*

5.1 Overview

This chapter represents the final results of the research starting from detected the changes of the Sea of Galilea area including shape, water level and volume over the time period of the research. Then, it debates the connection between area and water level. From that point onward, the results continue to show the conclusion of Markov chain analysis and Multicriteria evaluation. Next, displays the validation and statistical analysis results. Finally, it shows the predicted shapes of the sea of Galilea.

5.2 The changes in the area of the Sea of Galilea over time

After carrying out the supervised classification of the satellite images, which mentioned in chapter four using GIS and RS techniques, the areas of the Sea of Galilea derived and calculated for each satellite imagery. Table (5-1) shows the areas of the Sea of Galilea over the research time from 1972 until 2017.

The areas of the Sea of Galilee over the time are represented geographically also based on the change detection model, and it showed in figures (5-1), (5-2), (5-3), (5-4), (5-5) and (5-6) and graphically in figures (5-7), (5-8).

Table (5-1). The areas of the Sea of Galilea (1972-2017).

Year	Area km^2
1972	166.31
1975	166.25
1984	167.31
1986	162.61
1988	167.16
1990	163.00
1992	167.67
1998	163.43
2000	160.11
2004	166.34
2006	163.86
2008	161.42
2010	159.81
2014	162.46
2017	159.74

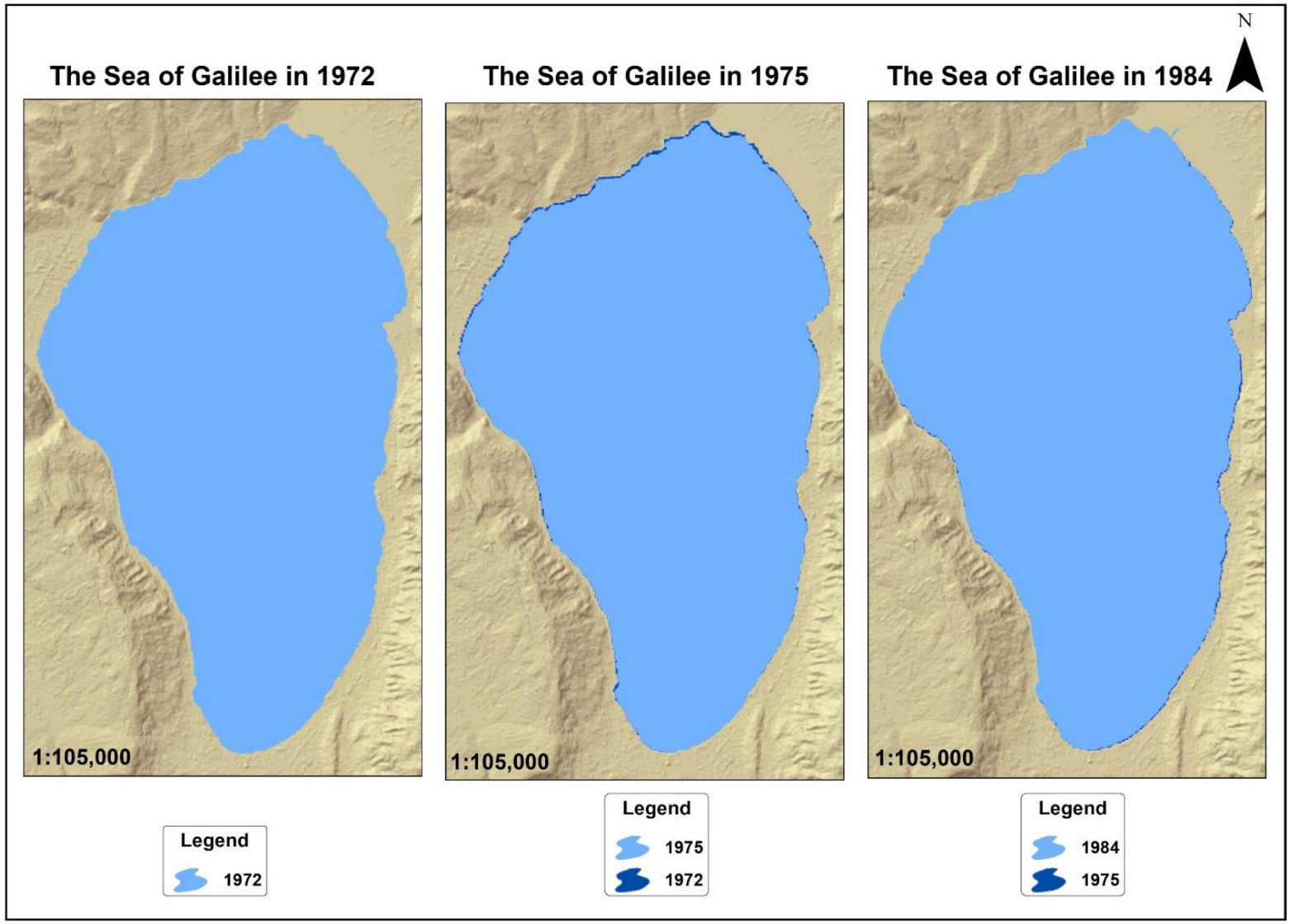

Figure (5-1). The Sea of Galilee in 1972, 1975 and 1984.

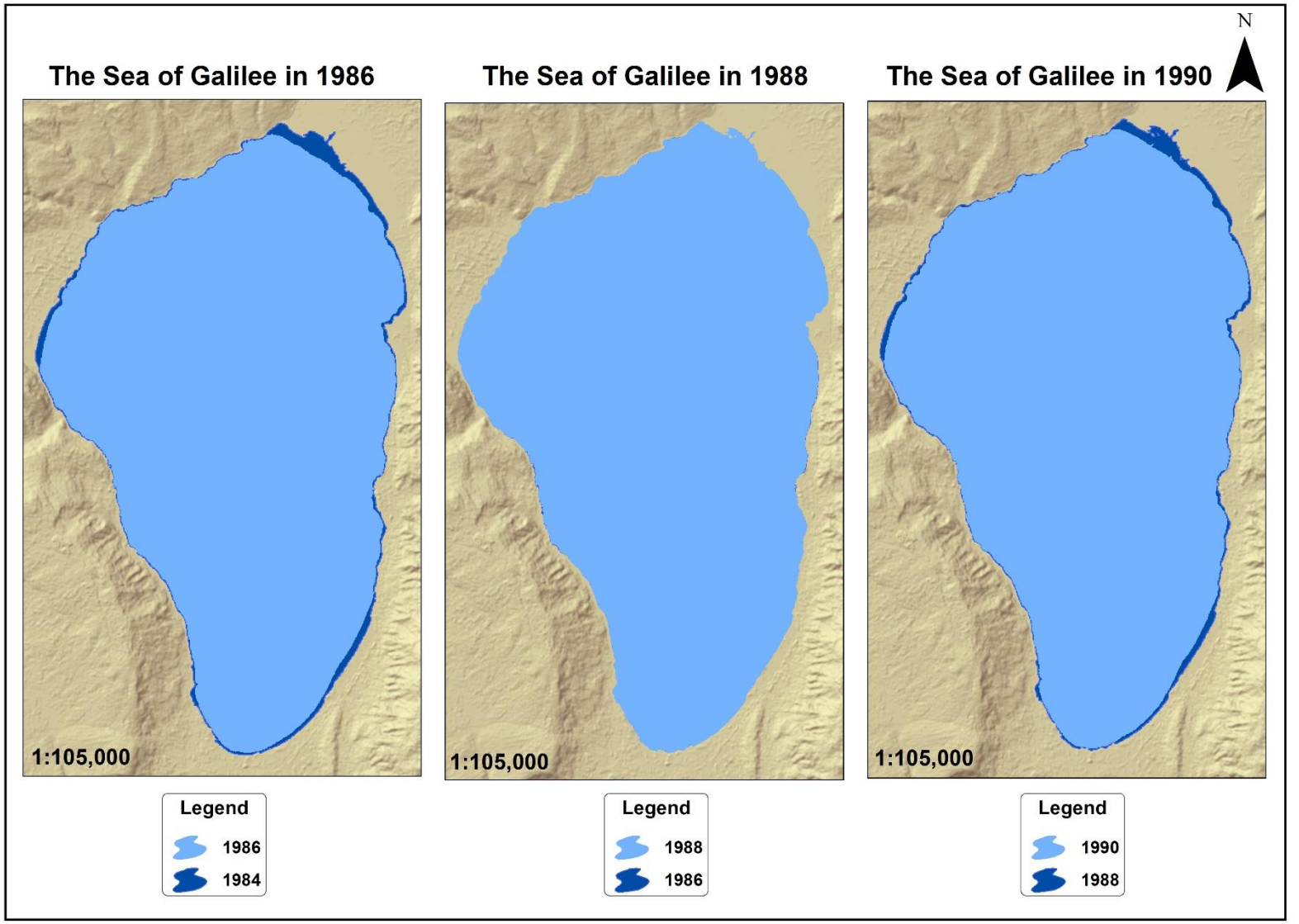

Figure (5-2). The Sea of Galilee in 1986, 1988 and 1990.

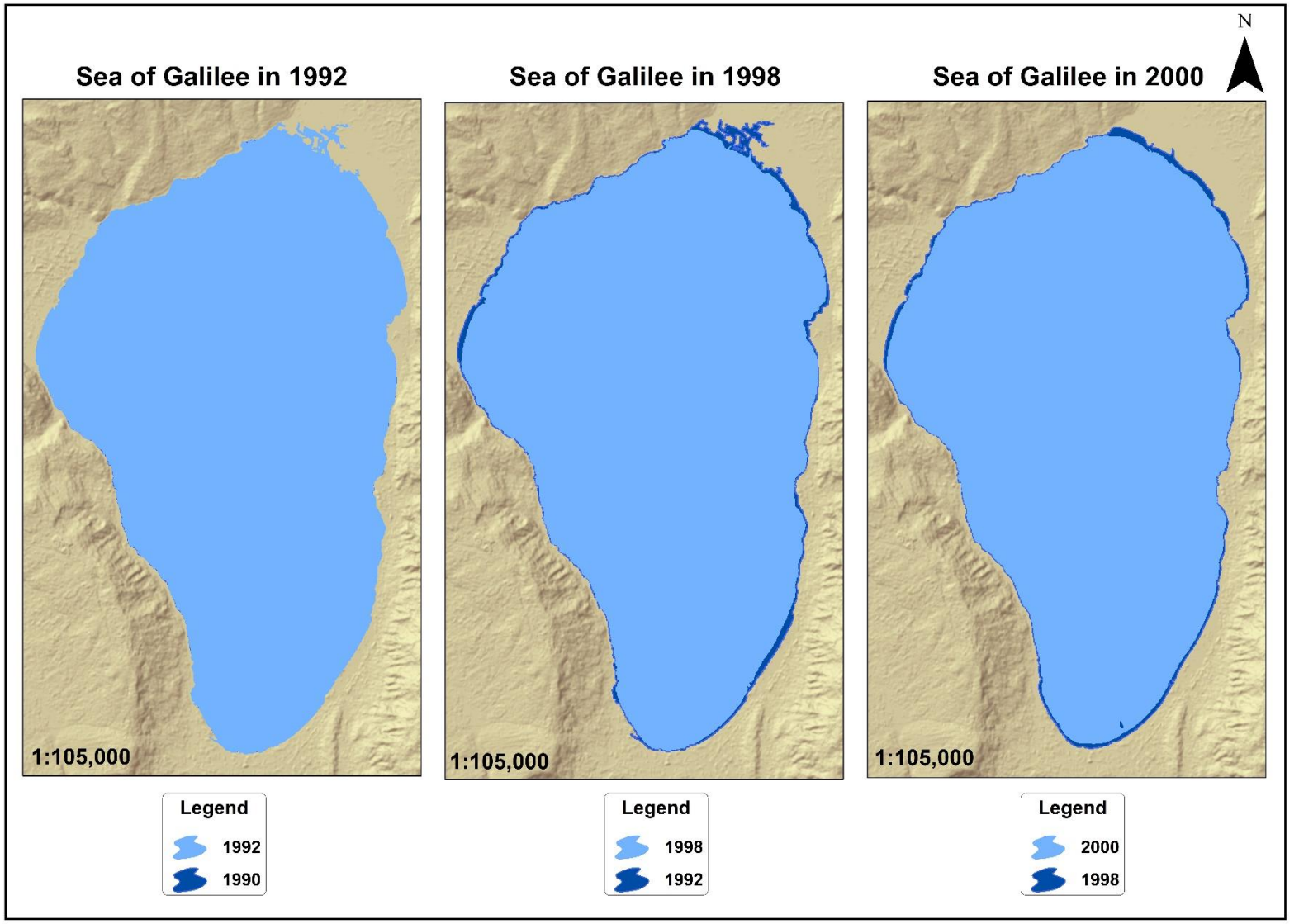

Figure (5-3). The Sea of Galilee in 1992, 1998 and 2000.

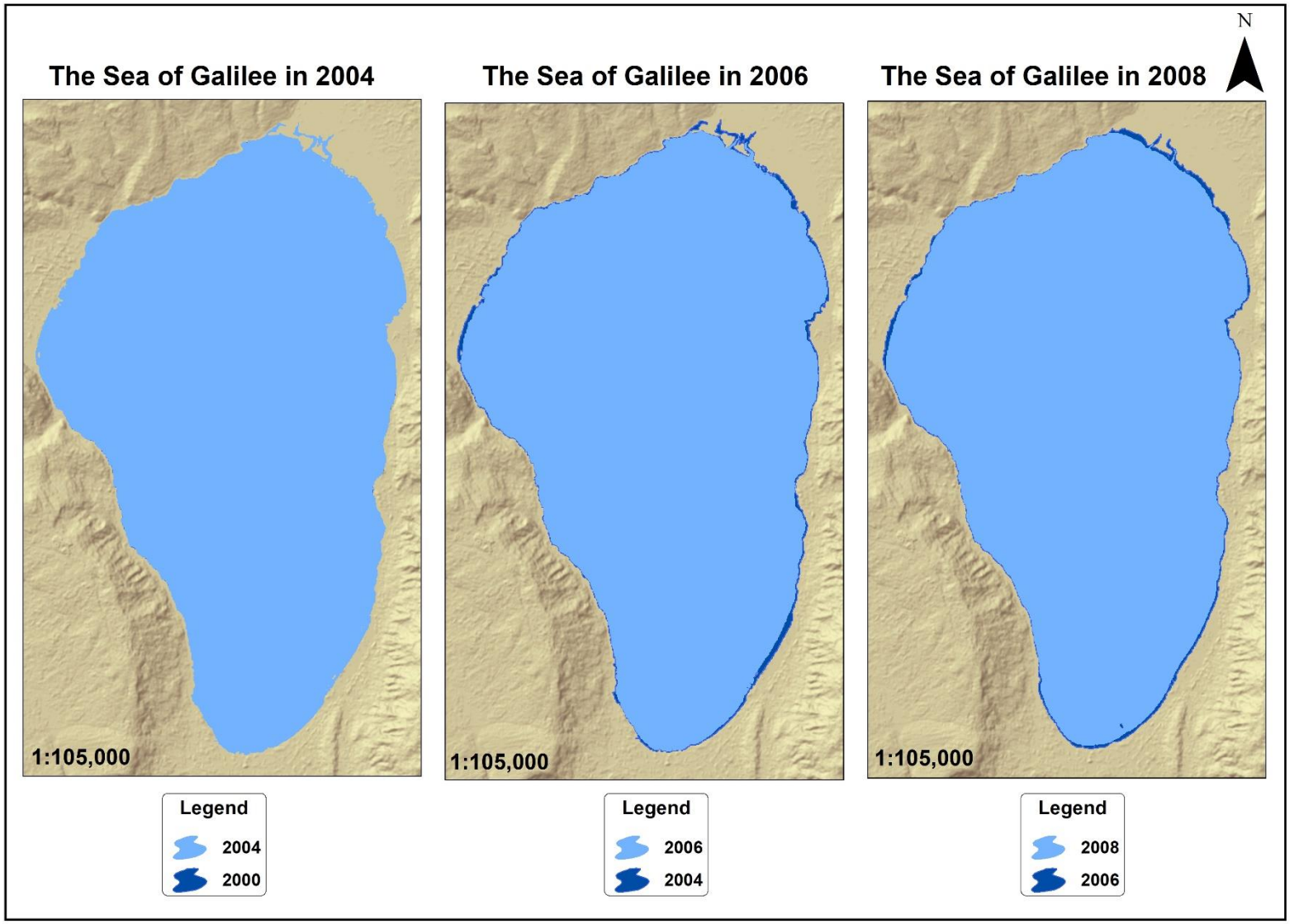

Figure (5-4). The Sea of Galilee in 2004, 2006 and 2008.

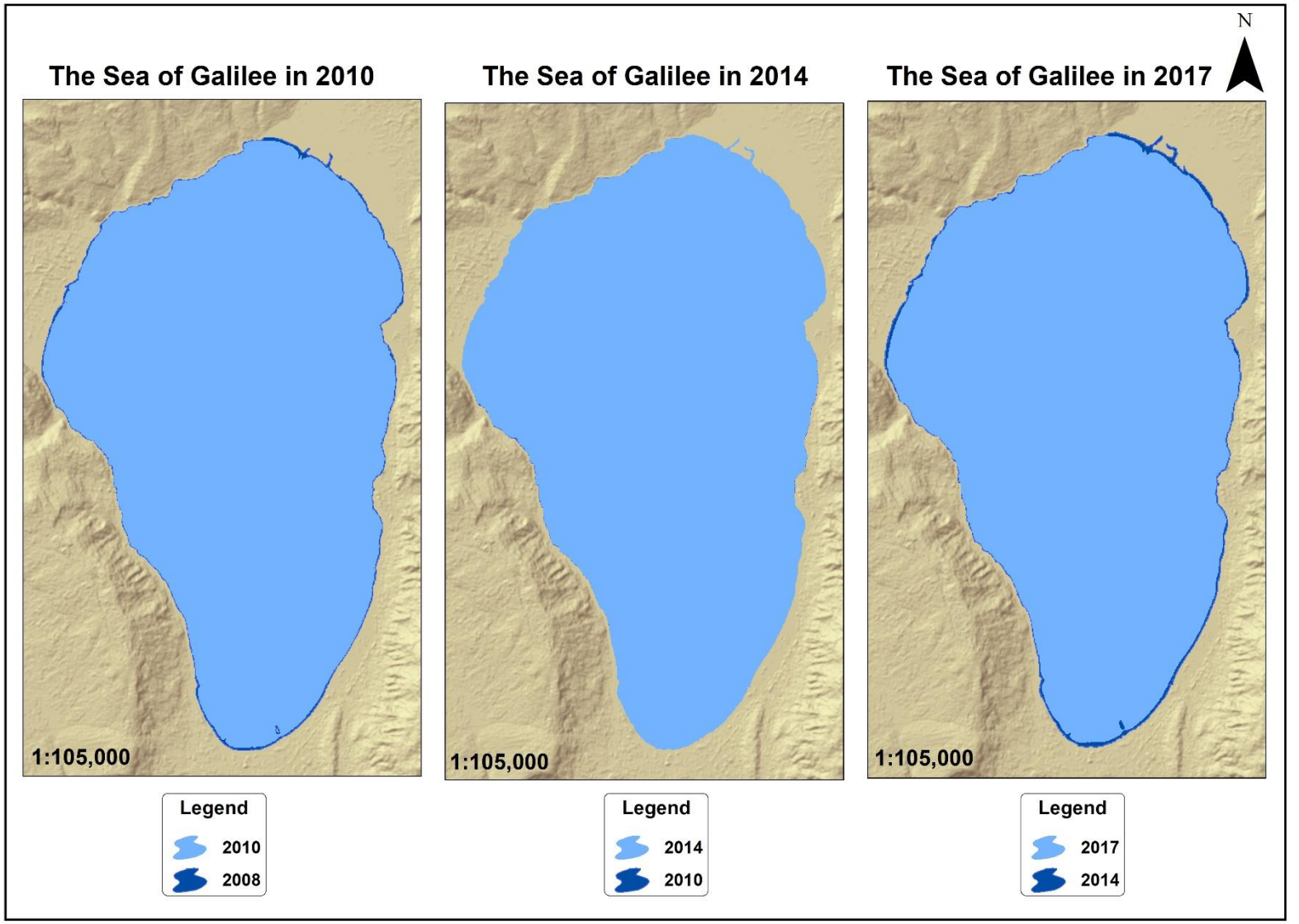

Figure (5-5). The Sea of Galilee in 2010, 2014 and 2017.

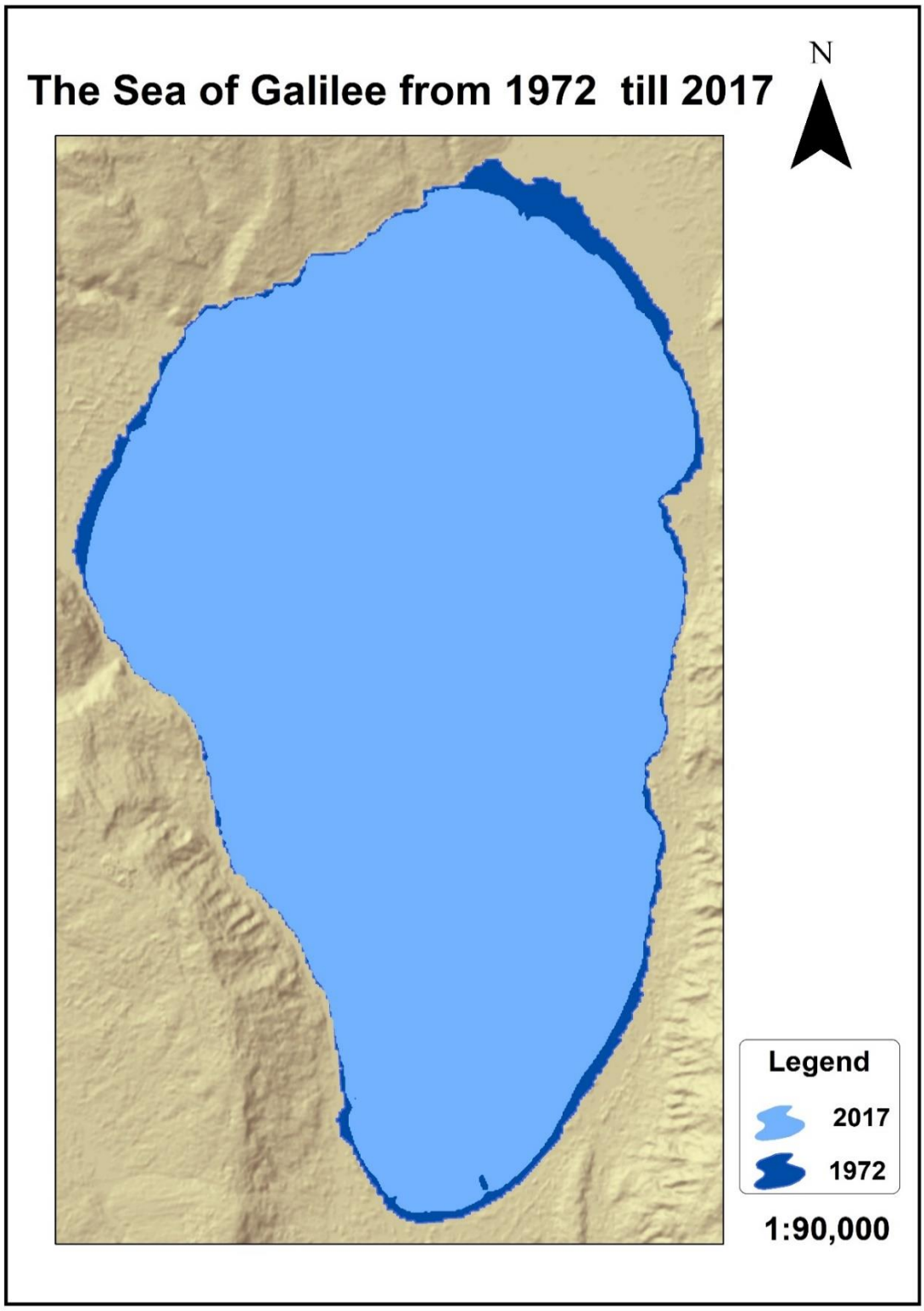

Figure (5-6). The Sea of Galilee from 1972 to 2017.

Figure (5-7). The Sea of Galilee areas (1972-2017).

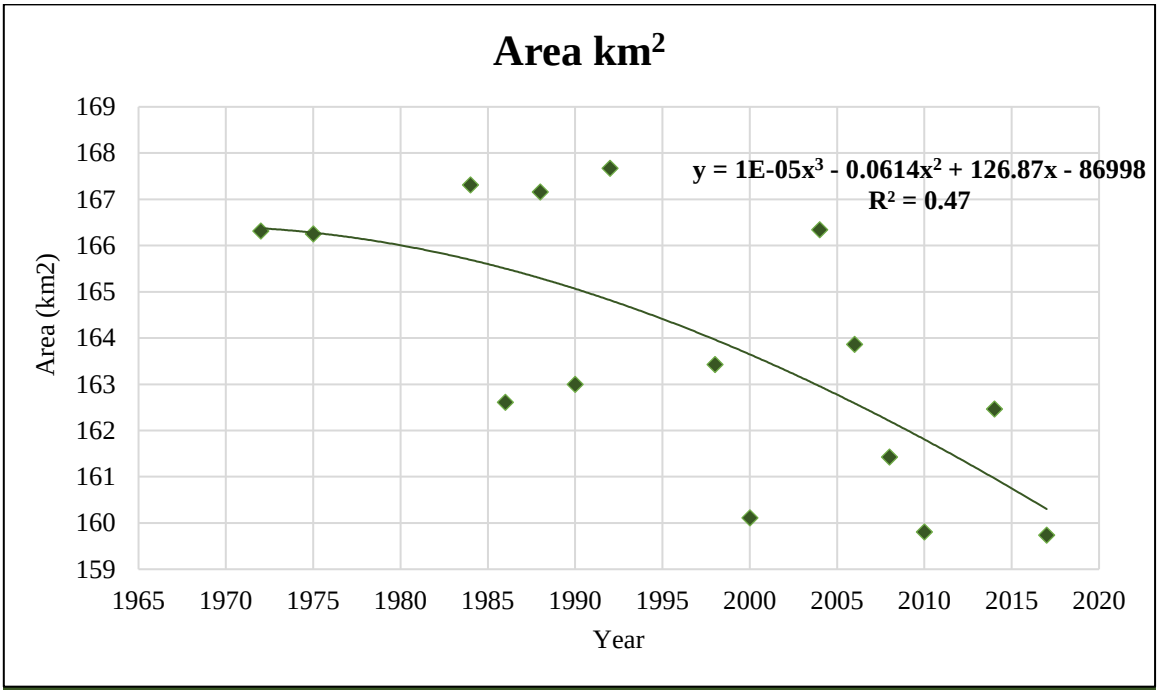

Figure (5-8). The Sea of Galilee area regression analysis over the time.

The overall trend of the Sea of Galilee is decreasing as is shown from the previous figures and it is apparently significant down to the yearly average area but not from the beginning.

Figure (5-1) shows the Sea of Galilee areas in 1972, 1975 and 1984. In 1975 the total area was 166.31 km^2, three years later and in 1975 the area did not change that much so it was 166.25 km^2, ten years later in 1984 the total area was a bit more than before 167.31 km^2 which might be justified because of the climatic conditions.

Figure (5-2) shows the Sea of Galilee areas in 1986, 1988 and 1990. This period connected with the previous period making such a cycle in the decreasing and increasing, starting from 1986 the area decreased around 5 km^2 than it was two years ago and became 162.61 km^2, then in 1988 it increased in the same amount 5 km^2 and became 167.16 km^2, in 1990 the area decreased again and became 163 km^2. Most of the decreasing and the increase in this period was in the north-eastern, the north-western and the south-eastern part of the Sea of Galilee, this variation is due the variation of the amount used water that can identify the main reason for this decreasing and increase.

Figure (5-3) represents the change in shape of the water-body over eight years from 1992 to 2000. This period is a bit mystery due to the lack of imageries from 1992 to 1998. In general, the annual average area change is -3 km^2 and the changes are detected in three essential directions; from the north, the north-eastern, the north-western and the south-eastern. In this period, the Sea of Galilee reaches the larges area over the research time, which is 167.67 km^2. Then it started to decrease dramatically and became 163.43 km^2 in 1998 and 160.11 km^2 in 2000.

Figure (5-4) and figure (5-5) illustrates the change occurred in shape over 17 years, from 2000 to 2017. The real significant decreasing of the yearly average area of the Sea of Galilee stared in this period. The shrinkage in the Sea of Galilee happened in every direction. From 2000 to 2008, the average area change is approximate -3 $km^{2,}$ and it is almost the same amount of shrinkage from 1992 to 2000. The decreasing continue till 2010 when the Sea of Galilee area reaches the deck 159.81 km^2, in 2014 the area became 162.46 km^2 it is somewhat precarious to recognize the fundamental explanation behind this, however, the area in 2017 followed the general trend of the 2000s period which is decreasing, so the Sea of Galilee area was 159.74 km^2. There is more than one reason affecting the water-body in this period like evaporation, the amount of inflow released from Jordan River, precipitation and the human overuse of the water.

5.3. The shrinkage Justifications

Finding out the exact reasons behind the shrinkage of the areas of the Sea of Galilee over the time is quite complicated and require bunches of researches and studies. However, the area of the Sea of Galilee can reflect more than one factor for this shrinkage.

The use of the Sea of Galilee water from Israel (Israeli occupation) is one of the primary factors that affect the area of the Sea of Galilee as they consider it the only significant surface water body. Since 1964, when the Israeli National Water Carrier began transferring water from the Sea of Galilee to the center and south of the country, supplying some 30% of the country's fresh water, the overconsumption of the water for urban and agricultural consumers has become the primary role of the lake while the water still decreasing.

Climatic conditions are playing an important role too in this behaviour of the water-body since this behaviour is the result of the balance between water running into the sea from the tributary area and direct precipitation, minus water evaporation. At all events, the main reason causing this recession in the Sea of Galilee area is the intensive human water consumption from the watershed including the Jordan River for another usage.

5.4 The changes in water level of the Sea of Galilea over time

In this part of the results, the water level of the Sea of Galilea over the research time derivated from the model that mentioned before in chapter four. The results were harmonious with area changing and the previous studies as well. In some cases, the water level from the previous studies submitted instead of the model results due to the repeating of the same values of the water level in different sources.

The average of the Sea of Galilea water over the time represents in Table (5-2). The water level values in meters and consistent with previous studies.

Table (5-2). The water level of the Sea of Galilee (1972-2017).

Year Water level	Mean Sea Level (m)	Year Water level	Mean Sea Level (m)
1972	-211.43	2000	-213.58
1975	-211.46	2004	-210.42
1984	-210.63	2006	-211.93
1986	-212.33	2008	-214.04
1988	-209.96	2010	-214.44
1990	-212.59	2014	-212.8
1992	-209.41	2017	-213.6
1998	-211.96		

In general, the water level of the Sea of Galilea from 1972 until 2017 looks much more like a wave decreasing and increasing. In the beginning, the change in water level was not observable for example the period from 1972-1975, but most of the times it is worthy to say there are changes. The wave started in 1984 when the water level increased 1 meter then decreased 2 meters in 1986. Then increased again to reach the highest water level over the research time, which is 209.41 m below the sea level in 1992; this is justified by changing in the water body area since this year the Sea of Galilee reaches the larges area.

In the 2000s period, it is evident that the general trend of the water level is decreasing. In 2008 and 2010 the water levels of the Sea of Galilea reached the deck which corresponds again to water-body areas in these years which were less than the before and after years.

Based on table 5-2 the changes in water level over the time calculated and in every year the average water level change of the Sea of Galilea is -0.89 m.

To analysis the overall trend behaviour of the decreasing in the water level of the Sea of Galilee through the years, a third-degree polynomial applied from regression analysis in Excel. The result illustrates in figure (5-9) where R^2= 0.39 which indicates a moderate positive linear relationship via a fuzzy-firm linear rule.

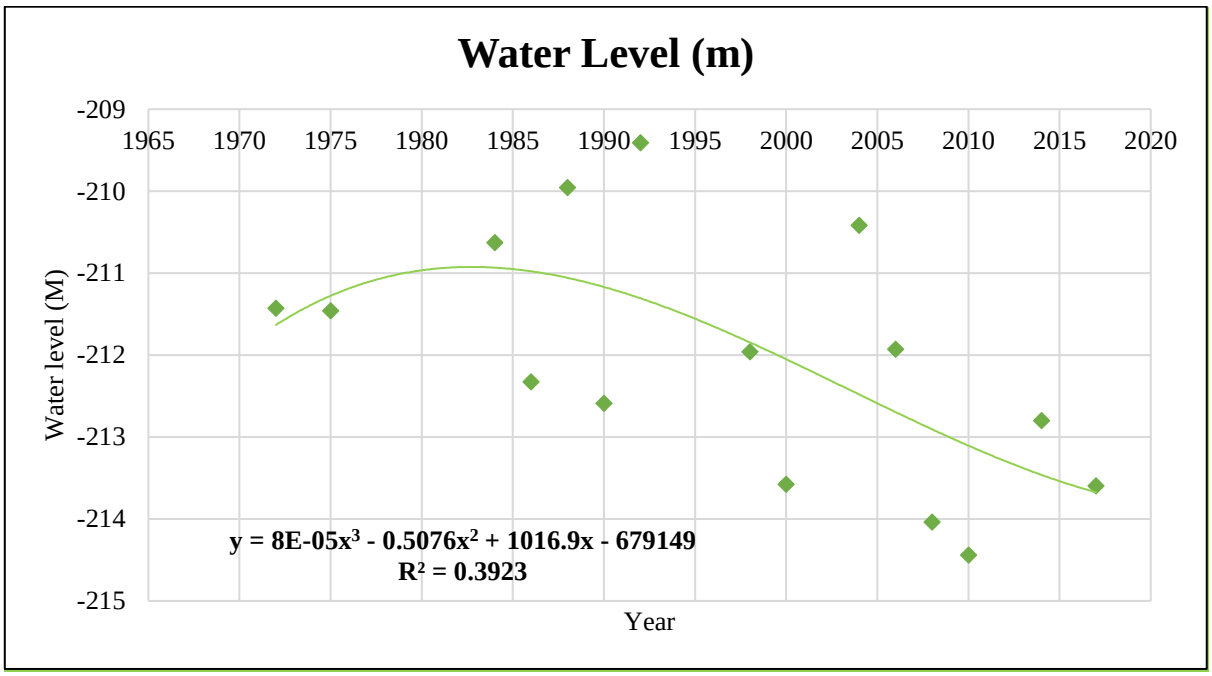

Figure (5-9). The Sea of Galilee water level regression analysis over the time.

5.5 Area-Water Mean Sea Level Relation

Concerning to discover the connection between the Sea of Galilee areas and the water levels over the research time, regression analysis applied again. The resulting analysis represents in figure (5-10). A linear equation where R^2= 0.905, that indicates a strong positive linear relationship via a firm, linear rule.

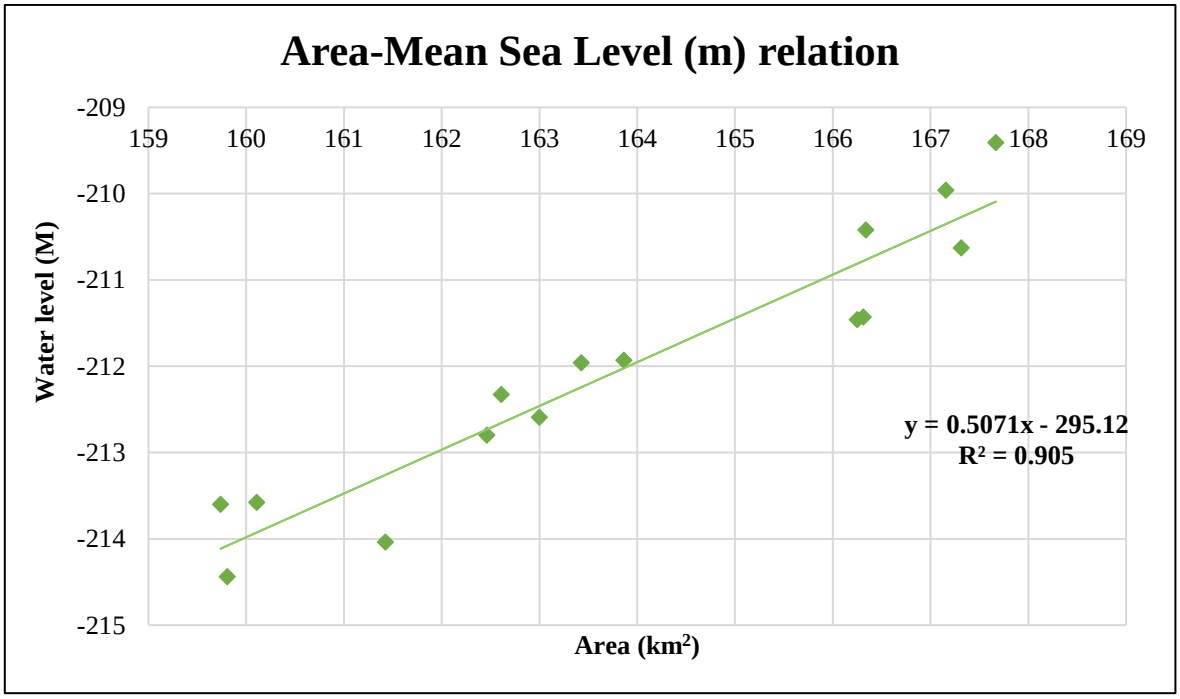

Figure (5-10). The Sea of Galilee water level regression analysis over the time.

5.6 The Change in volume over Time

(Habboub, 2013) explains that knowing the area and water level; the volume change could be calculated by using the following equation:

$$\Delta \boldsymbol{V} = \mathbf{0.5}\ (\boldsymbol{A_{1992}} + \boldsymbol{At}) \times (\boldsymbol{H_{1992}} - \boldsymbol{Ht}) \qquad \text{Equation 5-1}$$

Where:

Δ: The change in volume.

A_{1992}: The Sea of Galilee area in the year 1992.

: The Sea of Galilee area in a given time.

: The Sea of Galilee water level in a given time.

H_{1992}: The Sea of Galilee water level in the year 1992.

By applying this equation to the Sea of Galilee areas and water levels and taking into consideration, the applicable year is 1992 since this year recorded the largest area and the highest water level of the Sea of Galilee over the time. Table (5-3) and figure (5-11) show the Change in volume from the referential year, 1992. The average of the change in volume in the Sea of Galilee from the referential year, 1992 until 2017 is 0.565 km^3.

Table (5-3). Change in volume in the sea of Galilee from the referential year, 1992.

Year	Change in Volume km^3
1998	0.422
2000	0.683
2004	0.169
2006	0.418
2008	0.762
2010	0.824
2014	0.560
2017	0.686

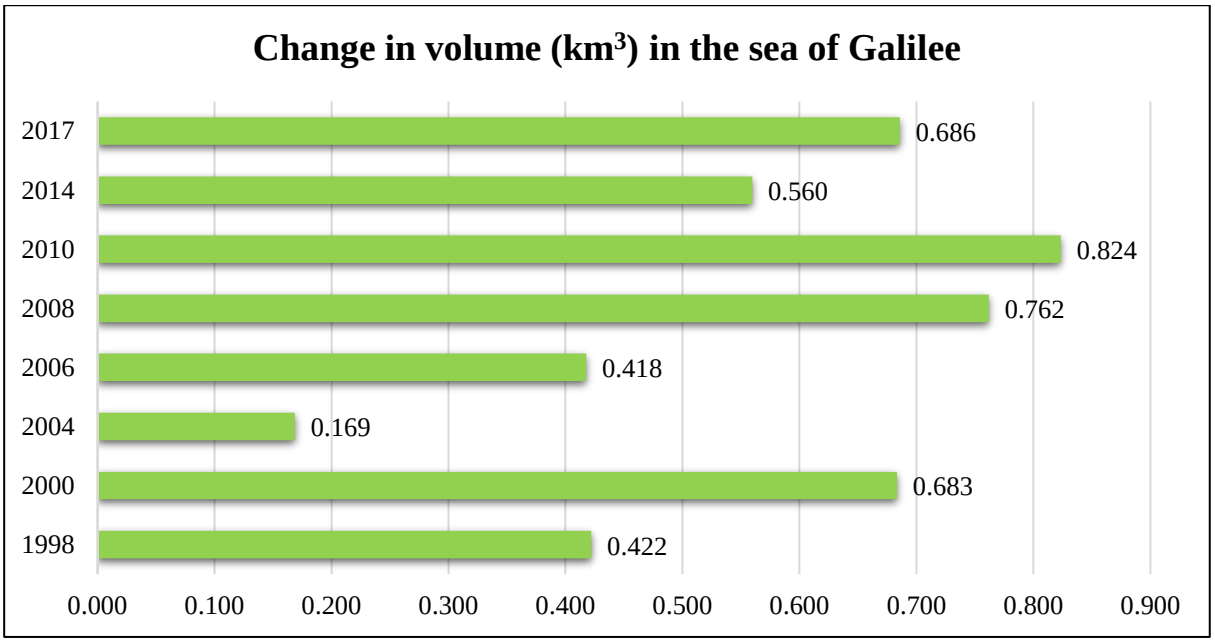

Figure (5-11). Change in volume in the sea of Galilee from the referential year, 1992.

5.7 The Sea of Galilee prediction

In this final part of the research, a prediction of the shape and the area of the Sea of Galilee done using Markov Chain Analysis, Multi-Criteria Evaluation model and CA-Markov analysis for the years 2036, 2055 and 2074 respectively. Figure (5-12) summarize all the processes.

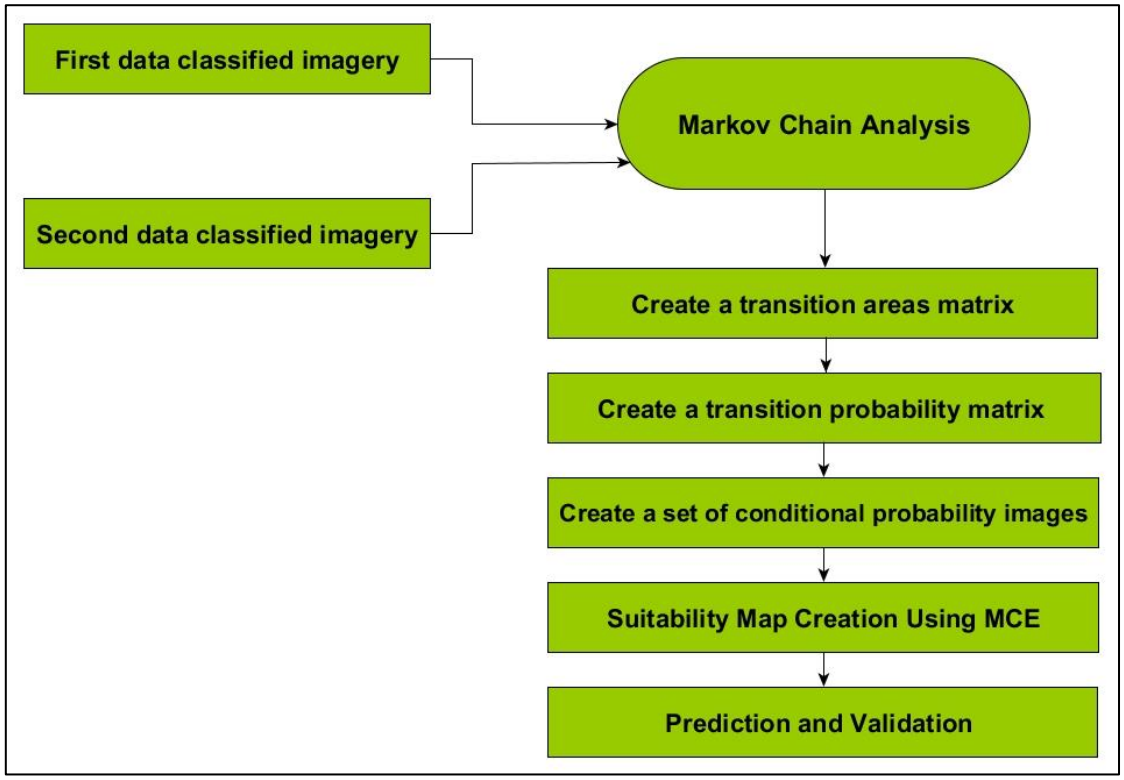

Figure (5-12). The Sea of Galilee prediction flowchart.

(Habboub, 2013) modified

5.7.1 Markov Chain Analysis

The Markov module analyses a pair of land cover images, which are the inputs. On the other hand, the outputs are a transition areas matrix, a transition probability matrix, and a set of conditional probability. The outputs use for prediction by using CA-Markov analysis.

In this research, the pair of classified imageries 1972 and 1998 used as inputs in the process of predicting the 2017 map.

1. The transition areas matrix (1972-1998-2017).

The transition areas matrix records the number of pixels that are expected to change from each land cover type to each other land cover type over the specified number of time units. The transition areas matrix of the years (1972, 1998, 2017) illustrates as follows:

Cells in: Expected to transition to :		
	Class 1 (Water)	Class 2 (Land)
Class 1 (Water) :	152469	29308
Class 2 (Land) :	37354	210250

Figure (5-13). The transition areas matrix (1972-1998-2017).

The transition areas matrix shows the total area (in cells) anticipated that would transform from the year of 1998 to the year of 2017 according to those changes occurred from 1972 to 1998. Based on the matrix above, there are 37354 land classified cells (30m/cell) will transform into water class, in the interim, there are 29308 water classified cells will transform into land class.

1. The transition probability matrix (1972-1998-2017).

The transition probability matrix records the probability that each land cover category will change to every other category. It could be gotten from transition areas matrix by knowing the aggregate cells of each class.

Given: Probability of changing to :		
	Class 1 (Water)	Class 2 (Land)
Class 1 (Water) :	0.8388	0.1612
Class 2 (Land) :	0.1509	0.8491

Figure (5-14). The transition probability matrix (1972-1998-2017).

1. A set of conditional probability images/maps (1972-1998-2017).

The conditional probability images report the probability that each land cover type would be found at each pixel after the specified number of time units. *"These images are calculated as projections from the later of the two input land cover images"*(Adhikari and Southworth, 2012) (IDRISI Selva Help System). The output is a raster group file listing all the conditional probability images. In another meaning, the outputs of this set are two images (land image and water image) these images are a cartographical presentation of the transition probability matrix (1972-1998-2017), and they will use as direct input for CA-Markov analysis to predict the Sea of Galilee map in 2017, figure (5-15) and figure (5-16).

5.7.2 Multi-Criteria Evaluation model for Suitability Map

After creating a set of conditional probability images in the previous step and before start predicting the Sea of Galilee map in 2017 using CA-Markov analysis. The MCE model that mentioned before in chapter four is used to create suitability map for land and water classes then after this both of suitability maps for land and water exported to IDRISI to predict the area Sea of Galilee in 2017.

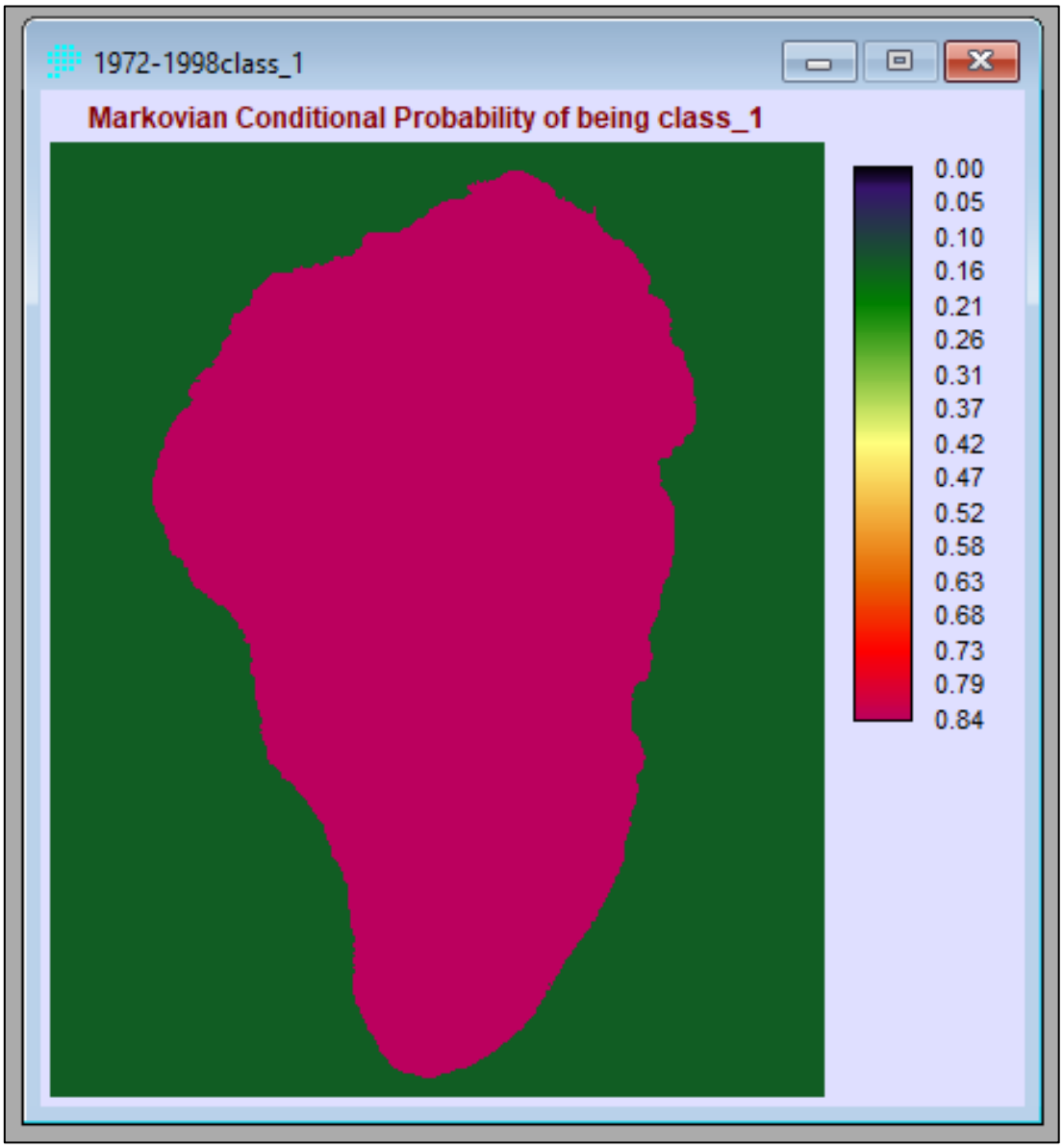

Figure (5-15). Conditional probability image for water class.

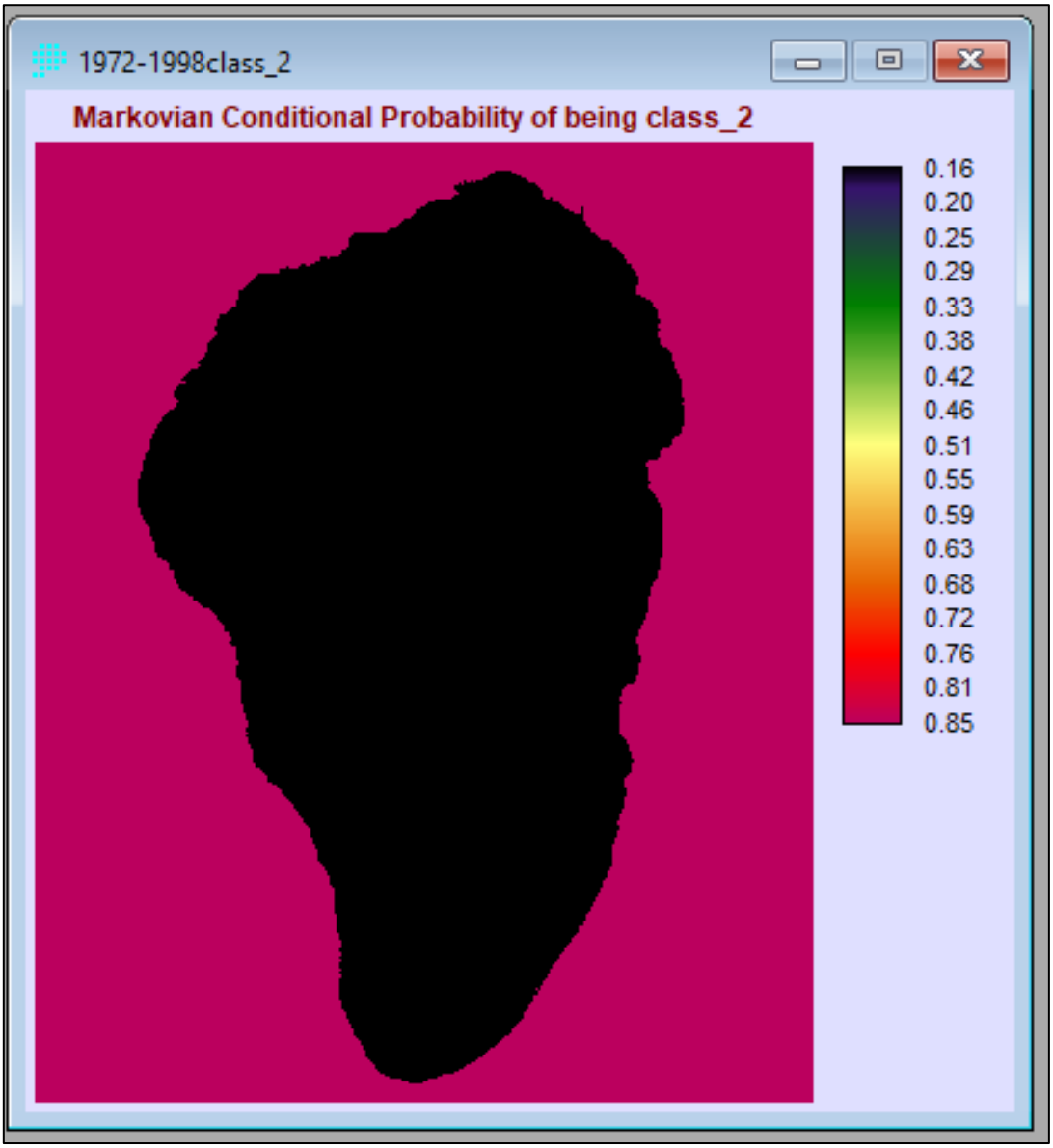

Figure (5-16). Conditional probability image for water class.

5.7.3 CA-Markov analysis (Prediction and Validation)

In this part the final output data that produced by the Markov chain analysis and MCE analysis used to predict the area of the Sea of Galilee in 2017 by applied CA-Markov analysis model. The predicted 2017 map is shown in Figure (5-17). After the prediction, an essential procedure made which is validation. Figure (5-18) summarizes the validation processes.

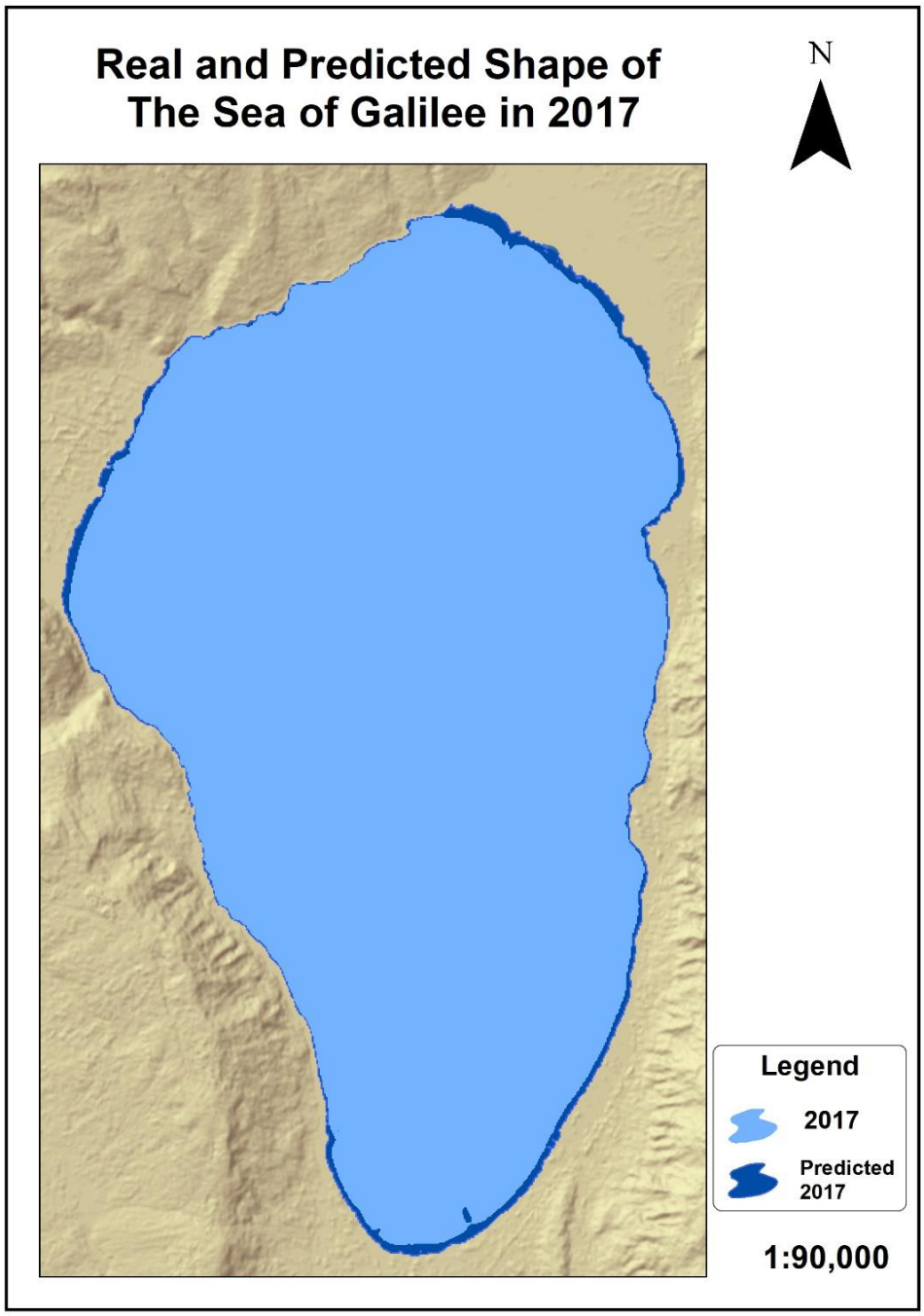

Figure (5-17). The predicted shape of the Sea of Galilee in 2017.

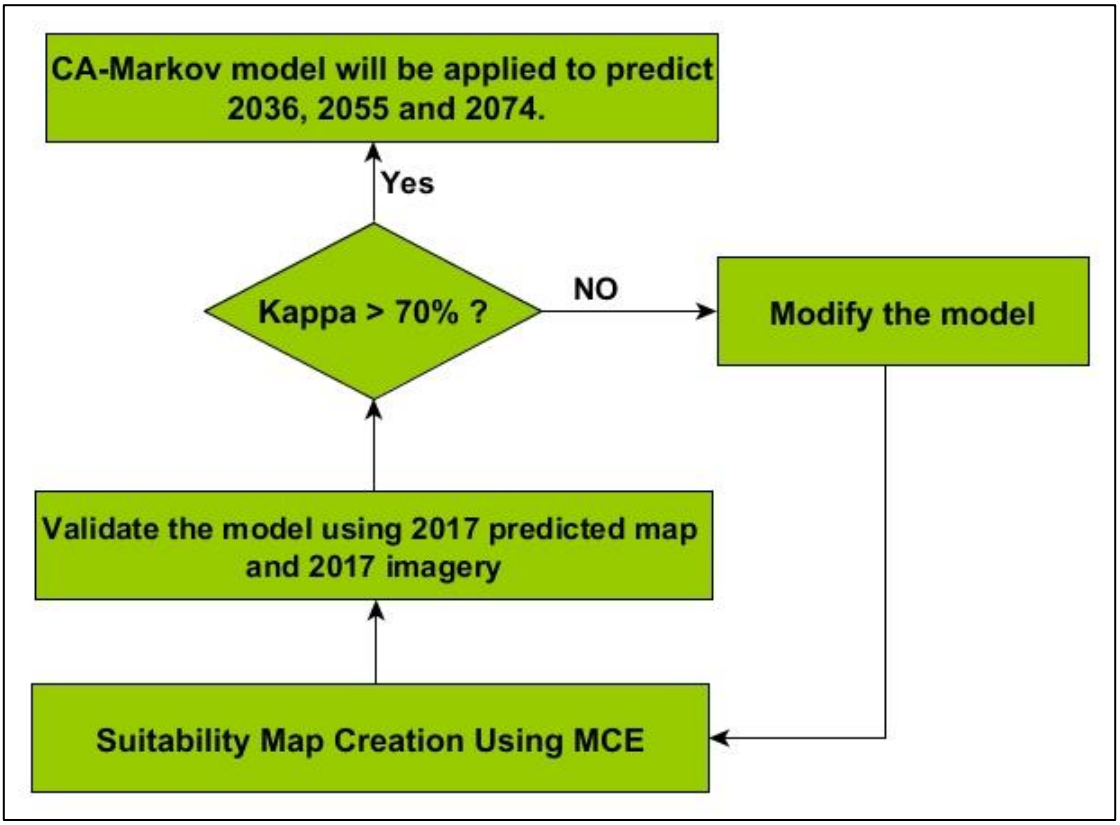

Figure (5-18). The validation processes.

(Habboub, 2013)

The validation provides a method to measure agreement between two categorical (integer or byte) images, a "comparison" map and a "reference" map. To check the previous model it is valid or not, standard Kappa index is used and as it mentioned before (The model can be valid if Kappa Index > 70 %) (Wen, 2008). If the model has the Kappa Index less than 70 %, then Markov Chain Analysis should be repeated by choosing different years than it was before. Otherwise, both MCE model and CA-Markov analysis model will be applied again to create the spatial model for 2036, 2055 and 2074 years.

By using the VALIDATE tool, IDRISI gave the following results:

- Standard Kappa of 0.9423
- Kappa for no information of 0.9435
- Kappa for the grid-cell level location of 1.0000
- Kappa for the stratum-level location of 1.0000

All of the given results above are more than 0.7 that means the model is valid and it can be used to predict the shape and the area of sea Galilee in the future Figure (5-19).

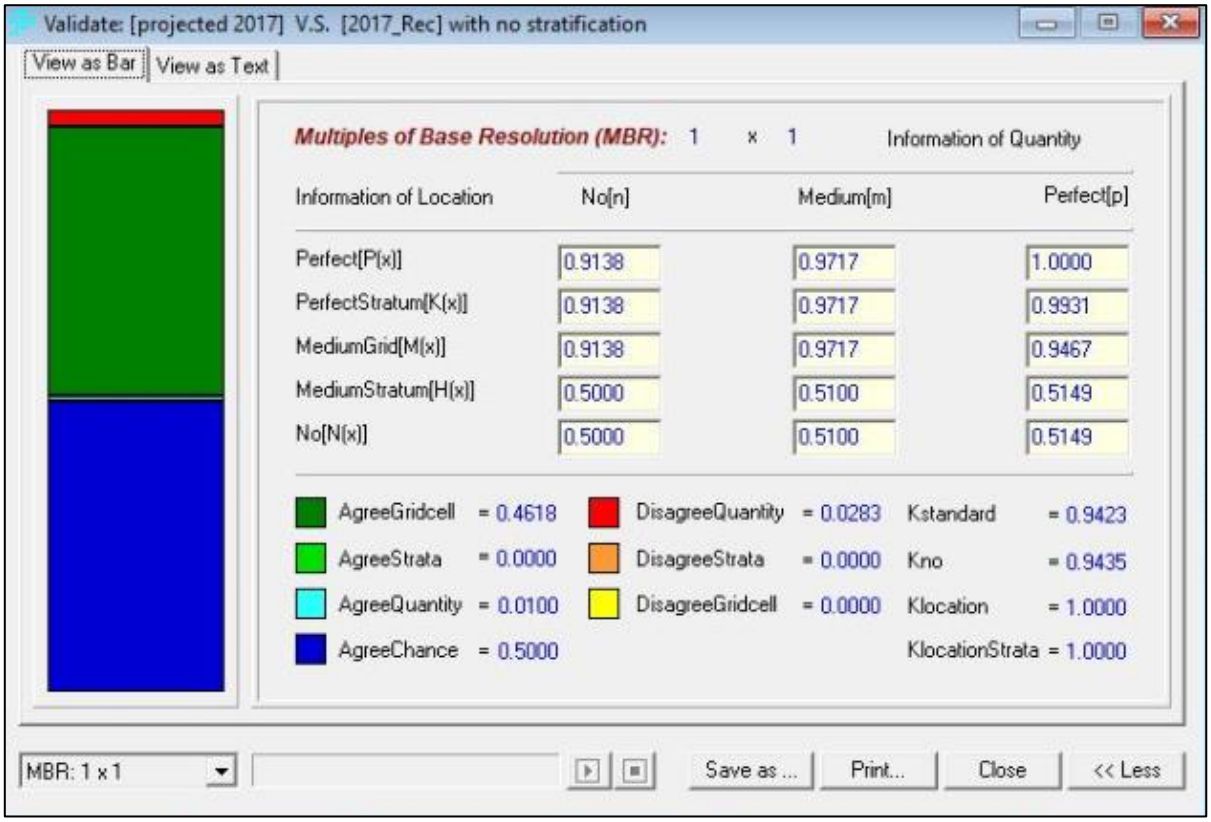

Figure (5-19). Validation results in IDRISI.

Based on the predicted map of the Sea of Galilee in 2017 the total area of the water-body calculated and it was 162.29 km^2 that show the water-body will decrease just 1.14 km^2 from 1998 to 2017. On the other hand, the real map of the Sea of Galilee in 2017 shows another tale since the decrease from 1998 to 2017 was 3.6 km^2 to equal 159.74 km^2. Those differences can be justified due to some pixels generated in random locations and not inside the water-body.

In view of these outcomes, the previous model is valid and will be applied again to generate and predict the shape and the area of the Sea of Galilee in every 19 years after 2017, because the number of years between 1998 and 2017 that they consider the base for the prediction and creating the transition matrixes is 19 years. In other words, the model will be used again to create the maps for 2036, 2055 and 2074 years. Very important to say that the predicted shapes of the Sea of Galilee follow up the same conditions and under the same circumstance from 1998 to 2017.

The areas of the water body of the predicted maps of the Sea of Galilee in 2036, 2055 and 2074 calculated and the results were as follows:

- In 2036, the total area of the water body is 158.50 $km^{2,}$ and it is 1.24 km^2 less than 2017 figure (5-20) shows the predicted shape of the Sea of Galilee and the shrinkage can be observed in the north-eastern.
- In 2055, the water body is 4.09 km^2 less than 2017, so the total area equals 155.65 $km^{2,}$ and the shrinkage is more in the north and the north-eastern figure (5-21).
- 2074 was an interesting year the total area of the water body equals 155.66 $km^{2,}$ so there were no significant changes than the previous prediction in 2055, that can be justified due to the extended period between 2017 and the prediction year 2077, which is 57 years figure (5-22) represents the predicted shape in the given year.

It is essential to know, and as it mentioned before, there are many factors may affect the shape and the area of the water-body of the Sea of Galilee. Either now or in the future, for example, the evaporation, the amount of inflow released from the watershed, the precipitation and the human use of the water. These factors must take in consideration before any prediction.

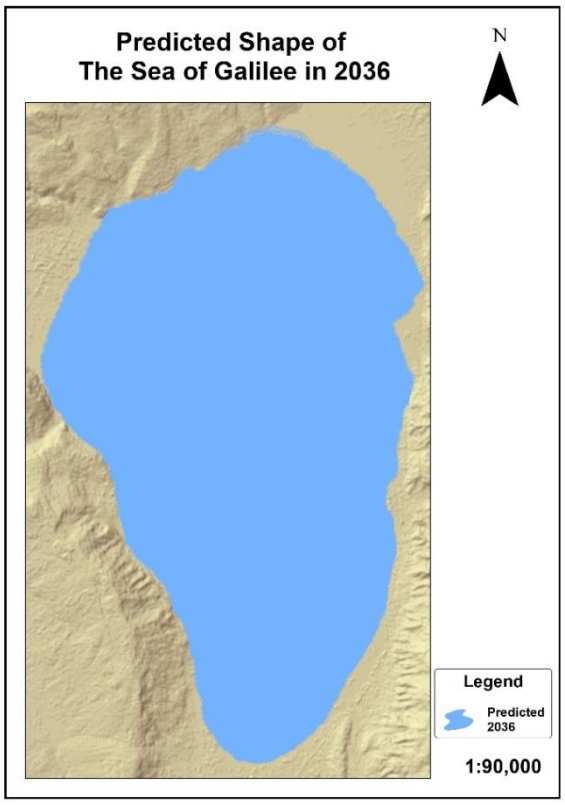

Figure (5-20). The predicted shape of the Sea of Galilee 2036.

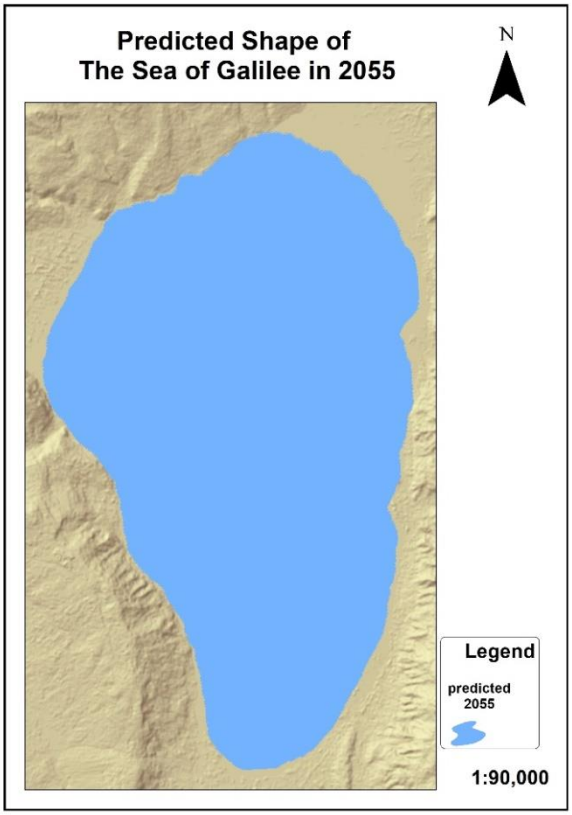

Figure (5-21). The predicted shape of the Sea of Galilee 2055.

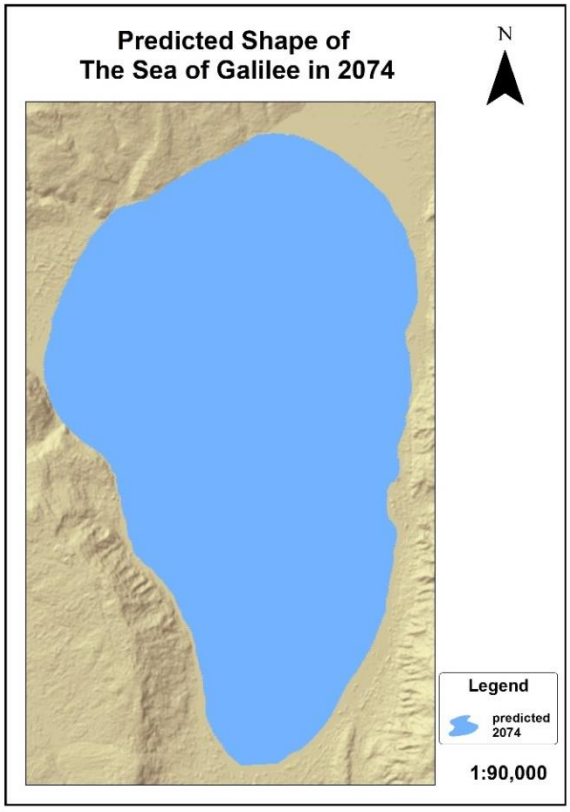

Figure (5-22). The predicted shape of the Sea of Galilee 2074.

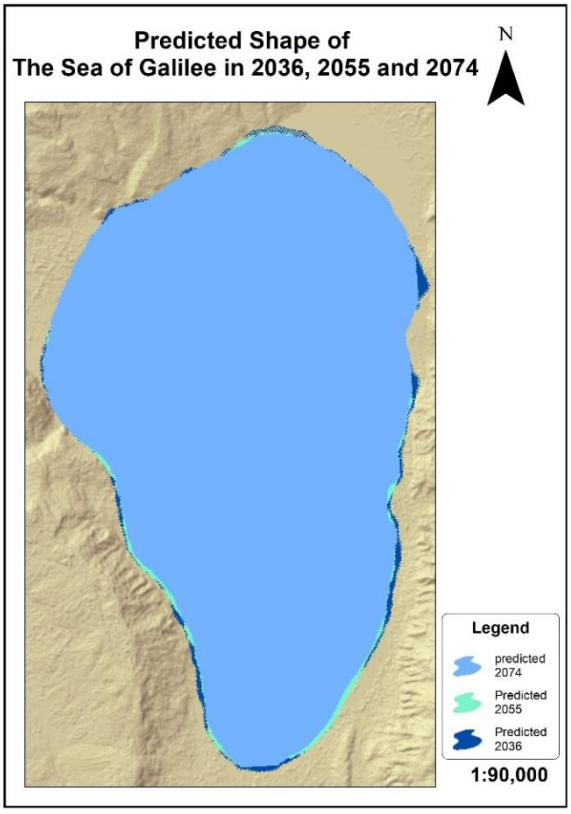

Figure (5-23).The predicted shape of the Sea of Galilee 2036, 2055 and 2074.

6. *Conclusion and Recommendations*

6.1 Conclusion

The period from 1972 to 2000, the decreasing and increasing of the water body of the Sea of Galilee behave as a wave. Consequently, the water level and the volume were changing. However, the Sea of Galilee in this era reaches the largest area and volume over the research time, which is 167.67 km^2 and 209.41 meters under the mean sea level. From 2000 to 2017 the real significant decreasing of the yearly average area of the Sea of Galilee started. The shrinkage in the Sea of Galilee happened in every direction mainly from the north, the north-eastern, the north-western and the south-eastern, the decreasing continue till 2010 when the Sea of Galilee area reaches the deck then started increasing again. The water body area in 2017 and nowadays follow the general trend of the 2000s period, which is decreasing. The essential explanation behind the shrinkage of the Sea of Galilee because of the intensive human water consumption by Israel in the first place knowing there are other factors affect the area of the Sea of Galilee like the evaporation, the amount of inflow released from Jordan River, and precipitation.

The research made a logical prediction of the Sea of Galilee [shape and area]. This prediction based on suitability maps and applying Markov chain analysis and Multicriteria Evaluation [MCE]. Spatial validation indices are used after that for validation. Base on the validation statistics the standard Kappa index was 0.9423 which means a complete agreement and strong relationship between the model and reality. After that, the predictions process continued knowing that the predicted water bodies [shape and area] of the Sea of Galilee in 2036, 2055 and 2074 following the same circumstances from 1998 to 2017. The final results were as follows: The predicted areas of 2036, 2055 and 2074 are 158.50, 155.65 and 155.66 km^2, which can be considered as a logical extension of the trend of the 2000s period, which is decreasing.

6.2 Recommendations

- Implement water rationing system and adopt regular programs for monitoring the Sea of Galilee by the local authorities and related agencies.
- Further research is needed on the methods of satellite-derived bathymetry of the Sea of Galilee.
- Use the results of this research to develop the prediction model by including the amount of inflow released from the watershed of the Sea of Galilee to get a very accurate prediction.

Bibliography

Abd Rabou, M. (2017). Assessing and Mapping the Coastal Zone Changes in the Gaza Strip, Palestine, Using GIS and Remote Sensing Techniques. Master degree. Islamic University of Gaza.

Adhikari, S. and Southworth, J. (2012). Simulating Forest Cover Changes of Bannerghatta National Park Based on a CA-Markov Model 58; A Remote Sensing Approach.

Aggarwal, S. (2003). Earth Resource Satellites. Satellite Remote Sensing and GIS Applications in Agricultural Meteorology, 39.

Akhter, M. (2006). Remote sensing for developing an operational monitoring scheme for the Sundarban Reserved Forest, Bangladesh. Department of World Forestry, University of Hamburg.

Akin, E. and Cooley, S. (2013). Lake Basin Volume. GIS 4 Geomorphology. [Online] Available at: http://gis4geomorphology.com/lake-basinvolume/#more-1239 [Accessed 04 Apr. 2018].

AUG signals. (2008). Change Detection. AUG SIGNALS. [Online] Available at: http://www.augsignals.com/page.php?menu=14 . [Accessed 15 Jan. 2018].

Australian Journal Of Basic And Applied Sciences. (2014). Utilization of High Spatial Satellite Images Reflectance's to Estimate the Nautical Charts for the Nile River. [Online] Available at: http://ajbasweb.com/old/ajbas/2014/July/541-547.pdf [Accessed 04 Apr. 2018].

Baker, Corey, et al. (2007). Change Detection Of Wetland Ecosystems Using Landsat Imagery And Change Vector Analysis. s.l. : The Society of Wetland Scientists, 2007. Vol. 27.

Belitzky, S. (1996). Geomorphology tectonic of the Lower Jordan Valley active continental rift. PhD dissertation, The Hebrew University, Jerusalem (in Hebrew).

Bell, E.and Hinojosa, R. (1977). Markov analysis of land use change: Continuous time and stationary processes. 1977. pp. 13-17.

Blaschke, T. (2010). Object-based image analysis for remote sensing. ISPRS Journal of photogrammetry and remote sensing, 65(1), 2-16.

Briassoulis, H. (2012). Analysis of Land Use Change: Theoretical and Modeling Approaches. [Online] Available at:

http://www.rri.wvu.edu/WebBook/Briassoulis/chapter4(models6).htm#4.7.2 [Accessed 12 Feb. 2018].

Burrough, P. (1986). Principles of GIS for land resources assessment. Monographs on soil and resources survey. Clarendon, Oxford.

Canadian Centre for Remote Sensing CCRS (1998). Fundamentals of Remote Sensing. [Online] Available at: http://www.nrcan.gc.ca/earth-sciences/geomatics/satellite-imagery-air-photos/satellite-imagery-products/educational-resources/9309 [Accessed 06 Jan. 2018].

Chavez (1996). Image-Based Atmospheric Corrections - Revisited and Improved. s.l. : PE & RS, 1996.

Collet, C. and Barboux, C. (2012). GITTA. [Online] Available at: http://gitta.info/SpatChangeAna/en/html/Spat_dyn_mod_discont_learningObject1.html [Accessed 20 Feb. 2018].

Cooley, S. (2013). Minimum Eroded Volume. GIS 4 Geomorphology. [Online] Available at: http://gis4geomorphology.com/calculate-basin-volume/#more-8 [Accessed 04 Apr. 2018].

Deer, P. (1999). Digital Change Detection Techniques. Civilian and Military Application Published in the UK. s.l. : Taylar & Francis Ltd, 1999.

Dewidar, K. and Frihy, O. (2007). Pre-and post-beach response to engineering hard structures using Landsat time-series at the northwestern part of the Nile delta, Egypt. Journal of Coastal Conservation, 11(2), 133-142.

Dueker, K. J. (1979). Land resource information systems: a review of fifteen years experience. Geo-Processing (Netherlands).

Eastman, J. (2001). Introduction to remote sensing and image processing. Idrisi for Windows User's Guide. Cap, 3.

Eastman, J. R., Jin, W., Keym, P. and Toledano, J. (1995). Raster procedures for multi-criteria/multi-objective decisions. Photogrammetric engineering and remote sensing, 61(5), 539-547.

Eastman, J. R. (2012). IDRISI Selva Manual. 2012.

Ehrlich, A. (1985). The eco-biostratigraphy significance of the fossil diatoms of Lake Kinneret. Current Research-Geological Survey of Israel 5, 24– 30.

Falk, M. et al. (2011). A First Course on Time Series Analysis. University of Wuerzburg : s.n., 2011.

Fonstad, M. A. (2006). Cellular automata as analysis and synthesis engines at the geomorphology–ecology interface. Geomorphology. s.l. : ELSEVIER, 2006. Vol. 77, 3-4.

Givati A., Rosenfeld D. (2007). Possible impacts of anthropogenic aerosols on water resources of the Jordan River and the Sea of Galilee. Water Resources Research Vol. 43.W10419, doi:10.1029/2006WR005771.

GPS 216 introduction to Remote sensing. (2018). GSP 216 Online Schedule. [Online] Available at: http://gsp.humboldt.edu/olm_2015/Courses/GSP_216_Online/images/radiance-diagram.PNG . [Accessed 05 May. 2018].

Green, E. P. et al. (2000). Remote Sensing Handbook for Tropical Coastal Management. 2000.

Habboub, M. (2013). Spatio -Temporal Analysis of the Dead Sea Area Using Remote Sensing and GIS-Based Model: Markov-Cellular Automata. Master degree. Islamic University of Gaza.

Hashimoto, T., Takagi, M., and Kajiware, K. (1999). Remote sensing note. Japan Association on Remote Sensing.

Hazana, J. et al. (2009). Detecting Changes in a Wetland: Using Multi-Spectral and Temporal Landsat in the Upper Noun Valley Drainage Basin-Cameroon. 2009.

Israel Meteorological Service. (2018). Climate information. [Online] Available at: http://www.ims.gov.il/IMSEng/CLIMATE [Accessed 12 Mar. 2018].

Israel Water Authority. (2012). The Kinneret watershed. [Online] Available at: http://www.water.gov.il/Hebrew/ProfessionalInfoAndData/2012/13-Israel-Water-Sector-Lake-Kinneret-watershed.pdf [Accessed 25 Mar. 2018].

Jagalingam, P. et al. (2015). Bathymetry Mapping Using Landsat 8 Satellite Imagery. Procedia Engineering, 116, 560-566.

Jesús D. Chinea. (2006). Supervised Classification. Universidad de Puerto Rico, Recinto Universitario de Mayagüez. . [Online] Available at: http://www.uprm.edu/biology/profs/chinea/gis/lectesc/tut4_3.pdf [Accessed 01 Apr. 2018].

Jianya, G., et al. (2008). A review of multi-temporal remote sensing data change detection algorithms. The International Archives of the Photogrammetry, Remote Sensing, and Spatial Information Sciences, 37(B7), 757-762.

Kandare, K. (2000). The time series change detection methods of remote sensing. 2000.

Kessler, S. (1999). Development, utilization and the state of the water sources in Israel until fall 1998.

Kiefer, R. W. (2004). Remote sensing and image interpretation: John Wiley and Sons.

Lillesand, T. M., and Kiefer, R. W. (1994). Remote sensing and photo interpretation. John Wiley and Sons: New York, 750.

Lu, D., et al. (2004). Change detection techniques. s.l. : Taylor & Francis Ltd, 2004. Vol.25.

Markel, D. (2004). Pollutants transfer from the Jordan River to Lake Kinneret during the winter of 2002/2003. Water and Irrigation, 448, 4–17, 35 (in Hebrew).

Markel, D. (2014). Monitoring and management Lake Kinneret (Sea of Galilee) preserving Israel's major surface water resource. [Online] Available at: http://www.water.gov.il/Hebrew/ProfessionalInfoAndData/Kinneret-monitoring/DocLib2/Monitoring_and_management_Lake_Kinneret-markel-20.10.14.pdf . [Accessed 03 Mar. 2018].

Markel, D., Somma, F. and Evans, B. (2006). Using a GIS transfer model to evaluate pollutant loads in the Lake Kinneret watershed, Israel, 2006.

Memarian, H. et al. (2012). Validation of CA-Markov for Simulation of Land Use and Cover Change in the Langat Basin, Malaysia. Journal of Geographic Information System. 2012.

Minimum Eroded Volume | Gis 4 Geomorphology. **(2018).** [Online] Available at: http://gis4geomorphology.com/calculate-basin-volume/ [Accessed 14 Apr. 2018].

Moayeri, M. et al. (2012). Change Detection of Wetland Development with Satellite Data and GIS. s.l. : American Journal of Scientific Research, 2012. 73. 2301-2005.

Neev, D. and Emery, E. O. (1967). The Dead Sea. Geological Survey of Israel. Bulletin 41, pp. 1 –147.

Pollinger, U., Ehrlich, A. and Serruya, S. (1986). The planktonic diatoms of Lake Kinneret (Israel) during the last 5000 years—Their contribution the algal biomass. In: Richard, M. (Ed.), Proceeding of the 8th International Diatom Symposium, Koeltz, pp. 459–470.

Pontius, R. G. (2000). Quantification error versus location error in comparison of catagoral maps. 2000.

Pontius, Robert G., and Millones, M. (2011). Death to Kappa: birth of quantity disagreement and allocation disagreement for accuracy assessment. International Journal of Remote Sensing. s.l. : Taylor & Francis, 2011. Vol. 32.

Radiometric Correction of Satellite Images: When And .., WITH BLACH. (2018). [Online] Available at: https://www.ncl.ac.uk/tcmweb/bilko/module7/lesson3.pdf [Accessed 11 Feb. 2018].

Ramsey, R. D. (2010). Image Standardization. RS/GIS Laboratory. [Online] Available at: http://earth.gis.usu.edu/imagestd/ [Accessed 08 Feb. 2018].

Reinert, G. (2010). Time Series. 2010. [Online] Available at: http://www.stats.ox.ac.uk/~reinert/time/notesht10short.pdf [Accessed 01 Feb. 2018].

Richard, J. et al. (2005). Image Change Detection Algorithms. A Systematic Survey. s.l. : IEEE Transactions on Image Processing, 2005.

Rimmer A. and Givati A. (2014). Hydrology. Chap. 31, In: Zohary T., Sukenik A, Berman T, Nishri A [eds] Lake Kinneret: Ecology and Management. pp. 97-111 Springer, Heidelberg.

Ruan, R., Zhang, Y. and Zhou, Y. (2008). Change Detection Of Wetland In Hongze Lake Using A Time Series Of Remotely Sensed Imagery. s.l. : The International Archives of the Photogrammetry, Remote Sensing and Spatial Information Sciences, 2008. Vol. XXXVII.

Samat, N. et al. (2011). Modeling Land Use Changes at the Peri-Urban Areas Using Geographic Information.

Schwabe, M. J., and Neevb, D. (2004). The late Quaternary limnological history of Lake Kinneret (Sea of Galilee), Israel (Israeli occupation).

Shaoqing, Z. (2008). The Comparative Study Of Three Methods Of Remote Sensing Image Change Detection. China.

Singh, A. (1989). Digital change detection techniques using remotely-sensed data. s.l. : Taylor & Francis.

Singh, A. (1989). Review article digital change detection techniques using remotely-sensed data. International Journal of Remote Sensing, 10(6), 989-1003.

Smith, R. B. (2012). Introduction to Remote Sensing of the Environment. Available at: http://www.microimages.com/documentation/Tutorials/introrse.pdf [Accessed 03 Jan. 2018].

Stein, M. (2001). The sedimentary and geochemical record of Neogene - Quatenary water bodies in the Dead Sea Basin - Inferences for the regional paleoclimatic history. Journal of Paleolimnology 26, 271–282.

Systems and Cellular Automata Model. Journal of Sustainable Development. (2011). Vol. 4. TANG, J., WANG, L. and YAO, Z. 2007. Spatiotemporal urban landscape change analysis using the Markov chain model and a modified genetic algorithm. 2007.

Théau, J. (2012). Change detection. [ed.] David M. Danko Wolfgang Kresse. Springer Handbook of Geographic Information. New York: Springer, 2012, 7.

U.S. Geological Survey. (1998). Overview of Middle East Water Resources. s.l. : Executive Action Team, 1998. p. 41.

Washah, D. (2002). Palestinian History Book. 2002. Palestine (in Arabic).

Water Level of Lake Kinneret. (2018). Weather In Israel. [Online] Available at: https://forecast.israelinfo.co.il/kineret [Accessed 20 Mar. 2018].

Weih Jr, R. C. and Riggan Jr, N. D. (2010). Object-based classification vs. pixel-based classification: comparative importance of multi-resolution imagery.

Wen, Wen. (2008). Wetland Change Prediction Using Markov Cellular Automata Model in Lore Lindu National Park Central Sulawesi Province, Indonesia. 2008.

Wikipedia. (2018). Degania Dam. [Online] Available at: https://en.wikipedia.org/wiki/Degania_Dam [Accessed 21 Mar. 2018].

WORLD SEA WATER TEMPERATURES. (2018). [Online] https://seatemperature.info/sea-of-galilee-water-temperature.html . [Accessed 20 Mar. 2018].

Yao, Xin. (2010). Cellular-automata. university of birmingham. 2010. [Online] Available at: http://www.cs.bham.ac.uk/internal/courses/intro-nc/current/notes/02-cellularautomata.pdf [Accessed 04 Apr. 2018].

Annex

A CD containing, the satellite images of the Sea of Galilee before and after image pre-processing, and the shapefiles extracted from the supervised classification which used for the spatiotemporal analysis.

ACKNOWLEDGEMENT

First of all, I would like to express my very profound gratitude to my family for their unlimited support and my sincere thanks to my love **Janka** for the motivation and the immense help that gave to me during my master degree.

I would like also to express my appreciation to my supervisor, **Prof. Dr. László ZENTAI**, who has cheerfully answered my queries, assisted me in myriad ways with the writing and helpfully commented on earlier drafts of this thesis. My deepest thanks as well to all colleagues from Palestine for their considerable guidance which helped a lot.

Furthermore, I would like to thank our honored teachers and professors in the department who reworded to us their knowledge simply and from their thoughts made a lighthouse guides us through the knowledge and success path.

I would like to extend my thanks to the university, the donor, and Hungary for this great opportunity to get my master degree and having the best time ever in my life

Finally, I am very grateful to my friends, and everybody supported and encouraged me throughout my years of study and through the process of researching and writing this thesis. This accomplishment would not have been possible without them. Thank you.

Ahmed Adwan